Helmholtz Zentrum München
Institut für Diabetesforschung
Direktorin: Prof. Dr. Anette-Gabriele Ziegler
und
Medizinischen Klinik und Poliklinik IV
Klinik der Ludwig-Maximilians-Universität München
Direktor: Professor Dr. med. Martin Reincke

The role of GLP1R signaling for the tissue-specific adaptation of regulatory T cells

Dissertation
zum Erwerb des Doktorgrades der Naturwissenschaften
an der Medizinischen Fakultät der
Ludwig-Maximilians-Universität zu München

vorgelegt von
Daria Opaleva
aus
Rostow am Don

Jahr
2022

Mit Genehmigung der Medizinischen Fakultät

der Universität München

Betreuerin:	Prof. Dr. phil. nat. Carolin Daniel
Zweitgutachter:	Prof. Dr. rer. nat. Ludger Klein
Dekan:	Prof. Dr. med. Thomas Gudermann
Tag der mündlichen Prüfung:	26. Juli 2023

Table of Contents

Abstract

During the last millennia, the organism of *Homo Sapiens* evolved under the pressure of positive selection driving the adaptation to occasional food scarcity and favoring energy accumulation and storage. The recent changes in demographics and lifestyle have altered the environment in which these adaptations have been advantageous, making them now responsible for the emerging of the obesity pandemic.

The disturbed regulation of systemic energy metabolism, as well as chronic low-grade visceral adipose tissue (VAT) inflammation are the main recognized factors driving the pathology of obesity and its associated comorbidities. Systemic energy metabolism is partially regulated by incretin hormones, e.g. glucagon-like protein 1 (GLP1), which has already been implicated in the development of anti-obesity drugs. Several GLP1 analogs are already approved or under current investigation and show multiple beneficial effects throughout the organism. The molecular mechanisms underlying the actions of GLP1 in various tissues have been intensively studied, but despite that, the knowledge about GLP1 signaling in immune cells, and specifically in regulatory T cells (Tregs), is very limited.

VAT resident Tregs are actively involved in the maintenance of systemic and local tissue metabolism. Their numbers decline upon obesity, thereby contributing to the progression of VAT inflammation and consequently the development of metabolic syndrome. The findings of this thesis provide the first evidence, to my knowledge, of the immunometabolic link between the GLP1/GLP1 receptor (GLP1R) signaling, VAT resident Tregs and systemic metabolic control. I show that the absence of GLP1R signaling in CD4 T cells (in a GLP1R TKO mouse model) affects the abundance of Tregs in metabolically active tissues, such as gut and VAT, fosters the pro-tolerogenic milieu within these tissues and ameliorates local inflammation. Upon hypercaloric challenge, the frequencies of VAT Tregs are restored in GLP1R TKO animals accompanied by a significant improvement of systemic metabolic parameters. The transcriptome analysis indicates that the specific cluster 2 Treg population, which is transcriptionally distinct from the classical VAT Tregs, is accountable for this local rise in Tregs in GLP1R TKO animals. This cluster 2

Treg population originates from classical VAT Tregs upon transcriptional dedifferentiation and downregulation of the tissue-specific program. At the same time, in absence of GLP1R signaling they are able to preserve the hallmarks of the classical VAT Treg signature while upregulating transcriptional programs supporting Treg stability and function. Collectively, this data indicates, that the absence of T cell-specific GLP1R signaling has beneficial effects on the adaptation and maintenance of Tregs in gut and VAT, contributing to the reduction of tissue inflammation and thereby safeguarding metabolic health.

Zusammenfassung

In den letzten Jahrtausenden entwickelte sich der Organismus des *Homo Sapiens* unter dem Druck einer positiven Selektion, die die Anpassung an gelegentliche Nahrungsmittelknappheit vorantrieb und die Energieakkumulation und -speicherung begünstigte. Die jüngsten Veränderungen in der Demografie und im Lebensstil haben das Umfeld, in dem diese Anpassungen vorteilhaft waren, verändert, sodass sie nun für die Entstehung der Adipositas-Pandemie verantwortlich sind.

Die gestörte Regulierung des systemischen Energiestoffwechsels sowie chronische Entzündungen des viszeralen Fettgewebes sind die wichtigsten anerkannten Faktoren, die für die Pathologie der Adipositas und der damit verbundenen Begleiterkrankungen verantwortlich sind. Der systemische Energiestoffwechsel wird teilweise durch Inkretin-Hormone, z. B. Glucagon-like protein 1 (GLP1), reguliert, die bereits in die Entwicklung von Medikamenten gegen Fettleibigkeit einbezogen wurden. Mehrere GLP1-Analoga sind bereits zugelassen oder werden derzeit untersucht und zeigen vielfältige positive Wirkungen im gesamten Organismus. Die molekularen Mechanismen, die den Wirkungen von GLP1 in verschiedenen Geweben zugrunde liegen, wurden intensiv erforscht, aber trotzdem ist das Wissen über die GLP1-Signalübertragung in Immunzellen und insbesondere in regulatorischen T-Zellen (Tregs) aktuell sehr begrenzt.

Tregs im viszeralen Fettgewebe sind aktiv an der Aufrechterhaltung des systemischen und lokalen Gewebestoffwechsels beteiligt. Ihre Zahl nimmt bei Fettleibigkeit ab und trägt damit zum Fortschreiten der Entzündung im viszeralen Fettgewebe und der daraus resultierenden Entwicklung des metabolischen Syndroms bei. Die Daten dieser Arbeit liefern meines Wissens den ersten Beweis für die immunometabolische Verbindung zwischen dem GLP1/GLP1 Rezeptor (GLP1R)-Signalweg, Tregs im viszeralen Fettgewebe und der systemischen Stoffwechselkontrolle. Ich zeige, dass das Fehlen von GLP1R-Signaltransduktion in CD4-T-Zellen (im GLP1R-TKO-Mausmodel) die Häufigkeit von Tregs in stoffwechselaktiven Geweben wie Darm und VAT beeinflusst, das pro-tolerogene Milieu in diesen Geweben fördert und Entzündungen lindert. Nach einer hyperkalorischen Diät wird die Häufigkeit von Tregs im viszeralen Fettgewebe von GLP1R-TKO-Tieren wiederhergestellt, begleitet von einer deutlichen Verbesserung der systemischen Stoffwechselparameter. Die Transkriptomanalyse von T-Zellen auf Einzelzellebene zeigt, dass eine Population von Tregs, die sich transkriptionell von den klassischen Tregs im viszeralen Fettgewebe unterscheidet, für diesen lokalen Anstieg der Tregs in GLP1R-TKO-Tieren verantwortlich ist. Diese Cluster-2-Treg-Population stammt von den klassischen Fettgewebe-Tregs ab, behält aber in GLP1R-TKO-Mäusen die Merkmale des klassischen Transkriptionsprogramms von Treg im viszeralen Fettgewebe bei. Gleichzeitig regulieren

Cluster-2-Tregs Transkriptionsprogramme hoch, die die Stabilität und Funktion der Tregs unterstützen. Insgesamt deuten diese Daten darauf hin, dass das Fehlen von T-Zell-spezifischer GLP1R-Signaltransduktion eine positive Wirkung auf die Anpassung und Aufrechterhaltung von Tregs im Darm und im viszeralen Fettgewebe hat, was zur Verringerung von Gewebeentzündungen beiträgt, und somit insgesamt die metabolische Gesundheit aufrechterhält und fördert.

List of figures

List of tables

List of abbreviations

AKT	Protein kinase B
AT	Adipose tissue
APC	Antigen-presenting cell
AREG	Amphiregulin
BAT	Brown adipose tissue
BSA	Bovine serum albumin
CNS	Conserved non-coding sequence
CpG	5’-C-phosphate-G-3’
CTLA4	Cytotoxic T lymphocyte antigen 4
DC	Dendritic cells
DPBS	Dulbecco's phosphate-buffered saline
EDTA	Ethylenediaminetetraacetic acid
Ex-4	Exendin-4
FACS	Fluorescence activated cell sorting
FC	Flow cytometry
FCS	Fetal calf serum
Foxp3	Forkhead box protein 3
GF	Germ-free
GLP1	Glucagon-like peptide 1
GLP1R	Glucagon-like peptide 1 receptor
GLP1R TKO	T cell-specific deletion of glucagon-like peptide 1 receptor
GSEA	Gene set enrichment analysis
HBSS	Hanks’ balanced salt solution
$HBSS^{+}$	Hanks’ balanced salt solution with supplements
HEPES	Hydroxyethylpiperazin-ethansulfonacid
HFHS	High-fat high-sugar
IFNγ	Interferon gamma

IL	Interleukin
i.p.	Intraperitoneal
IPEX	Immune polyendocrinopathy enteropathy X-linked
i.v.	Intravenous
IRF4	Interferon regulatory factor 4
KO	Knock-out
MACS	Magnetic activated cell sorting
MAPK	Mitogen activated protein kinase
MAT	Mesenteric adipose tissue
mesLN	Mesenteric lymph nodes
MHC	Major histocompatibility complex
mtDNA	Mitochondrial DNA
mTOR	Mammalian target of rapamycin
NFκb	Nuclear factor-κB
OXPHOS	Oxidative phosphorylation
PBS	Phosphate-buffered saline
PMA	Phorbol 12-myristate 13-acetate
PPAR-γ	Peroxisomal proliferator-activated receptor gamma
PTEN	Phosphatase and tensin homolog deleted on chromosome 10
RKI	Robert Koch Institut
PP	Peyer's patches
SAT	Subcutaneous adipose tissue
scRNAseq	Single cell RNA sequencing
SD	Standard diet
SI	Small intestine
SPF	Specific pathogen-free
STAT	Signal transducer and activator of transcription
TCR	T cell receptor

Th	T helper (cell subset)
TKO	T cell-specific knock-out
TNFα	Tumor necrosis factor
T2DM	Diabetes mellitus type 2
Treg	Regulatory T cell
UMAP	Uniform manifold approximation and projection
VAT	Visceral adipose tissue
WT	Wild type

1 Introduction

1.1 Obesity as a disease

Over the last few decades, obesity has evolved from just a cosmetic issue to the one of the world's largest health problems. Nowadays it is recognized as a major risk factor for the development and progression of Type 2 Diabetes Meletus (T2DM) and cardiovascular pathologies. It also contributes to the numerous cases of respiratory, neurological, immunological, gastrointestinal and musculoskeletal diseases, as well as some cancers. During the recent COVID-19 outbreak, obese individuals have been assigned to the group of risk for developing severe illness. Obesity, therefore, represents a multisystemic dysregulation, which significantly affects the quality of live and reduces the average life expectancy of millions of people (Bray et al., 2017, Ansari et al., 2020, Bhaskaran et al., 2014).

According to the World Health Organization (WHO), in 2016 39% and 13% of adults have been overweight and obese, respectively (WHO, 2021b). Much higher prevalence is estimated in Germany by Robert Koch Institute (RKI). Here, 67% of men and 53% of women are nowadays overweight, whereas about 23% of adults are obese (RKI). These numbers continue to rise steadily, but the most treatments have limited efficacy so far. The main reason for that is the heterogeneity and the multifactorial nature of the disease. Individual genetic and epigenetic factors in combination with environmental aspects influence molecular processes, which protect from or favor the development of obesity and associated complications (Ansari et al., 2020). Therefore, to successfully treat obesity, effective clinical programs are needed, which include screenings, risk factor assessment, prognosis and precise diagnosis. These data will then form a basis for personalized solutions incorporating the lifestyle and pharmacological management, possibly surgical intervention, as well as subsequent weight maintenance program. Therefore, a better understanding of the molecular mechanisms of the disease and its associated complications are required to design and implement such clinical programs.

1.2 Adipose tissue inflammation

One of the main mechanisms underlying the complications of obesity is a chronic low-grade inflammation, which primarily occurs in the white adipose tissue (AT) in abdominal cavity (visceral adipose tissue, VAT). Historically, the white AT has been considered to serve solemnly as a connective tissue and a site to store and release energy in form of lipids. However, in recent years it became clear, that the white AT is a complex metabolic and endocrine organ, which is able to secrete a variety of biologically active mediators and signaling molecules, called adipokines. These adipokines are crucial for the regulation of systemic lipid and glucose metabolism, appetite, insulin sensitivity, but also immune reactions and inflammatory responses. Adipokines exert both, pro- and anti-inflammatory functions, which are well balanced in the healthy steady state. Obesity and increasing AT mass induce oxidative stress, hypoxia and endoplasmic stress in adipocytes, which in turn leads to adipocyte dysfunction and prevailed expression of the pro-inflammatory adipokines, such as leptin and resistin (Hassan et al., 2012). It enhances the production of proinflammatory cytokines (e. g. IL6, IL12, IL18, TNFα) and chemokines (e.g CCL2), which activate proinflammatory signaling pathways not only in the VAT itself, but also affect the tissue residing immune cells, which comprise a substantial part of VAT cellular content (Hassan et al., 2012, Mathis, 2013). In the lean state, VAT residing immune cells are important for tissue repair, remodeling and metabolic function. However, with increasing AT mass, the numbers, composition and phenotype of these cells change.

The first identified and the most abundant immune cell subset involved in the development of VAT inflammation are macrophages (Xu et al., 2003). Being abundant in the lean AT (from under 10% of VAT cells), they strongly infiltrate AT upon obesity and may reach up to 50% of VAT cellular content (Weisberg et al., 2003). It is accompanied by their phenotypic polarization from anti-inflammatory alternatively activated (M2) towards proinflammatory classically activated (M1) state. These M1 macrophages were shown to be the main immune cell subset responsible for the production of proinflammatory cytokines (TNFα, IL6, IL1β, IL12 etc.) linked to the progression of obesity-associated VAT tissue inflammation and insulin resistance (Patsouris et al., 2008).

In addition, neutrophils, dendritic cells, mast cells, invariant natural killer T cells 1 (iNKT1), B and T lymphocytes have been shown to accumulate in obese VAT contributing to the progression of AT inflammation. On the contrary, the cells of the anti-inflammatory nature decrease in obesity. Among them are eosinophils and ILC2, which promote differentiation and survival of M2 macrophages, and a population of VAT resident regulatory T cells (Tregs), which are highly enriched in the lean VAT and are crucial modulators of both, immune and metabolic homeostasis in AT (Feuerer et al., 2009).

1.3 Tregs in self-tolerance

Tregs have been primarily discovered as the main mediators of immunological self-tolerance and negative regulation of immune-driven inflammation. These cells are able to modulate the strength of adaptive and innate immune responses by various mechanisms, such as secretion of inhibitory cytokines (Sundstedt et al., 2003), induction of apoptosis (Pandiyan et al., 2007), inhibition of proliferation (Kobie et al., 2006), sequestration of growth factors or modulation of dendritic cell (DC) maturation or function (Akkaya et al., 2019, von Boehmer, 2005). They are induced either in the thymus (tTregs) or peripherally (pTregs), however no conclusive markers distinguishing t- and pTregs have been discovered so far. Although the transcription factor Helios and surface protein Neuropilin1 (Nrp1) have been suggested to be characteristic for tTregs, this hypothesis has been lately challenged by the reports, that pTregs or Tregs induced *in vitro* (iTregs) are also potent of Helios and Nrp1 expression (Szurek et al., 2015).

Tregs are classically described as CD4 T cells positive for CD25 (the high-affinity interleukin-2-receptor α-chain (IL2Rα)), coinhibitory receptor cytotoxic T lymphocyte antigen 4 (CTLA4) and most importantly, a transcription factor Foxp3 (X-linked gene forkhead box P3). The essential role of Foxp3 for Treg cell lineage and for immunological self-tolerance in general is highlighted by the fatal autoimmune disorder, immune polyendocrinopathy enteropathy X-linked (IPEX) syndrome that is caused by mutation in the Foxp3 gene (Bennett et al., 2001). Patients with IPEX develop a broad variety of auto-antibodies and subsequent autoimmune enteropathy, psoriasiform or eczematous dermatitis, nail dys-

trophy, autoimmune endocrinopathies and autoimmune skin conditions such as alopecia universalis and bullous pemphigoid. Similarly, the mutant mouse strain *scurfy* or Foxp3^{DTR} mice, subjected to inducible ablation of Foxp3^{+} Tregs, experience aggressive and lethal autoimmunity (Brunkow et al., 2001, Kim et al., 2007). Collectively, these data indicate, that the continuous presence of Tregs and their expression of Foxp3 is essential for preventing severe autoimmunity.

1.4 Plasticity of Tregs

The profound consequences of Foxp3 absence for Tregs had led to the wide recognition of Foxp3 as a master regulator of Tregs, which is per definition essential and sufficient for acquisition of the full Treg signature. This idea has been though challenged by observations, that Foxp3 induction by TGFβ or retroviral transduction of Foxp3 elicit the Treg signature only partially (Hill et al., 2007). In addition, the characterization of Tregs harboring Foxp3^{null} allele, but lacking Foxp3 protein in healthy heterozygous female mice revealed the moderate expression of characteristic Treg cell surface markers, such as CD25, GITR and CTLA4, even in the absence of Foxp3. In comparison, in Foxp3 sufficient cells the expression of the same set of proteins was rather further amplified (Gavin et al., 2007). However, Foxp3^{null} T cells were not able to suppress CD4^{+}CD25^{-} T cell proliferation *in vitro* and after adoptive co-transfer into T cell-deficient recipient mice *in vivo*. These studies therefore set the foundation for the hypothesis, that Foxp3 is not the main factor initiating a *de novo* development of Tregs, but rather stabilizes pre-established Treg lineage signature and regulate Treg suppressive function.

Furthermore, by interaction with diverse binding partners downstream of Foxp3 (transcription factors and chromatin remodelers), Foxp3 can modulate the phenotypic and functional adaptation of Tregs to environmental cues. By these means, Tregs can adopt the transcriptional program of T helper effector (Th) cells to specifically control this particular Th subset. Such Tregs, referred to as Th-like Tregs, retain the classical features of Tregs and in addition express TFs and cytokines characteristic for the particular Th subset: IFNγ/TBET/CXCR3 for Th1-like Tregs, IL4/GATA3/IRF4 for Th2-like Tregs and IL17/RORγt/CXCR6 for Th17-like Tregs (Qiu et al., 2020).

1.5 Tregs in non-lymphoid tissues

The concept of Treg plasticity and phenotypic adaptation to enable specific functionality was further broadened by studies reporting existence of Tregs in non-lymphoid tissues, such as AT (Feuerer et al., 2009), colon and small intestine (SI) (Yang et al., 2016), lung (Faustino et al., 2012), skin (Nosbaum et al., 2016), liver (Li et al., 2020), muscle (Burzyn et al., 2013) and central nervous system (CNS) (Ito et al., 2019). In each of these sites of residence, Tregs form phenotypically unique and highly specialized subpopulations, characterized by the expression of tissue-specific surface markers, transcription factors and T cell receptor (TCR) repertoire. The DNA-methylation and transcriptome analysis delineated the developmental trajectories of tissue Tregs originating from common tissue Treg progenitors. Delacher et al. identified two precursor stages of tissue Tregs in spleen and LNs, which are defined by differential expression of Nfil3, PD1 and Klrg1 (Delacher et al., 2020). The reprogramming process is proposed to occur stepwise and include an early activation event in lymphoid organs (Delacher et al., 2020, Li et al., 2018). The transcription factor BATF has been shown to be crucial in this process of differentiation of Klrg1$^-$Nfil3$^-$ to the Klrg1$^-$Nfil3$^+$ and to the Klrg1$^+$Nfil3$^+$ precursor stages, directly modulating the accessibility of Th2-assosiated genes, such as *Il1rl1* (ST2), *IL10*, *Maf*, *Pparg*. The following transition of Klrg1$^-$Nfil3$^+$ to the later Klrg1$^+$Nfil3$^+$ stage includes the induction of characteristic tissue Treg markers (*Gata3*, *Il1rl1*, *Klrg1* and a switch from *Id3* to *Id2*). The further tissue-specific chromatin changes as well as phenotypic differentiation of tissue Tregs take place upon seeding in the respective tissue (Li et al., 2018). There, tissue Tregs do not only maintain an immunological tolerance by suppression of inappropriate inflammatory response, but are also indispensable for the organ and organismal homeostasis (Feuerer et al., 2009, Burzyn et al., 2013, Ito et al., 2019).

1.6 Abundance of Tregs in VAT

The first characterized in detail tissue Treg population are VAT Tregs (Feuerer et al., 2009, Cipolletta et al., 2012). In comparison to lymphoid organs, spleen and lymph nodes, where Tregs comprise about 5-15% of CD4$^+$ T cells, Tregs in VAT are much more

abundant (Cipolletta et al., 2015). However, their frequencies are very dynamic and are affected by several factors. *Ex vivo* Foxp3$^+$ Tregs are steadily increasing with age and can reach 50-70% of CD4$^+$ T cells. This peak in VAT Tregs is first evident at the age of 20-25 weeks in male C57Bl/6 mice. Later on, at the age of approximately 40 weeks, the abundance of Tregs decreases again (Cipolletta et al., 2015).

Another physiological factor, which modulates VAT Tregs is sex. Male and female mice are different in their AT physiology. So, males accumulate more VAT, especially upon high-fat/high-sugar diet (HFHS), whereas females are more protected from development of obesity and metabolic syndrome (Macotela et al., 2009, Salinero et al., 2018). Despite that, in comparison to female mice, lean male mice exhibit higher frequencies of Tregs in VAT, which are also different from female Tregs in their transcriptome and chromatin accessibility (Vasanthakumar et al., 2020). This effect has been shown to depend on sex hormone estrogen, which limits VAT inflammation in females. In males heightened VAT inflammation and specific to males IL33-producing stromal cells facilitate Treg recruitment, as a mechanism targeted to limit VAT inflammation.

Moreover, the adaptability and responsiveness of VAT Tregs to environmental cues is highlighted by their sensitivity to cold exposure, which was demonstrated by Kälin and Becker et al (Kalin et al., 2017). Here, the researchers could show, that cold exposure or direct beta3-adrenergic stimulation induce AT Tregs, which mechanistically relies on T cell-intrinsic STAT6/PTEN signaling.

An additional and well described factor, which strongly influences Tregs in VAT is obesity. The 8-20 weeks of HFHS diet or genetically induced (ob/ob mouse line) obesity cause significant reduction in percentages of Tregs in VAT (Feuerer et al., 2009, Li et al., 2021b). Moreover, the Tregs from obese VAT lose their tissue specific phenotype and characteristic expression of *Il1rl1*, *Klrg1* and *Il10* (Cipolletta et al., 2015). These results clearly demonstrate the dynamic nature of VAT resident Treg population and its ability to respond to environmental and physiological cues.

1.7 Phenotype of Tregs in VAT

VAT resident Tregs retain the expression of about 63% of canonical Treg signature genes, including those coding for Foxp3, CD25, GITR, OX40 and CTLA4 (Feuerer et al., 2009). At the same time, they are highly distinct in the expression of multiple genes, upregulating transcripts of characteristic chemokine receptors (e.g. CCR3, CCR2), surface markers and cytokine receptors (e.g. ST2, IL9R), transcription factors (PPARγ, BATF, BLIMP1, IRF4, ID2) and molecules involved in lipid metabolism (e.g. PCYT1A, DGAT1). Among the downregulated genes are chemokine receptors CCR6, CCR7 and several transcription factors (e.g. ID3). VAT Tregs possess rather an activated phenotype ($CD44^{hi}CD62L^{lo}$) (Cretney et al., 2011, Peters et al., 2013) and express much higher levels of IL10 which can act directly on adipocytes and suppress proinflammatory markers (Feuerer et al., 2009).

The major driver of VAT Treg phenotype is the adipocyte master regulator PPARγ. It was identified by a comparison of gene expression profiles of VAT Tregs vs lymph node (LN) Tregs, whereby *Pparg* was significantly increased in the former population. The expression of *Pparg* was strongly correlated with the most differentially expressed in VAT Treg compared to LN Treg genes (Cipolletta et al., 2012). The importance of PPARγ for the initiation and maintenance of VAT Treg phenotype is also outlined by the evidence that Treg-specific ablation of *Pparg* resulted in depletion of VAT Tregs, whereas their numbers in lymphoid organs remained unaltered (Cipolletta et al., 2012). Retroviral transfection of *Foxp3* and *Pparg* into $CD4^{+}CD25^{-}$ T cells has demonstrated that PPARγ collaborates with Foxp3 to upregulate the gene set characteristic for VAT Treg cell signature (Cipolletta et al., 2012). Recently, Li et al. identified a population of $PPAR\gamma^{lo}$ Tregs in spleen hypothesized to be the precursor stage of tissue Tregs and in particular of VAT Tregs (Li et al., 2018, Li et al., 2021a). Transfer of splenic $PPAR\gamma^{-}$ Tregs into wildtype (WT) C57Bl6 mice led to the appearance of $PPAR\gamma^{+}$ Tregs in the spleen followed by their rise in VAT. Transcriptomic analysis of these splenic $PPAR\gamma^{lo}$ Tregs demonstrated a partial induction of VAT Treg signature, but mostly genes related to the activated phenotype, whereas the tissue-specific part was induced only in VAT (Li et al., 2018).

Collectively, these studies indicate, that the accumulation, phenotype and function of VAT Tregs are dependent on PPARγ and Foxp3 expression, which however are not the

only crucial factors identified so far. VAT Treg accumulation has been shown to rely strongly on TCR and cell-intrinsic ST2/IL33 signaling. TCR repertoire of VAT Tregs is much more restricted and clonally expanded than that of their lymphoid tissue counterparts (Feuerer et al., 2009) and is hypothesized to be the one of the mechanisms of VAT Treg maturation and expansion. Li et al had accomplished to generate vTreg53 TCR-transgenic mice bearing the expression of an identified expanded VAT Treg TCR clone (Li et al., 2018). At steady state or upon adoptive transfer specifically, clonotype^{+} Tregs were enriched in VAT, but not in other tissues examined. In addition, TCR stimulation was shown to be necessary and sufficient to induce PPARγ expression in splenic PPARγ^{lo} Tregs (Li et al., 2018). These results support the hypothesis, that the accumulation of VAT Tregs and acquisition of VAT Treg phenotype is dependent on the TCR-antigen recognition, whereas the exact antigen (or multiple antigens) has not been identified so far.

Lastly, the Treg population in VAT is highly impacted by ST2/IL33 signaling. A vast majority of VAT Tregs express ST2 (encoded by Il1rl1), which is a receptor for alarmin IL33. The germline deletion of ST2 reduces the fraction of Tregs in VAT, but not in spleen (Kolodin et al., 2015). *In vitro* and *in vivo*, IL33 administration strongly promotes proliferation of VAT Tregs, as well as maintains their *Pparg* transcription and expression of Foxp3 and GATA3 (Vasanthakumar et al., 2015). Together these studies suggest, that VAT Tregs are sensitive to IL33, however controversial reports have been made on the mechanism of this interaction. Vasanthakumar et al. proposed that IL33 effect on VAT Tregs relies on cell-intrinsic IL33/ST2 signaling, since bone marrow chimeras reconstituted with ST2-deficient hematopoietic cells exhibit significant reduction of VAT Tregs (Vasanthakumar et al., 2015). At the same time, Molofsky and colleagues have argued, that the effect of IL33 on VAT Tregs is mainly indirect and is mediated by VAT resident ILC2s (Molofsky et al., 2015). The examination of mice with Treg-specific ablation of ST2 by two different research groups provided ambiguous results. Li et al. observed a significant reduction of VAT Tregs in Foxp3^{Cre} Il1rl1$^{fl/fl}$ mice (Li et al., 2018), whereas Hemmers et al. reported no changes in VAT Tregs in Foxp3^{Cre} Il1rl1$^{fl/fl}$ animals (Hemmers et al., 2020). These contradicting observations highlight the complexity of multi-layered regulation of Treg accumulation in tissues, where both, cell-intrinsic and extrinsic mechanisms may take part.

1.8 Functions of VAT Tregs

The intense phenotyping and characterization VAT Tregs have helped to study their function, which goes beyond the classical immunomodulation. Given the strong reciprocal correlation of VAT Treg frequencies with weight gain and progression of obesity, multiple studies have intensively investigated the role of VAT Tregs specifically in the setting of HFHS diet (Li et al., 2021b, Feuerer et al., 2009, Kalin et al., 2017, Vasanthakumar et al., 2020). It has been demonstrated, that by manipulating VAT Tregs systemic metabolic parameters could be affected. Depletion of Tregs by administration of anti-CD25 antibodies into WT C57Bl6 mice or induced in $Foxp3^{DTR}$ mice worsens metabolic parameters, such as glucose tolerance and insulin sensitivity (Feuerer et al., 2009, Eller et al., 2011). The expansion of Tregs with IL2/anti-IL2 complexes in mice on HFHS diet in contrary improves glucose tolerance (Feuerer et al., 2009). Later these effects have been confirmed by targeting Tregs specifically in VAT. Upon Treg-specific deletion of PPARγ, treatment with IL33 or PPARγ agonist Pio or in vTreg53 TCR-transgenic mice VAT Tregs have been significantly and specifically altered, which had an effect on VAT inflammation and metabolic parameters (Li et al., 2018, Cipolletta et al., 2012).

1.9 Intestinal Tregs

Similar to VAT, intestine is another site of an intense immunometabolic crosstalk and is highly populated by Tregs. There, Tregs establish immune tolerance towards dietary antigens and commensal microorganisms, but are also indispensable for the local tissue repair and the integrity of the epithelial barrier. These functions are performed by three specialized Treg subsets identified so far: $GATA3^{+}Helios^{+}(Nrp1^{+})$, $ROR\gamma t^{+}Helios^{-}$ and $ROR\gamma t^{-}Nrp^{-}(Helios^{-})$.

1.10 $ROR\gamma t^{+}$ intestinal Tregs

RORγt is a Th17 master regulator and is highly expressed in the intestinal Tregs. These $ROR\gamma t^{+}$ Tregs are mostly present as $Helios^{-}$ $Nrp1^{-}$ Tregs, which argues for their peripheral

induction (Kim Kwang et al., 2016, Sefik et al., 2015). In agreement with that, the frequencies of RORγt$^+$ Tregs are dependent on the complexity of microbiota. Germ-free (GF) mice, which are completely devoid of microbiota, as well as mice treated with a broad-spectrum antibiotic combination, exhibit a dramatic reduction of RORγt$^+$ Tregs (Sefik et al., 2015, Kim Kwang et al., 2016). Moreover, RORγt$^+$ Tregs in their abundance parallel microbiota, being more present in colon than in SI (ca. 40% vs 15% of all Foxp3$^+$, respectively) (Sefik et al., 2015).

In their gene expression RORγt$^+$ Tregs resemble rather intestinal Foxp3$^+$ Tregs than RORγt$^+$ Th17 cells (Yang et al., 2016). RORγt$^+$ Tregs expressed high levels of Th17 related genes (*Irf4*, *Maf*, *Il1r1*, *Il23r*, *Ikzf3*), as well as characteristic chemokine receptors (*Ccr4*, *Ccr6* and *Ccr9*). At the same time, the expression of Th17-associated effector cytokines (*Il17a*, *Il17f*, *Il21*) is repressed in RORγt$^+$ Tregs, which is facilitated by the expression of Blimp1 (Ogawa et al., 2018). Mechanistically, the induction of the RORγt$^+$ Treg program in the intestine is dependent on IL6 and TGFβ, which in combination with TCR signaling and in STAT3-dependent manner drives the expression of c-Maf and RORγt in Tregs (Wheaton et al., 2017). RORγt$^+$ Tregs possess an effector-like phenotype and express high levels of IL10, CTLA4, ICOS, CD39 and CD73. Accordingly, in the model of T cell-mediated transfer colitis RORγt$^+$ Tregs demonstrated a superior suppressive capacity, when compared with RORγt$^-$ Tregs (Yang et al., 2016). This argues for RORγt$^+$ Tregs being an important component of intestinal immune tolerance, especially towards microbial antigens.

1.11 GATA3$^+$ intestinal Tregs

The expression of GATA3 is mutually exclusive to RORγt (Sefik et al., 2015, Wohlfert et al., 2011). It is observed in approximately a third of the intestinal Tregs and can be induced and sustained by IL2 and TCR stimulation (Wohlfert et al., 2011). GATA3$^+$ Tregs in the intestine express Helios and are unaffected by microbiota, which suggests their thymic origin (Ohnmacht et al., 2015). Their phenotype and high expression of ST2 and amphiregulin (AREG) reflect their tissue repair function (Schiering et al., 2014). Schiering

et al. have demonstrated, that upon induction of chronic colitis the levels of IL33 in colonic epithelial cells were elevated (Schiering et al., 2014). However, in absence of ST2, Tregs were irresponsive to IL33, which affected their ability to accumulate in the inflamed tissue and abrogated their Foxp3 expression. Mechanistically, Schiering et al. have proposed, that IL33 can directly regulate Foxp3 expression through the activation and recruitment of GATA3 to the Foxp3 promoter. In accordance with that, GATA3-deficient Tregs were also impaired in their ability to accumulate and to suppress inflammation in the transfer colitis model (Wohlfert et al., 2011). Overall these data suggest the subpopulation of $GATA3^+$ Tregs to be adapted to accumulate to the sites of intestinal inflammation or damage and mediate tissue repair, although this model has yet to be proven.

1.12 RORγt$^-$Nrp$^-$ intestinal Tregs

While the colon is highly populated by RORγt$^+$Helios$^-$ Tregs responsive to microbiota, the substantial proportion of Tregs in SI is rather driven by dietary antigens (Ag). This RORγt$^-$Nrp$^-$ population is unaffected by changes in the microbiota, since GF mice possess normal numbers of Tregs when compared to SPF (specific pathogen-free) control mice. The treatment of SPF mice with a cocktail of antibiotics also does not affect the RORγt$^-$Nrp$^-$ Treg population. On the contrary, feeding of SPF mice with diet devoid of macromolecules (Ag-free diet) caused a severe reduction of RORγt$^-$Nrp$^-$ Tregs in SI, but not in colon (Kim Kwang et al., 2016). These data suggest, that the population of RORγt$^-$Nrp$^-$ Tregs are the Tregs induced peripherally and in response to dietary antigens. Since SI is primarily a compartment, specialized on nutrient absorption, high abundance of RORγt$^-$Nrp$^-$ Tregs once more highlights the plasticity and superior tissue specialization of Tregs, governed by the local microenvironment.

1.13 GLP1

An additional component of the intestinal Treg microenvironment, which can potentially affect Treg function, are the bioactive molecules produced within this microenvironment. One of such bioactive molecules is the incretin hormone glucagon-like peptide 1 (GLP1). GLP1 is involved in postprandial regulation of glucose levels by inducing the insulin secretion and suppressing the glucagon secretion after the oral food intake. GLP1 is produced mainly by intestinal L cells, which are distributed with increasing density from duodenum to the colon (Jorsal et al., 2018), and to some degree in the CNS (Larsen et al., 1997). It is expressed as a proglucagon gene (*Gcg*), which encodes a precursor for glucagon, GLP1 and GLP2. Although the same mRNA is transcribed in the intestinal L cells, in the pancreatic α-cells and in the neurons of hypothalamus and brainstem (Drucker and Asa, 1988, Mojsov et al., 1987), the tissue-specific post-translational processing by different prohormone convertase (PC) enzymes generates different proteins. In the pancreas, the action of PC2 ensures the processing of proglucagon mainly to glucagon, whereas PC1/3 in brain and intestine is responsible for GLP1, GLP2 and oxyntomodulin expression (Rouillé et al., 1995). However, the initial full-length GLP1 (1-37) product is devoid of biological activity and undergoes subsequent proteolytic cleavage. This process gives rise to two forms, GLP1(7-36) amide and GLP1(7-37), with similar bioactivity, but GLP1(7-36) form being more abundant (Orskov et al., 1994).

The half-life of GLP1 after release into systemic circulation is very short (ca. 2 min) (Deacon et al., 1995, Deacon et al., 1996), which is mainly a result of the rapid degradation by the enzyme dipeptidylpeptidase-4 (DPP4). DPP4 cleaves both forms, GLP1(7-36) amide and GLP1(7-37), at the N-terminal dipeptide generating an inactive GLP1(9-36) amide (Deacon et al., 1995, Vahl et al., 2003).

GLP1 acts on its receptor (GLP1R), which is a member of the class B family of G protein-coupled receptors (GPCRs). GLP1R signaling can occur via multiple pathways, whereas the best documented is a signaling through $G_{\alpha s}$ with a subsequent activation of adenylate cyclase and increase in cAMP levels (Koole et al., 2013).

The expression of GLP1R has been identified in a variety of tissues including pancreas, heart, kidney, lung, intestine and brain (Bullock et al., 1996, Campos et al., 1994, Wei

and Mojsov, 1995). In AT, the reports on the GLP1R expression for a long time have been controversial (Wei and Mojsov, 1995, Bullock et al., 1996), however, the most recent studies argue for GLP1R being expressed in adipocytes and pre-adipocytes (Vendrell et al., 2011, Challa et al., 2012). By acting on its receptor GLP1 exert tissue-specific functions. The best characterized is the action of GLP1 in pancreas, where it increases insulin secretion from β-cells and inhibit glucagon secretion from α-cells in a glucose-dependent manner (Simonsson and Ahrén, 1998, Fernandez and Valdeolmillos, 1999, Hare et al., 2010). Moreover, GLP1 and GLP1R agonists were demonstrated to stimulate proliferation and inhibit apoptosis of β-cells (Buteau et al., 2003, Buteau et al., 2004).

In addition to its insulinotropic effects, the beneficial effects of GLP1 on the cardiovascular system have been reported. These include cardioprotective effects and inhibition of apoptosis in an acute model of myocardial infarction or hypoxia-reoxygenation induced injury (Noyan-Ashraf et al., 2009, Wang et al., 2010). GLP1 as well as GLP1R agonists have been reported to increase heart rate and blood pressure (Barragán et al., 1996). However, these effects seem to be species-specific and the underpinning mechanisms are complex and may involve the sympathetic as well as parasympathetic nervous system (reviewed in (Ussher and Drucker, 2014)).

Over the last decades, the effects of GLP1 and its analogs on the CNS have gained the great interest, first of all to promote satiety and reduce food intake. This anorectic effect has been proposed to be directly mediated by GLP1R in CNS and vagal afferents (Kanoski et al., 2011, Secher et al., 2014, López-Ferreras et al., 2018). Moreover, the effects of GLP1 on energy expenditure in rodents appeared at least partially to involve GLP1R signaling in the brain to control BAT thermogenesis (Heppner et al., 2015, Bagger et al., 2015). Furthermore, systemically administered GLP1 was demonstrated to improve neuroprotection and hippocampal dependent associative and spatial learning in rats (During et al., 2003). In line with that, the weekly administration of a GLP1R agonist exenatide could ameliorate symptoms of Parkinson's disease and improve patients' motor function (Athauda et al., 2017). Conversely, astrocyte-specific deletion of GLP1R impairs mitochondrial function in astrocytes, but improved memory formation and systemic glucose metabolism (Timper et al., 2020). Therefore, the exact cellular targets of GLP1 in the CNS and molecular mechanisms have to be further investigated.

Quite recently, reports implicating GLP1R in the regulation of inflammation have emerged. In 2008 Hadjiyanni et al. for the first time have detected mRNA transcripts of GLP1R in spleen, thymus and lymph nodes from NOD (non-obese diabetic) and C57BL6 mice (Hadjiyanni et al., 2008). Later in 2010 the same research group demonstrated GLP1R mRNA transcripts in several sorted immune cell populations, including $CD4^+$ T cells and sorted as $CD4^+CD25^+$ Tregs (Hadjiyanni et al., 2010). In this study, Hadjiyanni et al. have shown, that GLP1R signaling in mixed leucocyte populations leads to the cAMP accumulation, but did not affect the *in vitro* migratory behavior of thymocytes and splenocytes. In the model of Type 1 Diabetes (T1D) in NOD mice, Xue et al. specifically addressed the effect of systemic administration of GLP1R agonist exendin-4 (Ex-4) on Tregs (Xue et al., 2008). Although, no effect of Ex-4 on the disease progression has been observed, the treatment increased the frequencies of splenic $CD4^+CD25^+Foxp3^+$ Tregs. In addition, Tregs isolated from treated animals possessed improved suppressive power and produced more IL10 *in vitro*.

2 Objective

Due to its insulinotropic, anorexigenic, neuroprotective, cardiovascular protective and metabolic regulatory effects GLP1/GLP1R axis has become an appealing target for the treatment of obesity and diabetes. Multiple GLP1R agonists have already been approved for obesity and T2DM treatment with many more currently undergoing preclinical and clinical trials. Although, multiple GLP1 analogs with improved stability and pharmacokinetics have been proven effective in regulation of metabolic parameters, a lot of effort is currently directed towards making these drugs safer and their production more affordable. Yet, to avoid side effects and to improve the efficacy of these drugs, the molecular mechanisms underlying the actions of GLP1 and its analogs in various tissues and immune cells specifically have to be further specified. Therefore, the main objective of this study was to fill this gap of knowledge and to describe the role of intrinsic GLP1R signaling for CD4 T cells and Tregs.

As highlighted above, Tregs reside in almost every tissue in the organism, where they are critically involved in the maintenance of tissue homeostasis and systemic metabolic health. Their plasticity and adaptability ensure the unique ability of tissue Tregs to respond to signals derived from their metabolic microenvironment, including endocrine hormones. It has been described, that CD4 T cells and Tregs express receptors for several endocrine hormones, including GLP1R. However, the information on how GLP1R signaling influences the biology of these immune cell subpopulations is largely missing. In the present PhD thesis, I therefore aimed to test the hypothesis, that endocrine hormone signaling, specifically GLP1R signaling, represents a potential means of synchronizing environmental and metabolic cues with Treg induction, stability and function. By means of T cell-specific loss-of-function mouse model (GLP1R TKO) the role of T cell-intrinsic GLP1R signaling for Treg induction, stability, maintenance and phenotype in multiple tissues was investigated. Since the absence of GLP1R signaling appeared to have the impact mainly on the Tregs in VAT and intestine, the major focus of the study was set on these Treg subpopulations. In various *in vivo* mouse models of acute and chronic metabolic inflammation, the stability and suppressive capacity of GLP1R-deficient VAT and intestinal Tregs was assessed. Additional *in vitro* assays and methylation analysis served to confirm the observations from *in vivo* experiments.

Along with the functional and phenotypical characterization, the second objective of this study was to delineate the mechanism of the observed changes in tissue Treg maintenance and phenotype induced by the absence of T cell-specific GLP1R signaling. For that, the unsupervised transcriptional profiling of VAT Tregs by single cell RNA sequencing (scRNAseq) was performed. This analysis could provide insights about differentiation dynamics and signaling pathways most strongly affected in VAT Tregs by GLP1R-deffiiciency and most probably underlying the observed *in vivo* phenotype.

3 Material

Table 1: Mouse strains

Strain	Description
GLP1R TKO (C57Bl/6 $CD4^{Cre}$ $GLP1R^{fl/fl}$) and floxed controls ($GLP1R^{fl/fl}$ littermate controls)	Strain has a T cell-specific depletion of the *Glp1r* gene (by CD4-Cre mediated excision of *Glp1r* floxed exons). The strain was generated by crossing the $CD4^{Cre}$ and $GLP1R^{fl/fl}$ mice. $GLP1R^{fl/fl}$ ($Glp1r^{tm1.1Stof}$, MGI:5551409) mice were generated by the Prof. Randy J. Seeley's group (Hilary E. Wilson-Pérez, 2013) and kindly provided by Prof. Timo Müller, Helmholtz Center Munich. $CD4^{Cre}$ mouse line was purchased at The Jackson Laboratory (JAX#017336).
GLP1R KO	Strain has global deletion of the *Glp1r* gene, was generated by Prof. Dan Drucker's group (Scrocchi et al., 1996) and kindly provided by Prof. Timo Müller, Helmholtz Center Munich. MGI: 2150310
CD45.1	Strain (B6.SJL-$Ptprc^{a}Pepc^{b}$/BoyJ) carries the differential $Ptprc^{a}$ pan leukocyte marker commonly known as CD45.1 or Ly5.1. The mouse line was purchased at The Jackson Laboratory (JAX#002014).
Rag KO	Strain (B6.129S7-$Rag1^{tm1Mom}$/J) are homozygous for the $Rag1^{tm1Mom}$ mutation and produce no mature T or B cells. The mouse line was purchased at The Jackson Laboratory (JAX#002216).
ob/ob	Strain (*ob,* Lep^{ob}) carries the spontaneous mutation in both alleles of the leptin (*Lep*) gene. The mouse line was purchased at The Jackson Laboratory (JAX#000632).

Table 2: Reagents and chemicals

Chemical	Manufacturer	Item code
Bovine serum albumin (BSA)	Sigma Aldrich	A7906
Collagenase II	Sigma Aldrich	C6885
Collagenase D	Roche	11088882001
D(+)-Glucose	Karl Roth	HN06.1
Dispase II	Roche	4942078001
DNase I	Roche	11284932001
DreamTaq Green DNA-Polymerase (5 U/µl)	Thermo Fisher Scientific	EP0712
DSS (Lot S4140)	MP Biomedicals	02160110-CF
DTT (1M)	BioChemica	A1101
Dulbecco's phosphate buffered saline (DPBS)	Fisher Scientific	5001223
eF450 Viability Dye	eBioscience	65-0863-18
Ethylenediaminetetraacetic acid (EDTA)	Lonza	51234
Fc-block	BioLegend	101320
Fetal calf serum (FCS)	Biowest	S1810-500
Hank's balanced salt solution	Sigma Aldrich	H6648
Hydroxyethyl-piperazineethanesulfonic acid solution (HEPES, 1M)	VWR	5000961
Interleukin 2 recombinant human (50,000 U/ml)	ReproTech	200-02
Insulin	Lilly	HI0210

Invitrogen™ Ambion™ DNase I (RNase-frei)	Fisher Scientific	10229144
Ionomycin	Cayman Chemicals	10004974-1
Non-essential amino acids (100x)	Biochrom AG	K 0293
Penicillin/Streptomycin (Pen/Strep)	Sigma Aldrich	P4333
Percoll	GE Healthcare	17-0891-01
Phorbol 12-Myristate 13-Acetate (PMA)	abcam	ab120297
RPMI 1640 + Glutamax	Life technologies	61870-010
Sodium Pyruvate Solution	Sigma Aldrich	S8636
Streptavidin Microbeads	Miltenyi	130-048-101
Sytox® Blue Live Dead Stain	Thermo Fisher Scientific	S34857
β-Mercaptoethanol	BioConcept	5-69F00-E

Table 3: Media and buffers

Media and Buffer	**Composition**
Cell culture medium (RPMI+)	RPMI, 10% (v/v) FCS, 1x Pen/Strep (100 U/ml Penicillin, 100 µg/ml Streptomycin), 50 nM β-Mercaptoethanol, 1 mM Sodium-Pyruvat, 1x Non-essential amino acids
Coating buffer	0.1 M sodium bicarbonate buffer, pH 8.2
Extraction medium	RPMI 1640, 9.6 mM DTT, 1 mM EDTA, 1.7% FCS

Hank's Balanced Salt Solution with supplements (HBSS+)	HBSS, supplemented with 5% (v/v) FCS, 10 mM HEPES
MACS-PBS	DPBS, supplemented with 0.5% (w/v) BSA, 2 mM EDTA
PBS+BSA	DPBS, supplemented with 0.5% BSA
Digestion medium	RPMI 1640, 0.5 mg/ml Dispase II, 2 mg/ml Collagenase D, 15 µg/ml DNase I, 3 mM $CaCl_2$ and 1.2% FCS

Table 4: Antibodies

Antibody	**Fluorophore**	**Clone**	**Manufacturer**
B220	PB	RA3-6B2	BioLegend
CD11b	PB	M1/70	BioLegend
CD11c	BV421	N418	BioLegend
CD14	V450	rmC5-3	BD
CD25	PerCP-Cy5.5	PC61	BioLegend
CD3	PE-Dazzle 594	145-2C11	BioLegend
CD4	A700	RM4-5	BioLegend
CD4	Biotin	GK1.5	BioLegend
CD44	PE	IM7	BioLegend
CD45.1	APC-Cy7	A20	BioLegend
CD45.2	Briliant Violet 480	104	BioLegend
CD62L	APC	MEL-14	eBioscience
CD8a	PB	53-6.7	BioLegend

F4/80	PB	BM8	BioLegend
Foxp3	FITC	FJK-16s	eBioscience
GATA3	Briliant Blue 700	L50-823	BD
Helios	Alexa Fluor 647	22F6	BioLegend
IFNγ	Alexa Fluor 647	XMG1.2	BD
IL10	Brilliant Violett 711	JES5-16E3	BioLegend
IL17	Brilliant Violett 605	TC11-18H10.1	BioLegend
IL4	PE-Cy7	11B11	BioLegend
RORγt	PE	AFKJS-9	eBioscience
ST2	BB700	U29-93	BD
Strep-PE	Strep	-	BioLegend

Table 5: Coating antibodies for Treg induction assay

Antibody	**Concentration**	**Clone**	**Manufacturer**
Anti-CD28	5 µg/ml	37.51	BD
Anti-CD3	5 µg/ml	145-2C11	BD

Table 6: Primers

Purpose	**Forward sequence (5'-3')**	**Reverse sequence (5'-3')**
Genotyping/floxed	TGAGCCATCTCCTCAGCTCT	AGGCATGTATCCACCTCTGG
Genotyping/CD4Cre	TGTGGCTGATGATCCGAATA	GCTTGCATGATCTCCGGTAT

Genotyping/WT control	TTCCATCCAGTTGCCTTCTTGG	TTCTCATTTCCACGATTTCCCAG
Cre-recombination	TGAGCCATCTCCTCAGCTCT	CTGATTGCCCTGCACTGGGT
Glp1r qPCR	AGCACTGTCCGTCTTCATCA	AGAAGGCCAGCAGTGTGTAT
Histone qPCR	ACTGGCTACAAAAGCCG	ACTTGCCTCCTGCAAAGCAC
Foxp3 CNS2 Methylation	TTGGGTTTTGTTGTTATAATTTGAATTTGG	ACCTACCTAATACTCACCAAACATC

Table 7: Commercial assays

Kit	**Manufacturer**	**Item code**
$CD4^+CD25^+$ Regulatory T Cell Isolation Kit, mouse	Miltenyi Biotec	130-091-041
Cytofix/cytoperm Plus with GolgiStop/GolgiPlug™	BD	555028
Foxp3/Transcription factor staining buffer	eBioscience	00-5523-00
iScript Advanced cDNA Synthesis Kit	BioRad	1725038
Ssofast™ EvaGreen Supermix	BioRad	1725202
Zymo Methylation-Direct™ 200	Zymo Research	D5021
PyroMark Gold Q24 Reagents	Qiagen	970802
RNAdvance Cell v2 Kit	Beckman Coulter	A47942
RNAdvance Tissue Kit	Beckman Coulter	A32649
SensiFAST™ HRM Kit	Bioline	5001484

Table 8: scRNAseq reagents (10x Genomics)

Product	Item code
3' Feature Barcode Kit	1000276
Chromium Next GEM Single Cell 3' Kit v3.1	1000268
Dual Index Kit NT Set A	1000242
Dual Index Kit TT Set	1000215
Chromium Next GEM Chip G Single Cell Kit	1000120

Table 9: Hashtag Antibodies

Hashtag Antibody	Clone	Sequence	Item code
TotalSeq™-B0301	M1/42, 30-F11	ACCCACCAGTAAGAC	155831
TotalSeq™-B0302	M1/42, 30-F11	GGTCGAGAGCATTCA	155833

Table 10: Technical equipment

Instrument	Manufacturer
Accu-Chek® Aviva Glucometer	Roche
BD FACSAria™ III	BD
CFX96 Touch RT-PCR system	Bio-Rad
Cooling System HAAKE SC100	Thermo Scientific
CO_2-Incubator BBD 6220	Thermo Scientific
EchoMRI™	Zinsser Analytic GmbH

Epoch	BioTek
Heraeus Multifuge 3 S-R	Thermo Scientific
Heraeus Multifuge X3R	Thermo Scientific
HiSeq4000 sequencer	Illumina
MACS Multistand, QuadroMACS	Miltenyi Biotec
Mars Safety Class Cabinet II	ScanLaf
Microscope, Primo star	Zeiss
peqStar 2X thermal cycler	Peqlab
PyroMark Q24	Qiagen
Rotator	VWR
Vortex Mixture, Lab Dancer	VWR

Table 11: Software

Software (Version)	**Company**
Bio-Rad CFX Manager 3.1	Bio-Rad
Cell Ranger	10x Genomics
FACSDiva™ (V6.1.3)	BD
FlowJo (V10.0.8r1)	TreeStar Ink
GraphPad Prism® (V7-V9)	GraphPad Software Inc.
R (V4.2.0)	RStudio

4 Methods

4.1 Mice

Mice were bred in the animal facility of the Helmholtz Center Munich in individually ventilated cages (IVC) under specific pathogen (SPF)-free conditions. They were maintained group-housed on a 12-h/12-h light dark cycle at 25 °C with free access to food and water. 14-18-weeks-old mice were used for experiments if not indicated otherwise. In case of HFHS diet, mice were fed the diet composed of 58% kcal fat with sucrose starting from the age of 8 weeks and for 8 weeks (Research Diet#12331).

Ethical approval has been received by the District Government of Upper Bavaria, Munich, Germany (approval numbers: ROB-55.2-2532.Vet_02-17-63, ROB-55.2-2532.Vet_02-18-173). All animal care was executed according to the guidelines established by Institutional Animal Committees and in accordance with the ARRIVE guidelines and the Directive 2010/63/EU.

The genotype of the GLP1R TKO mice was determined by PCR on ear punches collected upon weaning and after each experiment. The genotyping PCR, as well as the PCR to confirm the deletion of the floxed gene were performed using Dream Taq Green DNA Polymerase according to the manufacturer's instructions with the primers listed in the **Table 6**.

4.1.1 DSS Colitis

10-12-weeks-old mice were treated with 2% DSS-supplemented drinking water *ad libitum*. The mice were weighed daily and monitored for the signs of colitis development. The analysis occurred 7 days after the treatment.

4.1.2 Adoptive transfer

For the adoptive transfer into the Rag KO animals, female 8-10-weeks-old animals were used as recipients. Cells were isolated from pooled LNs and spleen of female GLP1R TKO or floxed mice (for isolation procedure see section 4.2.1). Naïve T cells were isolated

from female 15-18-weeks-old CD45.1 C57BL/6J WT mice and pre-enriched with CD4 microbeads by Magnetic Activated Cell Sorting (MACS). After that they were FACS-sorted as live, exclusion channel negative (CD11b, CD11c, CD14, B220, CD8a, F4/80), $CD4^+CD25^-CD44^{low}$ and 1 x 10^6 cells per recipient were injected *i.p.*. Tregs were isolated from female 15-18-weeks-old either GLP1R TKO or floxed mice, pre-enriched with CD25 microbeads by MACS, FACS-sorted as live, exclusion channel negative (CD11b, CD11c, CD14, B220, CD8a, F4/80), $CD4^+CD25^{hi}$ and 5 x 10^5 cells were injected *i.p.*. Animals were analyzed 8 weeks after transfer or when severe colitis developed (humane endpoint).

For the adoptive transfer into the ob/ob mice, Tregs from either GLP1R TKO or floxed mice were isolated with $CD4^+CD25^+$ Regulatory T cell Isolation Kit according with manufacturer's protocol. 1 x 10^6 Tregs were then injected *i.v.* into the 8-10-weeks-old male ob/ob recipients.

Post-sort and post-injection sample aliquots were taken to assess Foxp3 expression by FACS in all sorted cell populations. The purity of sorted Tregs was >95%, the percentage of $Foxp3^+$ cells in sorted naïve T cells was <1.5%.

4.1.3 Intraperitoneal glucose tolerance test (ipGTT), intraperitoneal insulin tolerance test (ipITT), EchoMRI™

Mice were fasted for 6 h prior to GTT and ITT, except for the model of adoptive transfer into the ob/ob mice, where fasting period was extended to 12 h prior to GTT. The mice were then injected *i.p.* with glucose (2 g/kg of body weight of D-glucose in 0.9% saline) or insulin (1 U/kg in 0.9% saline). Blood glucose was measured from the tail vein with Accu-Chek® Aviva glucometer. Whole body fat and lean mass was measured by EchoMRI™.

4.2 T cell isolation and flow cytometry

4.2.1 T cell isolation from lymphoid organs

Single cell suspensions were obtained by straining lymph nodes, spleens and Peyer's Patches (PP) through 70 µm cell strainers into HBSS+ provided. After final centrifugation

step at 400 xg and 4 °C for 5 min the cell pellet was subjected to the surface FACS staining or PMA/Ionomycin stimulation.

4.2.2 T cell isolation from VAT, SAT and MAT

VAT, mesenteric AT (MAT) and subcutaneous AT (SAT) were digested with Collagenase II solution (4 mg/ml, 10 mM $CaCl_2$ in PBS+BSA) for 8-15 min at 37 °C. The digestion was stopped by adding MACS-PBS. The cell suspension was passed through a 200 µm filter membrane, centrifuged at 400 xg and 4 °C for 5 min, and resuspended in HBSS+ for further processing.

4.2.3 T cell isolation from BAT

Brown AT (BAT) was minced and digested with Collagenase D solution (1 mg/ml in HBSS+) for 20 min at 37 °C in three rounds. After each round, the obtained suspension was passed through a 200 µm filter membrane whereas the remaining tissue was again subjected to a Collagenase D digestion. The filtrates were collected, combined, centrifuged at 400 xg and 4 °C for 5 min, and resuspended in HBSS+ for further processing.

4.2.4 T cell isolation from SI and colon

Prior to processing of SI tissue, PP were removed. The SI or colon were cut in 3-5 cm long pieces, turned inside out and cleaned. To remove mucus and epithelial cells, tissues were incubated in Extraction medium (**Table 3**) for 20 min at 37 °C upon rotation. Tissues were washed with cold DPBS, wiped with paper towels to remove the epithelium and remaining mucus. After that tissues were minced and digested (Digestion medium, see **Table 3**) for 2x20 min at 37 °C. Supernatants were collected and filtered through 100 µm and 40 µm cell strainers.

4.2.5 T cell isolation from skeletal muscle

Skeletal muscle (*Musculus gastrocnemius*) pooled from both legs was minced and digested with Collagenase II (0.5 mg/ml in DPBS with 0.5% BSA and 0.18 mg/ml $CaCl_2$) at 37 °C for 20-30 minutes. Cells were passed through 100 µm cell strainer.

4.2.6 T cell isolation from brain

Prior to the cell isolation from brain, cerebellum and olfactory bulbi were removed. Brain was then homogenized with the cell homogenizer in RPMI medium. After that the density gradient centrifugation with Percoll™ was performed. For that, cell suspension was layered in the 30% layer over the 70% Percoll™ layer and centrifuged at 22 °C and 500 xg without acceleration and deceleration for 30 min. Cells were collected from the interphase and washed once with cold HBSS+.

4.2.7 T cell isolation from pancreas

Pancreas was minced and digested with Collagenase D solution (1 mg/ml in HBSS+) for two rounds for 15 min at 37 °C. Obtained suspension was passed through a 200 µm filter membrane after each round. The filtrates were collected, combined, centrifuged at 400 xg and 4 °C for 5 min, and resuspended in HBSS+ for further processing.

4.2.8 Flow cytometry (FC) and Fluorescence Activated Cell Sorting (FACS)

Isolated single cell suspensions were incubated with Fc-blocking reagent (diluted 1:50 in HBSS+) for 10 min on ice to prevent unspecific antibody binding. This was followed by the surface staining with antibodies for 30 min on ice in the dark.

Live cells for Treg induction, mRNA expression analysis and scRNAseq were sorted for purity into HBSS+ at 4 °C. Dead cells were excluded prior to sort by staining with Sytox® Blue Live Dead Stain.

For *ex vivo* analysis or sorting for methylation analysis, the cell surface staining was combined with fixable viability dye eFluor450. Afterwards, using the Foxp3 Staining Buffer Set cells were fixed and permeabilized for 40 min on ice in the dark and then stained intracellularly for 30 min on ice in the dark.

For cytokine staining, prior to the staining procedures, cells were stimulated with PMA (0.5 µg/ml) and ionomycin (0.5 µg/ml) in RPMI+ (see **Table 3**) for 4 h. After 2 h of stimulation the protein transport inhibitor brefeldin A (GolgiPlug™) was added (1:1000).

Details of used antibodies are listed in the **Table 4**.

Samples were acquired on the BD FACSAria™ III system with BD DIVA™ software and the data was further analyzed using FlowJo (v7.6.1-v10.8). Doublets were excluded based on FSC-A/FSC-W and SSC-A/SSC-W.

4.3 In vitro assays and molecular biology approaches

4.3.1 In vitro Treg induction assay

For polyclonal Treg induction, 96-well plates were pre-coated over night with anti-CD3 (5 µg/ml) and anti-CD28 (5 µg/ml) in the Coating buffer (see **Table 3**). Naïve T cells were sorted for purity as live, exclusion channel negative (CD11b, CD11c, CD14, B220, CD8a, F4/80), $CD4^+$ and $CD44^{low}$ with the FACSAria™ III. Sorted cells (10 000 cells/well) were cultured for 18 h in pre-coated 96-well plate in the presence of 100 U/ml recombinant human IL2. After 18 h, cells were transferred into uncoated wells and cultured for further 36 h.

4.3.2 Methylation analysis

The procedure for the methylation analysis was established in our lab and previously reported (Scherm et al., 2019). For that, up to 2000 Tregs were sorted as live $CD3^+CD4^+Foxp3^+$ and processed with EZ DNA Methylation-Direct™ Kit according to the manufacturer's instructions for lysis and bisulfite conversion. The quantitative methylation analysis accrued in the subsequent methylation-sensitive high-resolution melting (MS-HRM) PCR followed by pyrosequencing. PCR and sequencing primers were designed as described in (Scherm et al., 2019) (for sequences see **Table 6**). MS-HRM was performed with Sensi-FAST™ HRM Kit and the CFX96 real time system. Pyrosequencing was performed on the PyroMark Q24 system using PyroMark Gold Q24 Reagenst and according to the manufacturer's instructions.

4.3.3 qPCR

Total RNA from tissues was extracted using the RNAdvance Tissue Kit following the manufacturer's instructions. From cells RNA was extracted with RNAdvance Cell v2 Kit. For that, up to 100 000 cells were sorted as live $CD3^+CD4^+$ and processed according to the manufacturer's instructions. The transcription into cDNA was performed using iScript Advanced cDNA Synthesis Kit, followed by mRNA expression analysis by RT-qPCR using the CFX96 Touch Real-Time PCR Detection System and SsoFast™ Evagreen Supermix reagents. The data were processed with Bio-Rad CFX Manager 3.1 Software and obtained Cq values were normalized to the expression of *Histone*.

4.4 Statistical analysis

All FC and qPCR data, the as well as the results of metabolic studies were analyzed with GraphPad Prism (V7-9). The results are presented as bar, box-and-whiskers or XY graphs including or depicted as mean and standard error of the mean (SEM). For normally distributed data, unpaired Student's t-test was applied to compare means of two independent groups. Multiple comparisons were performed with one-way ANOVA and Šídák's multiple comparisons test. For all tests, a two-tailed P value < 0.05 was considered as significant. *P < 0.05, **P < 0.01, ***P < 0.001, ****P < 0.0001.

4.5 Single cell RNA sequencing (scRNAseq)

4.5.1 Cell sorting

For scRNAseq cells were isolated from VAT and stained with surface and Hashtag antibodies (TotalSeq™, Biolegend, **Table 9**). Up to 10 000 cells were sorted as live, exclusion channel negative (CD11b, CD11c, CD14, B220, CD8a, F4/80), $CD3^{+}CD4^{+}$ and pooled within one experimental group (2 biological replicates per group). The scRNAseq library was prepared using the 10x Genomics Chromium Next GEM technology according to the manufacturer's instructions. Libraries were sequenced on the Illumina HiSeq4000 with 50000 reads/cell (Samples) and 2000 reads/cell (Hashtags).

4.5.2 Data pre-processing

For all downstream procedures except for the velocity analysis, the transcripts were counted and filtered using Cell Ranger software. The transcript count matrices each containing hashtagged cells from two mice were filtered using Seurat package for R (V 4.1.0) using commands:

m<-CreateSeuratObject(counts = …, min.cells = 3, min.features = 200)

m[["percent.mt"]]<-PercentageFeatureSet(m, pattern = "^mt-")

m<-subset(object = m, subset = nFeature_RNA > 200 & nFeature_RNA < 4500 & percent.mt < 7.5)

The velocity analysis was performed on the transcript counts generated by Velocyto software (La Manno et al., 2018).

4.5.3 Noise reduction, batch-effect correction and clustering

For noise reduction, the transcript count matrices were log1p-transformed, normalized to median library size and subjected to MAGIC with parameters kNN = 5, t = 2 (van Dijk et al., 2018). Next, the matrices were subjected to batch effect correction and merged (Stuart et al., 2019), and the cells were clustered (resolution = 0.2) following the recommendations for Seurat from Satija Lab.

4.5.4 Supervised signature enrichment analysis

For the supervised analysis (**Figure 22**, B) we used the expression values subjected to noise reduction, but not to the batch effect correction step (see above). We compiled several short gene sets specific to particular cell populations. Some of them consisted of two parts – the positive one (containing the genes upregulated in the corresponding population) and the negative one (containing the downregulated genes). For every gene present in these gene sets the ratio of average expression in cluster 2 to cluster 4 (denoted as $\frac{cl.2}{cl.4}$) was calculated in each mouse individually. Next, the codirection score between each mouse and each gene set was calculated as the sum of the number of genes in the positive part with $\frac{cl.2}{cl.4} \geq 1.2$ and the number of genes in the negative part with $\frac{cl.2}{cl.4} \leq \frac{1}{1.2}$ divided by the size of the gene set.

In **Figure 25** another collection of gene sets was used with 30 genes in total. The transcript counts were normalized using *Seurat::NormalizeData*. Next, the expression of each of the mentioned 30 genes in each mouse was compared to its expression in every other mouse in cluster 2 and in cluster 4 individually using two-side Wilcoxon rank sum test followed by Bengamini-Hochberg correction.

The genes that had adjusted p-value ≥ 0.05 in all comparisons within the same genotype and at the same time had adjusted p-value < 0.05 in at least three out of 4 possible comparisons between different genotypes were considered statistically-significant.

4.5.5 Unsupervised signature enrichment analysis

For the unsupervised analysis (**Figure 24**) we used 6 libraries of gene sets: “canonical pathways”, “GO biological process”, “GO molecular function”, “GTRD transcription factor targets” (all downloaded from http://www.gsea-msigdb.org), the library with 61 gene sets compiled in (Bi et al., 2021) and the library of 1445 gene sets manually selected from the “immunologic signature gene sets” library available at http://www.gsea-msigdb.org. The gene names in the libraries were converted from HUGO format to the

mouse gene symbols using BioMart tool (http://useast.ensembl.org/biomart/martview/c0a53d4785d930f83bf91ca0b07f7f18) in conjunction with the ENSEMBL_mouse_gene.chip dictionary available in the GSEA web page. If a gene was absent in these dictionaries, we converted its name to lowercase, while retaining the first letter capital. Mitochondrial genes (all genes whose symbols start with "mt-") and ribosomal protein-coding genes (*Rpf1, Rpf2, Rpl10, Rpl10-ps3, Rpl10a, Rpl11, Rpl12, Rpl13, Rpl13a, Rpl14, Rpl15, Rpl17, Rpl18, Rpl18a, Rpl19, Rpl21, Rpl22, Rpl22l1, Rpl23, Rpl23a, Rpl24, Rpl26, Rpl27, Rpl27a, Rpl28, Rpl29, Rpl3, Rpl30, Rpl31, Rpl32, Rpl34, Rpl35, Rpl35a, Rpl36, Rpl36a, Rpl36a-ps1, Rpl36al, Rpl37, Rpl37a, Rpl38, Rpl39, Rpl39l, Rpl4, Rpl41, Rpl5, Rpl6, Rpl7, Rpl7a, Rpl7l1, Rpl8, Rpl9, Rpl9-ps6, Rplp0, Rplp1, Rplp2, Rps10, Rps11, Rps12, Rps13, Rps14, Rps15, Rps15a, Rps16, Rps17, Rps18, Rps18-ps4, Rps18-ps5, Rps18-ps6, Rps19, Rps19bp1, Rps2, Rps20, Rps21, Rps23, Rps24, Rps25, Rps26, Rps27, Rps27a, Rps27l, Rps27rt, Rps28, Rps29, Rps3, Rps3a1, Rps4x, Rps5, Rps6, Rps6ka1, Rps6ka2, Rps6ka3, Rps6ka4, Rps6ka5, Rps6kb1, Rps6kb2, Rps6kc1, Rps7, Rps8, Rps9, Rpsa*) were excluded from the analysis.

The transcript count matrices from GLP1R TKO and floxed mice both fed HFHS diet were merged without the batch-effect correction step and then subjected to noise reduction via MAGIC (see above). Merging of the matrices without batch-effect correction was valid, because, as shown in **Figure 27**, the variation between batches was not global. Next, we compared gene expression in each mouse to gene expression in each of the other mice in cluster 2 and in cluster 4 individually. For this we first identified the genes, whose expression distribution overlapped between the two compared mice in the given cluster by < 80%, and at the same time whose average expression value was ≥ 0.5 in at least one of them. Next, we used the difference in average expression values as the input for fgsea algorithm in R (https://doi.org/10.1101/060012). This procedure was performed in two variants: (var.1) the noise reduction was done on the whole population of $CD4^+$ T cells; and (var.2) the noise reduction was performed only on the cells of cluster 2 and cluster 4 pooled together.

After running fgsea, we selected the gene sets that have the adjusted p-value ≥ 0.2 in all comparisons within each genotype and at the same time have the adjusted p-value < 0.05 in at least one comparison between genotypes. If these conditions were satisfied

both in var.1 and var.2 for the same gene set and for the same individual comparison, then we defined the pair of the gene set and the corresponding comparison to be statistically significant. The leading-edge genes (Subramanian et al., 2005) and user's guide of fgsea) present in both var.1 and var.2 in a particular statistically significant pair were identified and pooled together across all selected gene sets and all statistically-significant pairs. Among these genes, we identified those that were found in the leading edges of ≥ 8 gene sets in cluster 2 or in the leading edges of ≥ 8 gene sets in cluster 4 and visualized them in **Figure 24**.

4.5.6 Identification of differentially expressed genes

The markers of clusters were identified using *Seurat::FindAllMarkers* with parameters *min.pct = 0.25, logfc.threshold = 0.5*. Next, only those genes were retained that had *p_val_adj < 0.05*. For visualization in **Figure 20** the average expression values obtained via noise reduction and batch-effect correction were used. For each gene, those values were averaged across all cells in each individual cluster and divided by the average expression of that gene in the whole data set.

The markers of experimental groups (**Figure 26**) were identified from the transcript counts merged together without noise reduction and batch effect correction. We compared the gene expression in each mouse to the gene expression in each of the other mice (6 comparisons in total) in cluster 2 and cluster 4 individually using the commands *Seurat::NormalizeData* and *Seurat::FindMarkers* with default parameters. Only those genes were retained, whose expression was consistently altered (only upregulated or only downregulated) in those comparisons between different genotypes that had *p_val_adj < 0.05*, and at the same time had *p_val_adj ≥ 0.05* in all comparisons within each genotype.

4.5.7 Gene expression heat maps

For visualization the transcript counts previously processed with *Seurat::NormalizeData* were averaged across the cells and then scaled across all experimental groups and across both examined clusters (denoted as z.score, **Figure 26**) or across the cells in cluster 2 and cluster 4 individually (denoted as cl.z.score, **Figure 24** and **Figure 25**) via subtraction of the arithmetic mean and dividing by the standard deviation.

4.5.8 Velocity analysis

Differentiation trajectories were constructed for every mouse individually using scVelo software according to the authors' guidelines (Bergen et al., 2020).

5 Results

5.1 GLP1R TKO mouse model: validation of CD4 T cell-specific deletion of GLP1R in $CD4^{Cre}GLPR^{fl/fl}$ mice

In order to study the function of GLP1R specifically in CD4 T cells we generated a CD4 T cell-specific KO (TKO) of GLP1R by making use of the Cre-LoxP system and crossing $CD4^{Cre}$ and $GLP1R^{fl/fl}$ mice. The presence of Cre and loxP sites was verified by PCR (**Figure 1**, A). The DNA recombination specifically in CD4 T cells and only in TKO mice was confirmed by PCR from sorted $CD4^+$ T cells (**Figure 1**, B).

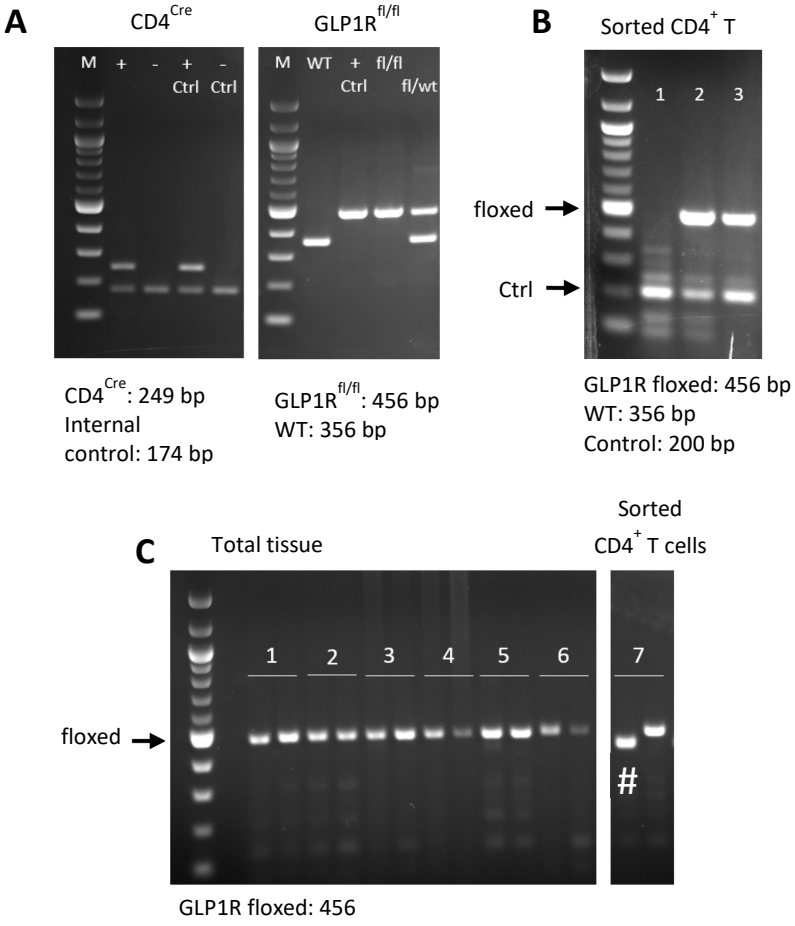

Figure 1: Genotyping and verification of the functional Cre-LoxP system in GLP1R TKO mice. (A) Representative genotyping. Detection of Cre (left) and floxed (right) constructs by PCR. (B) Detection of floxed construct in sorted $CD4^+$ T cells from GLP1R TKO (1) and floxed (2) mice by PCR. (3) An ear biopsy as a positive control. (C) PCR-assay for detection of the DNA recombination of the floxed region in tissues (1-6) and sorted $CD4^+$ T cells (7) of GLP1R TKO (left band) and floxed controls (right band). (1) Pancreas, (2) brain, (3) SI, (4) colon, (5) VAT, (6) liver, (7) sorted $CD4^+$ T cells. (#) The larger PCR product formed upon binding of the second reverse primer, which is only possible upon DNA recombination.

In order to prove, that DNA recombination takes place exclusively in T cells rather than in other non-lymphoid tissues, I designed a PCR-assay aiming at detecting DNA recombination by forming a larger product. As expected, this PCR product was present only in the sorted from GLP1R TKO mice CD4$^+$ T cells and not in other tissues analyzed (**Figure 1**, C).

Next, by qPCR it was verified, that the expression of *Glp1r* was not altered in GLP1R TKO mice in tissues with its known expression (**Figure 2**, A). In addition, the effective deletion of *Glp1r* was confirmed on mRNA level on sorted CD4$^+$ T cells from various tissues and secondary lymphoid organs (**Figure 2**, B).

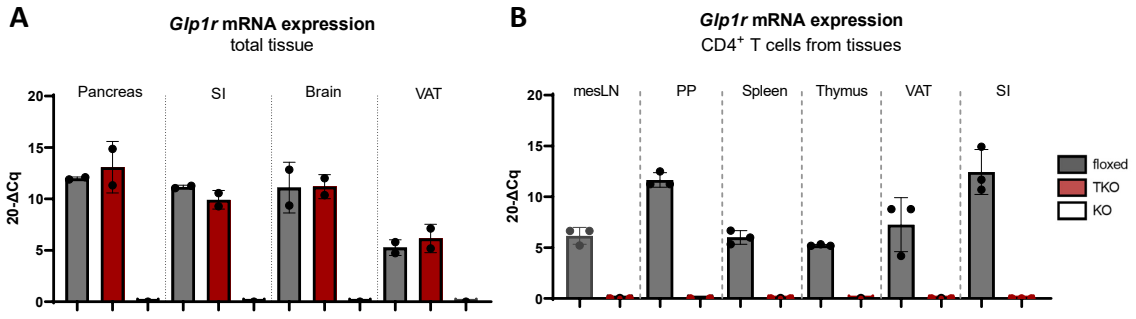

Figure 2: Detection of the *Glp1r* mRNA expression in total tissues and tissue-resident CD4$^+$ T cells. RT-qPCR analysis of the *Glp1r* expression from total tissue (A) or sorted CD4$^+$ T cells (B) from GLP1R TKO, floxed and global GLP1R KO mice. Summary bar plots, each data point represents biological replicate.

By these means, the efficient and specific to CD4 T cells deletion of *Glp1r* gene was confirmed. In addition, the expression of *Glp1r* in metabolically-active tissues, in which GLP1R signaling is involved in the regulation of systemic metabolism, was proven to be unaffected in GLP1R TKO mice.

5.2 CD4 T cell-specific GLP1R signaling is involved in the regulation of Treg frequencies in VAT and SI at steady state

Having validated the genetic deletion of GLP1R and its specificity, I next assessed whether it has an impact on tissue Tregs. For that, the frequencies of Tregs were examined in various tissues of GLP1R TKO and floxed control mice (**Figure 3**).

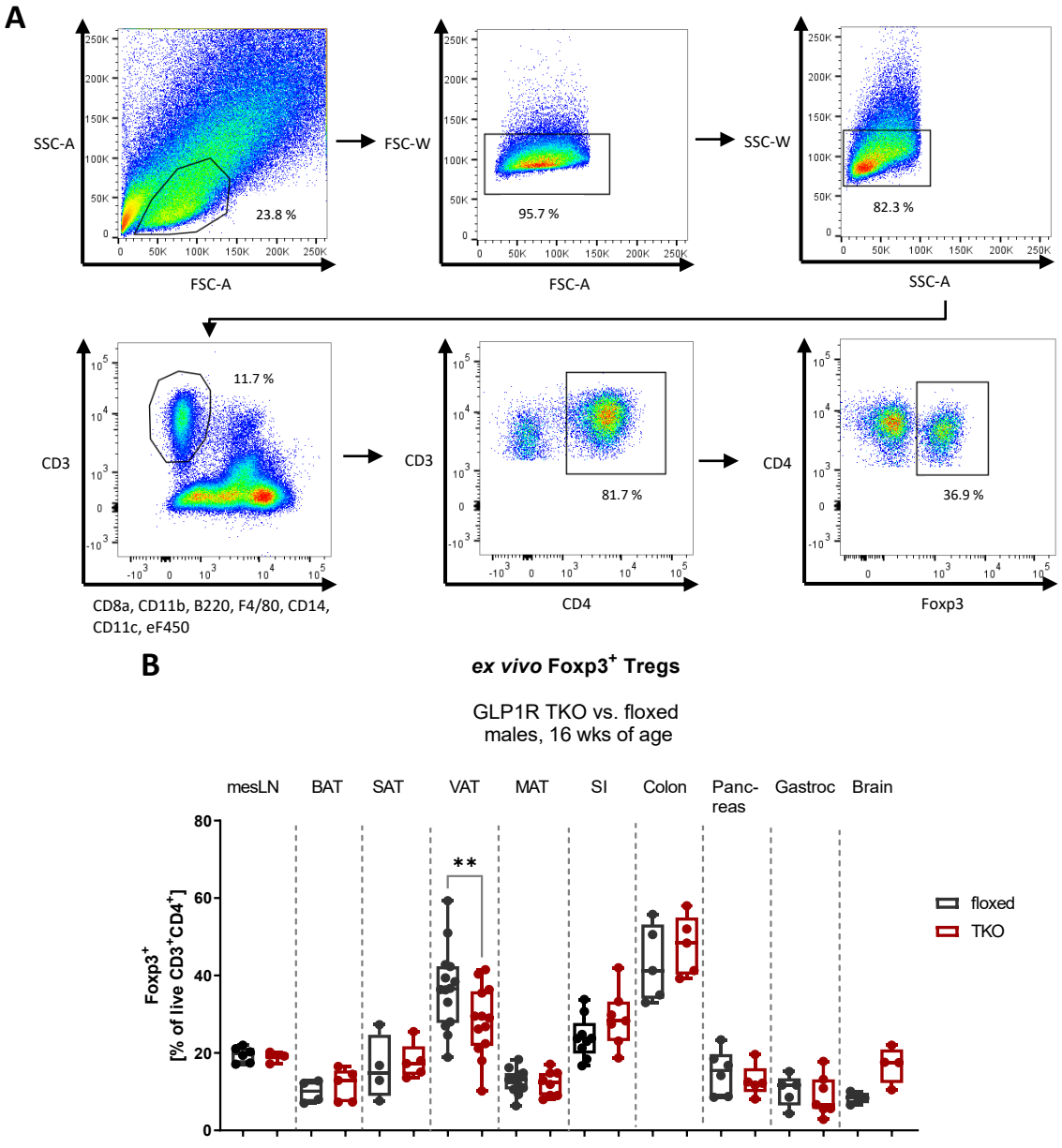

Figure 3: Examination of the non-lymphoid metabolically active tissues for Treg frequencies in GLP1R TKO mice. (A) Representative FC staining and gating strategy for the analysis of Treg frequencies in tissues of 16-weeks-old male GLP1R TKO and floxed control mice. (B) Summary plot. Data is presented as box-and-whiskers plot, each data point represents biological replicate. **P < 0.01, ordinary one-way ANOVA.

Most prominently, the effect of the absence of the T cell-specific GLP1R signaling on the tissue Tregs was observed in VAT, with a significant decline in their frequencies and numbers in GLP1R TKO animals vs. floxed controls (**Figure 3**, **Figure 4**, A-C). It was accompanied by a significant reduction in the expression of characteristic for VAT Tregs marker ST in GLP1R-deficient Tregs (**Figure 4**, D, E).

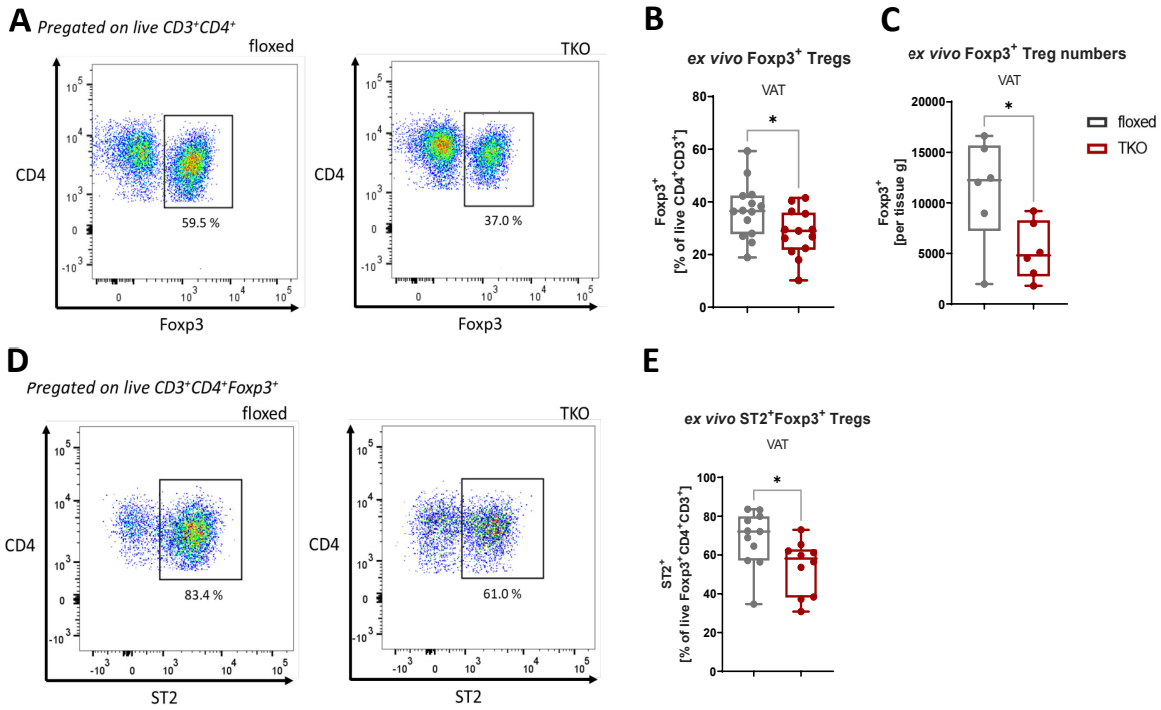

Figure 4: In absence of GLP1R signaling in CD4 T cells the frequencies of VAT Tregs are reduced. (A-C) *Ex vivo* frequencies and numbers of Foxp3⁺ Tregs and (D-E) ST2 expression in Tregs in VAT of GLP1R TKO vs. floxed mice. (A, D) Representative FC stainings. (B, C, E) Summary plots. Data are presented as box-and-whiskers plots, each data point represents a biological replicate. *P < 0.05, Student's t-test.

Since a trend towards an increase in Treg frequencies was also observed in SI of GLP1R TKO mice, I assessed the phenotype of this Treg population by analyzing characteristic SI markers.

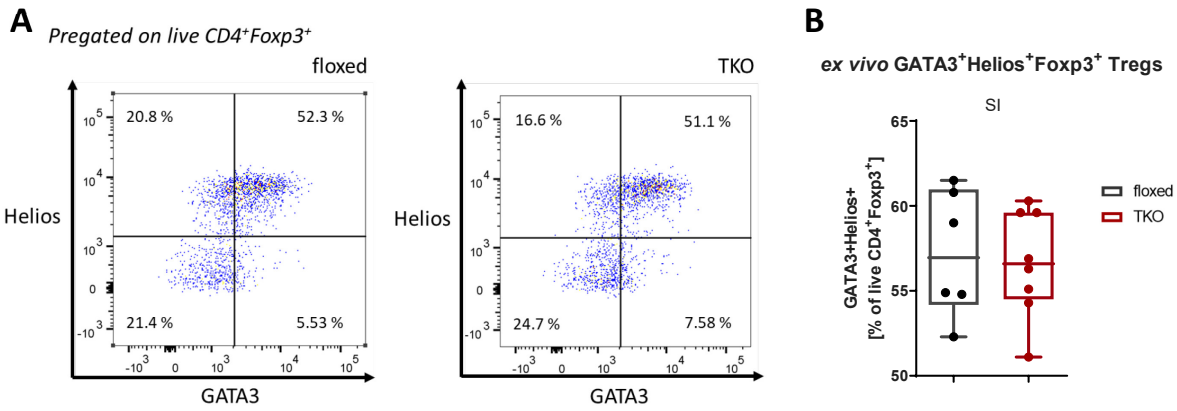

Figure 5: GLP1R TKO and floxed mice possess similar frequencies of Helios$^+$GATA3$^+$ Tregs in SI. *Ex vivo* frequencies of GATA3$^+$Helios$^+$ among the Tregs in SI of GLP1R TKO vs. floxed mice. (A) Representative FC stainings. (B) Summary plots. Data is presented as box-and-whiskers plot, each data point represents a biological replicate. Student's t-test.

Whereas the GATA3 expressing Treg population was unaffected by GLP1R deficiency in CD4 T cells (**Figure 5**), an increase in RORγt and CCR6 expression in SI Tregs in GLP1R TKO animals in comparison to their floxed counterparts was detected (**Figure 6**). This observation may indicate, that the lack of GLP1R signaling specifically fosters the peripheral Treg induction in SI, since RORγt$^+$ Tregs are known to be induced in the gut in response to intestinal microbiota. The more profound Th17-like phenotype of SI Tregs in GLP1R TKO mice may suggest a tissue-specific adaptation and a more robust *in vivo* induction of Tregs in SI.

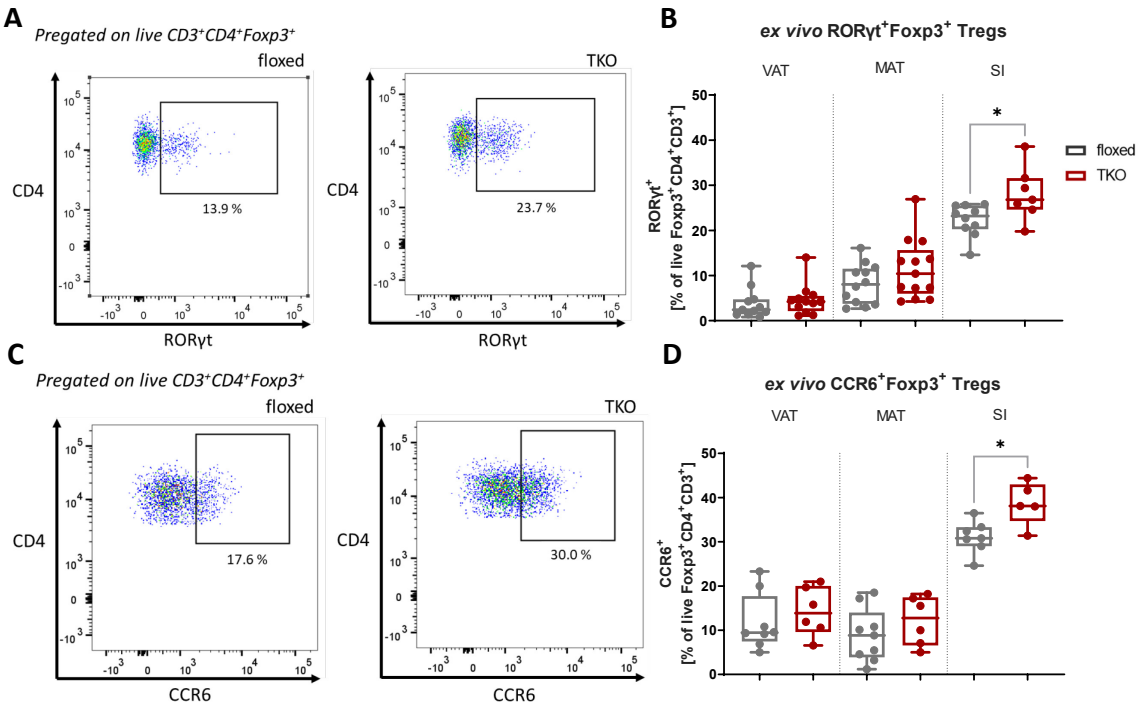

Figure 6: Absence of GLP1R promotes tissue-specific adaptation in SI. *Ex vivo* frequencies of RORγt$^+$ and CCR6$^+$ Tregs in VAT, MAT and SI of GLP1R TKO vs. floxed mice. (A, C) Representative FC stainings. (B, D) Summary plots. Data is presented as box-and-whiskers plot, each data point represents a biological replicate. *P < 0.05, ordinary one-way ANOVA.

5.3 GLP1R TKO animals are less prone to the development of DSS-induced colonic inflammation

Given the indications of tissue-specific adaptation of GLP1R-deficient Tregs in SI, I aimed to assess the relevance of these phenotypic changes in Tregs in the context of acute intestinal inflammation. For that, the model of chemically induced acute DSS colitis was used.

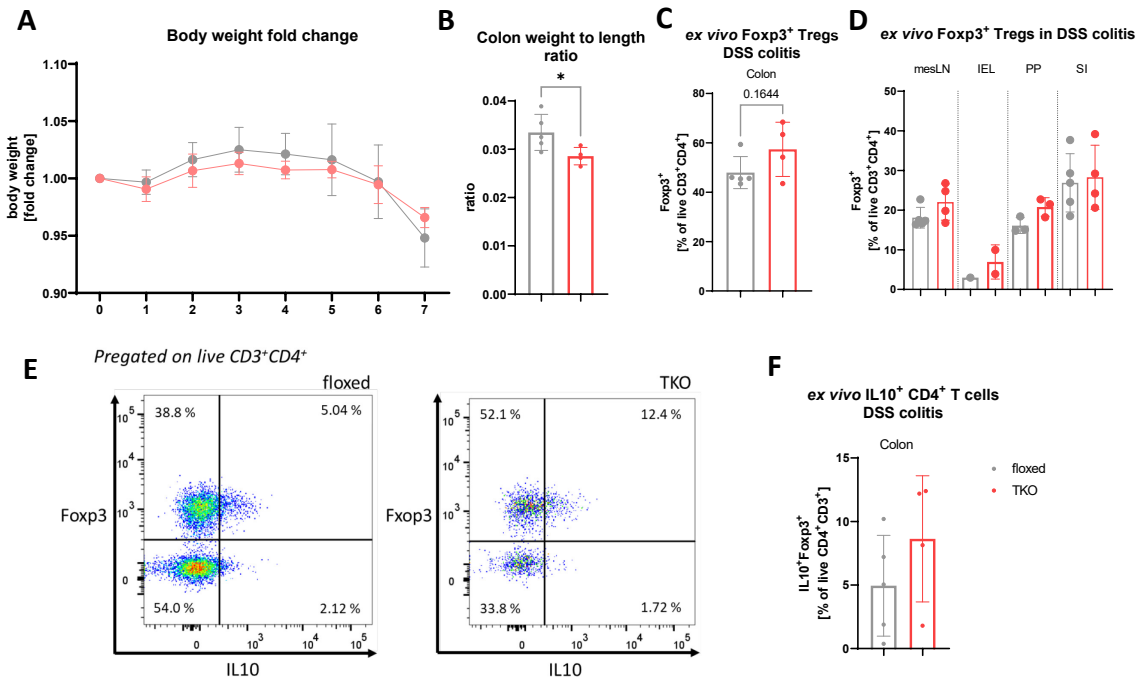

Figure 7: GLP1R TKO mice show reduced signs of colonic inflammation upon DSS treatment. Monitoring of the colitis progression and the final *ex vivo* analysis of GLP1R TKO vs. floxed mice upon 7 days of DSS treatment. (A) Body weight progression as the fold change (n = 4 for GLP1R TKO and n = 5 for floxed mice). (B) Colon weight to length ratio. (C, D) *Ex vivo* Treg frequencies. (E, F) IL10 expression in Tregs. (E) Representative FC stainings of IL10 in Tregs. (B-D, F) Summary bar plots, each data point represents a biological replicate. (B, C, F) *P < 0.05, Student's t-test. (D) Ordinary one-way ANOVA.

Although the body weight reduction between the different genotypes was similar, GLP1R TKO animals showed significantly reduced colon weight to length ratios suggesting reduced colonic inflammation when compared to floxed controls (**Figure 7**, A, B). This was accompanied by trending yet not significant increase in colonic Tregs and IL10$^+$ Tregs (**Figure 7**, C-F). Collectively, these data indicate the enhanced tolerogenic capacity of GLP1R-deficient Tregs in the setting of acute tissue inflammation.

5.4 Adoptive transfer of Tregs lacking GLP1R ameliorates inflammation in SI and VAT in Rag-deficient mice

To specifically study the suppressive capacity of GLP1R-deficient Tregs, as well as their stability and ability to repopulate various tissues *in vivo*, the model of adoptive transfer

was utilized. Here, CD45.2 Tregs, isolated from GLP1R TKO or floxed control animals in combination with congenically marked CD45.1 WT T naïve responder cells were adaptively transferred into immunodeficient Rag KO mice (**Figure 8**). The third control group received the WT naïve T cells only.

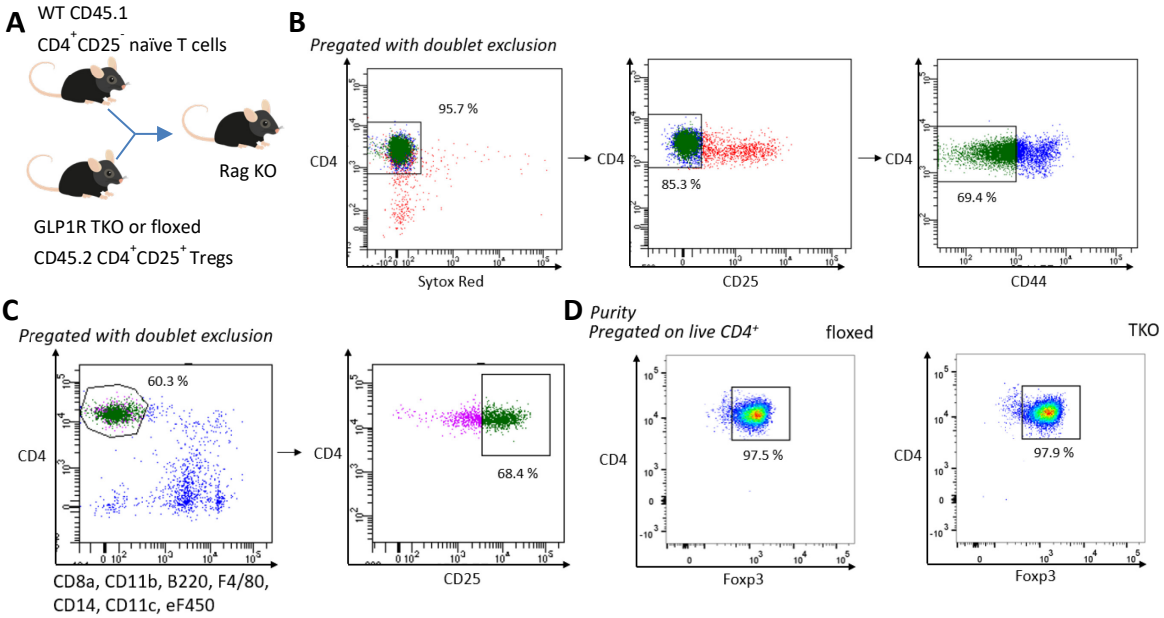

Figure 8: Adoptive transfer. Experimental design. (A) Schematic representation of the experimental design. (B) Sorting strategy for WT CD45.1 $CD4^+CD25^-CD44^{lo}$ T naïve responder cells. (C) Sorting strategy for GLP1R TKO or floxed CD45.2 $CD4^+CD25^+$ Tregs. (D) Representative purity control staining for Foxp3 on sorted GLP1R TKO or floxed CD45.2 $CD4^+CD25^+$ Tregs.

Both groups, which received either GLP1R-deficient or floxed Tregs remained healthy, in contrast to the WT naïve T cells only control group, which started to lose weight approximately 2 weeks after transfer and developed severe colitis (**Figure 9**, A, B). The ratios of CD45.1 and CD45.2 T cells were similar within the tissues irrespective whether GLP1R-defficient or floxed Tregs were transferred (**Figure 9**, D, E). This evidence argues

for similar migration and distribution of transferred GLP1R-deficient or floxed Tregs throughout the tissues.

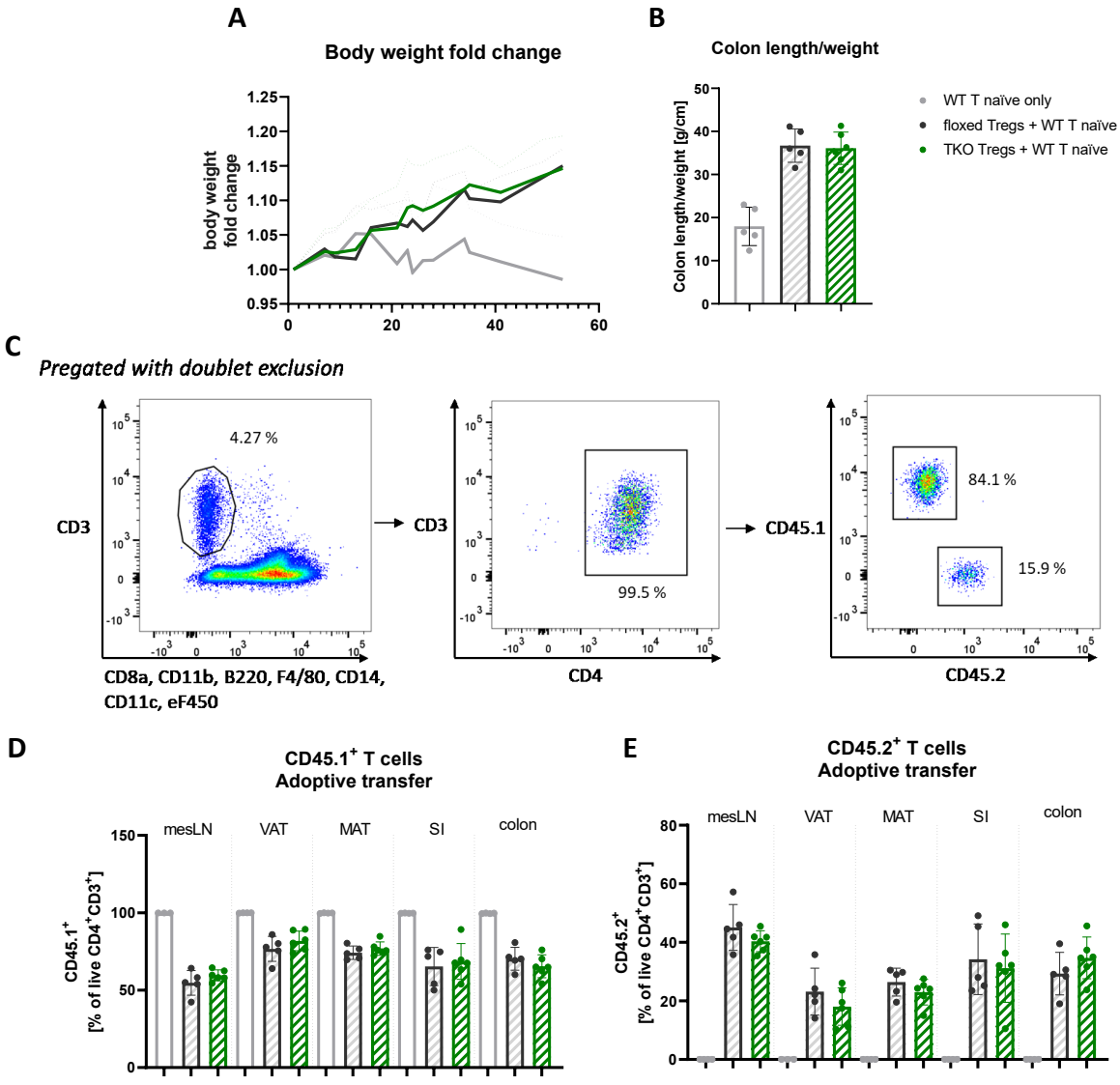

Figure 9: Similar health conditions and CD45.1/CD45.2 T cell distribution in GLP1R TKO or floxed Treg recipients. Adoptive transfer of CD45.1 naïve T cells alone or in combination with CD45.2 GLP1R TKO or floxed Tregs. (A) Body weight progression as the fold change (n = 6 for naïve T cells + GLP1R TKO Tregs recipients, n = 5 for both other groups). (B) Colon weight to length ratio. (C-E) FC analysis of CD45.1 naïve T cells and CD45.2 Tregs in various tissues. (C) Gating strategy to distinguish CD45.1 and CD45.2 T cells by FC. (D-E) Summary bar plots, each data point represents a biological replicate. Ordinary one-way ANOVA.

However, having evenly populated various tissues, GLP1R-deficient and floxed Tregs were different in their ability to retain Foxp3 expression there. In contrast to the mes-LNs, where similar frequencies of Foxp3 expressing CD45.2 T cells were detected among

the both groups, in all analyzed non-lymphoid tissues the frequencies of Foxp3$^+$ CD45.2 T cells were slightly higher in the recipients of GLP1R-deficient Tregs (**Figure 10**). This effect was most prominently observed in VAT, where this difference reached statistical significance.

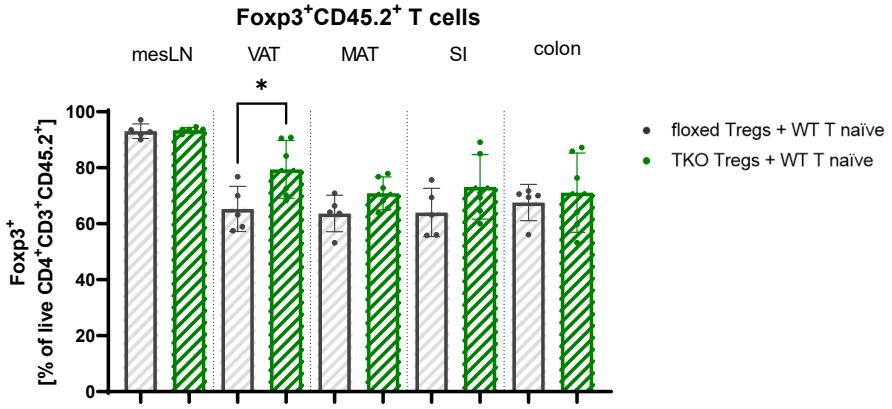

Figure 10: GLP1R-deficient Tregs better retain Foxp3 expression in tissues. Adoptive transfer model. *Ex vivo* Foxp3$^+$ Treg frequencies in tissues analyzed by FC. Summary bar plot, each data point represents a biological replicate. *P < 0.05 identified with ordinary one-way ANOVA.

In accordance with that, the recipients of GLP1R-deficient Tregs exhibited lower degree of inflammation in VAT, as evidenced by reduced secretion of proinflammatory cytokines IFNγ and IL17 in both, CD45.1 and CD45.2 T cell populations (**Figure 11**, A, B). On the contrary, the production of anti-inflammatory cytokine IL10 and the production of IL4, which is associated with tissue repair and maintenance, was increased in CD45.2 T cells in VAT of GLP1R-deficient Treg recipients (**Figure 11**, C, D).

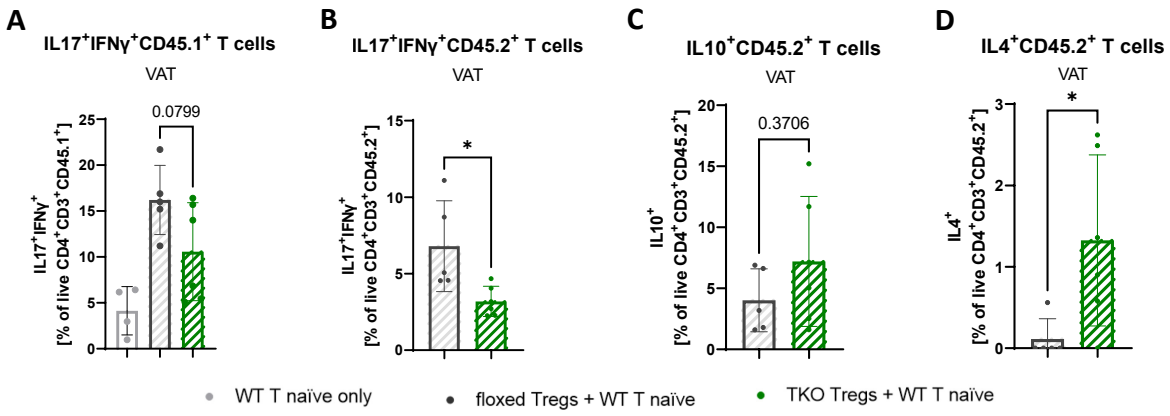

Figure 11: Tregs from GLP1R TKO mice possess higher tolerogenic potential. FC analysis of the cytokine expression in VAT upon adoptive transfer. Summary bar plots, each data point represents a biological replicate. *P < 0.05, Student's t-test.

Another interesting observation was made in colon, where significantly higher expression of Foxp3 was detected in GLP1R-sufficient CD45.1 responder cells, which were transferred in the presence of GLP1R-deficient Tregs (**Figure 12**, A). It suggests, that GLP1R-defecient Tregs are more capable to support Treg induction in colon, which is a prominent site of peripheral Treg induction. In the model of adoptive transfer, colon is usually also a site of the strongest inflammation. Therefore, the higher peripheral Treg induction in the proinflammatory milieu, accompanied by a reduced expression of pro-inflammatory cytokines IFNγ and IL17 by CD45.2 T cells in GLP1R TKO Treg recipients (**Figure 12**, B, C) are potential mechanisms directed towards the amelioration of tissue inflammation.

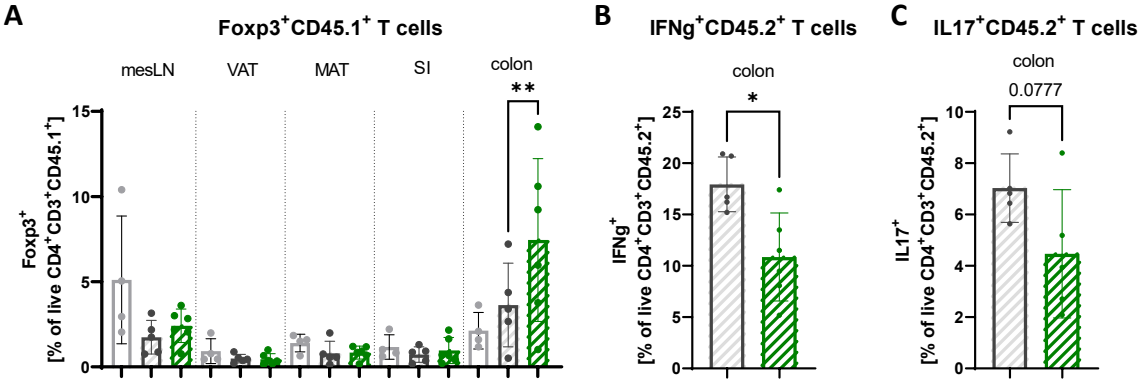

Figure 12: Tregs lacking GLP1R support Treg induction from WT responder T cells *in vivo*. Adoptive transfer model. (A) *Ex vivo* frequencies of Foxp3+ Tregs among the CD45.1 T cells in tissues analyzed by FC. **P < 0.01, ordinary one-way ANOVA. (B-C) Cytokine expression in CD45.2 T cells in colon analyzed by FC. *P < 0.05, Student´s t-test. (A-C) Summary bar plots, each data point represents a biological replicate.

Collectively, in the model of adaptive transfer I could show, that in the absence of GLP1R signaling Tregs better retain their Foxp3 expression, suppress the production of proinflammatory cytokines and promote the induction of *de novo* Tregs in SI. These data led us to the hypothesis, that in the absence of GLP1R signaling Tregs can better tolerate the proinflammatory milieu and contribute to the suppression of tissue inflammation.

5.5 Loss of GLP1R signaling in T cells enhances *de novo* Treg induction

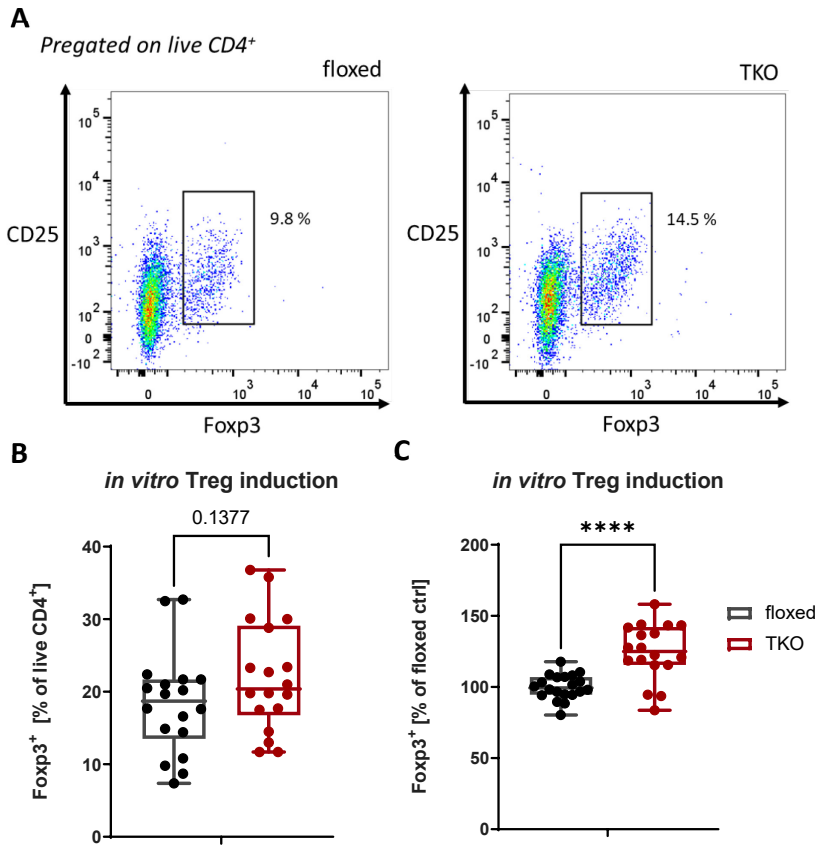

Figure 13: GLP1R-deficient naïve T cells possess an increased intrinsic capacity for *in vitro* Treg induction. FC analysis of the *in vitro* Foxp3$^+$ Treg induction from naïve T cells. (A) Representative FC staining. (B-C) Summary box-and-whiskers plot of absolute values (B) or normalized to floxed control (C). Each data point represents a biological replicate. ****P < 0.0001, Student's t-test.

Since multiple evidence of improved peripheral Treg induction from GLP1R-deficient T cells, as well as WT T cells in the presence of GLP1R-deficient Tregs were observed throughout the study, I aimed to test, whether the lack of GLP1R indeed has an impact on Treg induction in an isolated system *in vitro*. According to the protocols established

in our lab conversion of naïve CD4$^+$ T cells into the Foxp3$^+$ Tregs is achieved best upon non-activating, so called subimmunogenic conditions. To mimic these conditions in our lab we use premature withdrawal of polyclonal TCR stimulation (Sauer et al., 2008, Serr et al., 2014). In accordance with the increased Treg induction in the colon of GLP1R-deficient Treg recipients in the adoptive transfer model, more efficient *in vitro* Treg induction was detected when started from the GLP1R-deficient CD4 naïve T cells (**Figure 13**). Improved capacity of GLP1R-deficient naïve CD4 T cells to convert to Tregs or to support the Treg induction as bystanders may therefore represent one of the components of the superior tolerogenicity observed in GLP1R TKO mice, especially in the context of proinflammatory environment.

5.6 GLP1R TKO mice are protected from the HFHS diet-induced decline of Tregs in VAT and show improved metabolic parameters

Given the strong phenotype in VAT observed at steady state and in the adoptive transfer model, I aimed to examine the role of GLP1R signaling for VAT Tregs in the setting of mild chronic inflammation. Therefore, GLP1R TKO and floxed control mice were subjected to 8 weeks of HFHS diet.

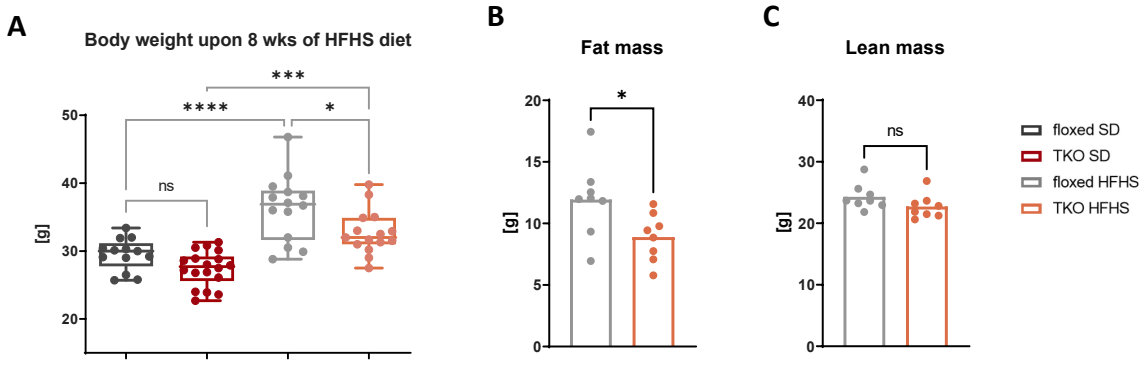

Figure 14: GLP1R TKO mice fed HFHS diet have reduced body weight and body fat content. (A) Body weight of GLP1R TKO vs. floxed control mice upon SD or 8 weeks of HFHS. *P < 0.05, ***P < 0.001, ****P < 0.0001, ordinary one-way ANOVA. (B) Fat mass and (C) lean mass of GLP1R TKO vs. floxed mice upon 8 weeks of HFHS measured by EchoMRI^{TM}. *P < 0.05, Student´s t-test. (A) Summary box-and-whiskers or bar (B, C) plots, each data point represents a biological replicate.

8 weeks of HFHS diet induced body weight gain in both mouse strains, however, to a much lesser degree in the GLP1R TKO mice. GLP1R TKO animals fed HFHS diet demonstrated significantly lower body weight and body fat content, whereas the lean body mass was similar to that of their GLP1R-sufficient counterparts (**Figure 14**).

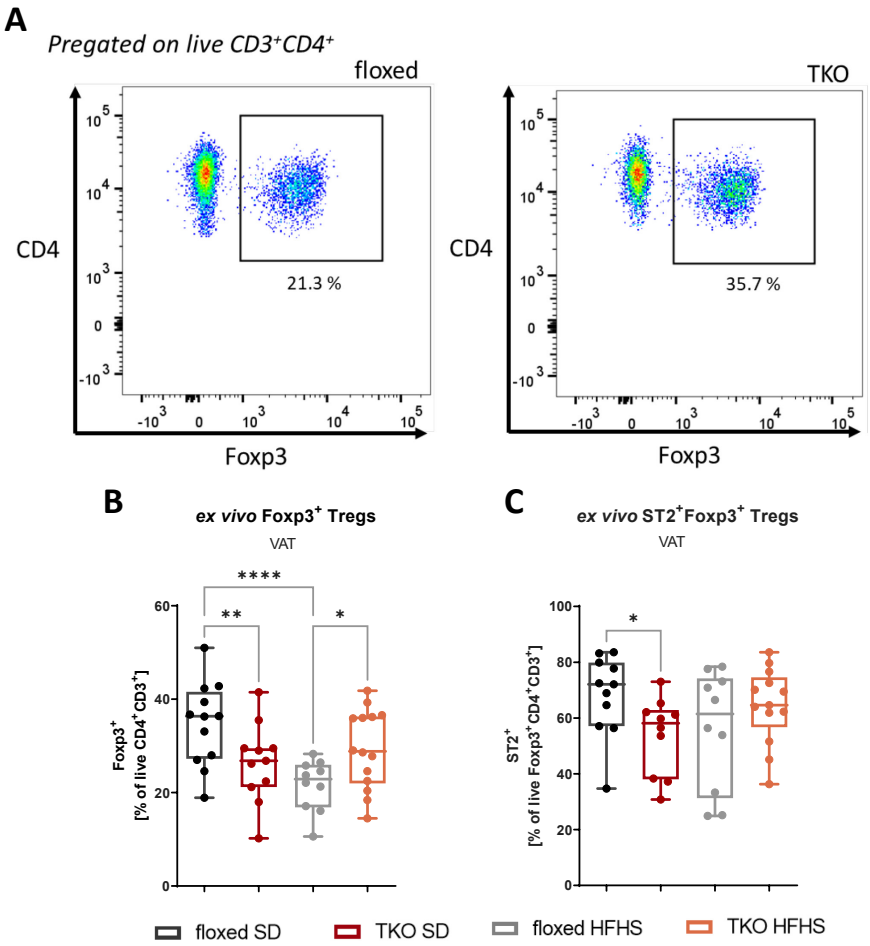

Figure 15: GLP1R TKO mice are protected from the HFHS diet-induced decline of Tregs in VAT. *Ex vivo* frequencies of Foxp3⁺ Tregs and ST2 expression in Tregs in VAT of GLP1R TKO vs. floxed control mice upon SD or 8 weeks of HFHS. (A) Representative FC staining of Foxp3⁺ Tregs in VAT upon HFHS. (B-C) Summary box-and-whiskers plots, each data point represents a biological replicate. *P < 0.05, **P < 0.01, ****P < 0.0001, ordinary one-way ANOVA.

As outlined above, 8 weeks of HFHS diet are sufficient to induce strong reduction of Tregs in VAT (Li et al., 2021b), which indeed was observed in floxed controls. Interestingly, mice lacking T cell-specific GLP1R signaling were protected from this negative effect of HFHS diet on VAT Tregs. In GLP1R TKO mice the VAT Treg frequencies tended to be slightly higher, than upon SD and were significantly higher when compared to HFHS

diet-fed floxed controls (**Figure 15**, A, B). However, the analysis of ST2 expression could neither confirm the significant impairment of Treg ST2 expression by HFHS diet, nor demonstrate any differences in the ST2 expression in Tregs in mice of both genotypes.

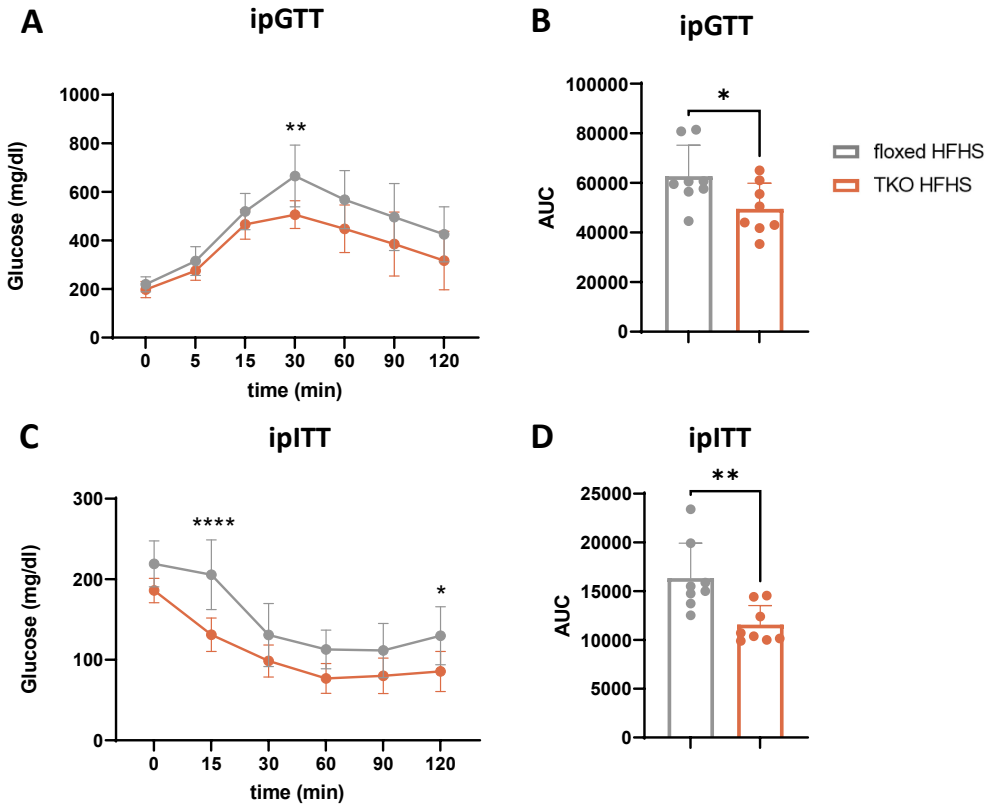

Figure 16: Metabolic parameters upon HFHS diet are improved in GLP1R TKO mice. (A, B) intraperitoneal glucose tolerance test (ipGTT) with HFHS diet-fed GLP1R TKO (n = 8) and floxed (n = 8) mice. (C, D) intraperitoneal insulin tolerance test (ipITT) with HFHS diet-fed GLP1R TKO (n = 8) and floxed (n = 8) mice. *P < 0.05, **P < 0.01, ****P < 0.0001. (A, C) Ordinary one-way ANOVA. (B, D) Area under the curve (AUC), each data point represents a biological replicate. Student's t-test.

The positive correlation between the abundance of Tregs in VAT and improved metabolic parameters is well described in the literature (Feuerer et al., 2009, Cipolletta et al., 2012). To examine, whether significantly higher Treg frequencies in VAT of GLP1R TKO mice have a direct implication in the control of systemic metabolism, I performed a series of glucose and insulin tolerance tests in HFHS diet-fed mice. Indeed, a significant improvement of both, glucose and insulin tolerance, was observed in GLP1R TKO mice compared to floxed animals (**Figure 16**, A-D). These data support our hypothesis, that

GLP1R-deficient Tregs better tolerate the inflammatory environment, which in turn positively impacts the systemic metabolism.

5.7 Adoptive transfer of GLP1R-deficient Tregs tends to improve metabolic control in ob/ob mice

To rule out the possibility, that the improvement of the glucose tolerance and insulin sensitivity in GLP1R TKO mice were solemnly attributed to the reduced body weight, the adoptive transfer of Tregs from GLP1R TKO or floxed mice into the genetically induced obese ob/ob mice was performed.

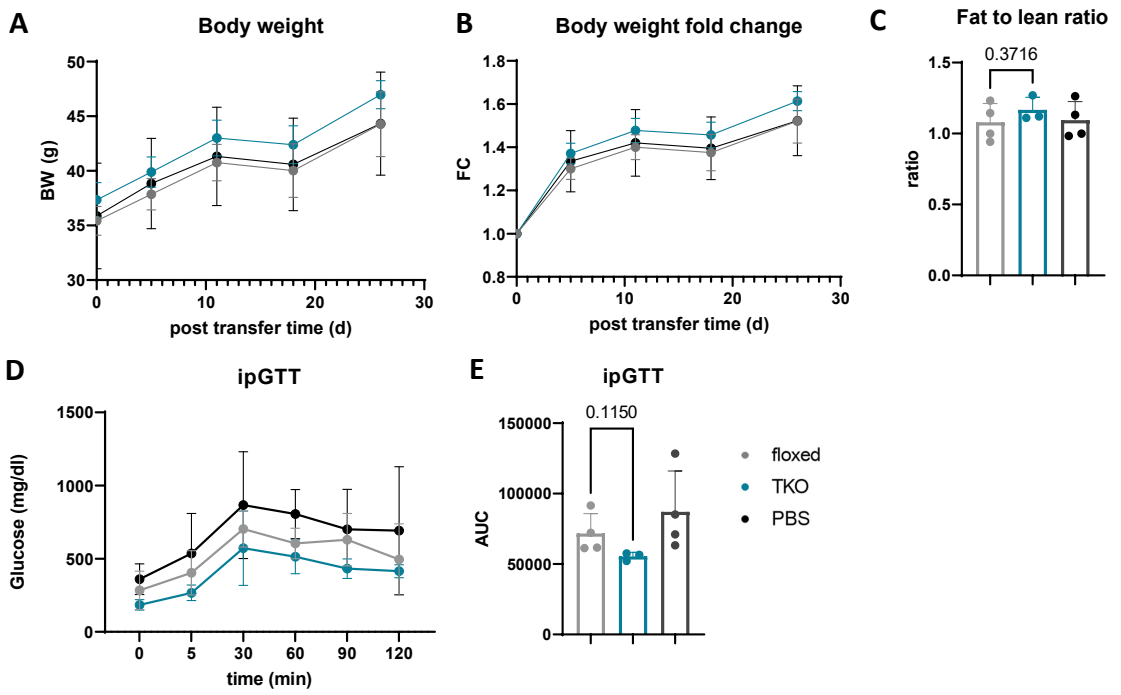

Figure 17: Adoptive transfer of GLP1R-deficient Tregs improves glucose tolerance of ob/ob mice. Adoptive transfer of Tregs from GLP1R TKO or floxed mice into the ob/ob animals. (A, B) Body weight (A) absolute or (B) as fold change. (C) Fat mass to lean mass ratio measured by EchoMRI™. Ordinary one-way ANOVA. (D-E) Intraperitoneal glucose tolerance test (ipGTT) with GLP1R TKO Treg recipients (n = 3), floxed (n = 4) Treg recipients and PBS control (n = 4) mice. (E) Area under the curve (AUC). (C, E) Each data point represents a biological replicate, Student's t-test.

All three experimental cohorts, including the PBS injected control mice, equally gained weight and had similar fat mass to lean mass ratios (**Figure 17**, A-C). Nevertheless, the preliminary results of the glucose tolerance tests showed tendentially lower blood glucose response in GLP1R-deficient Treg recipients (**Figure 17**, D, E). Flow cytometric analysis of *ex vivo* Tregs in VAT could not identify any significant differences among the experimental groups, most probably due to abundant indigenous ob/ob VAT Tregs, which could not be excluded from the analysis. However, in accordance with the slightly improved glucose tolerance in GLP1R TKO Treg recipient animals, the expression of proinflammatory cytokine IFNγ in VAT of these mice also tended to be slightly lower (**Figure 18**, A-C). These preliminary results thereby support our hypothesis, that GLP1R deficient Tregs can better suppress tissue inflammation positively affecting metabolic control. This effect therefore seems to be at least partially Treg-specific and body weight independent.

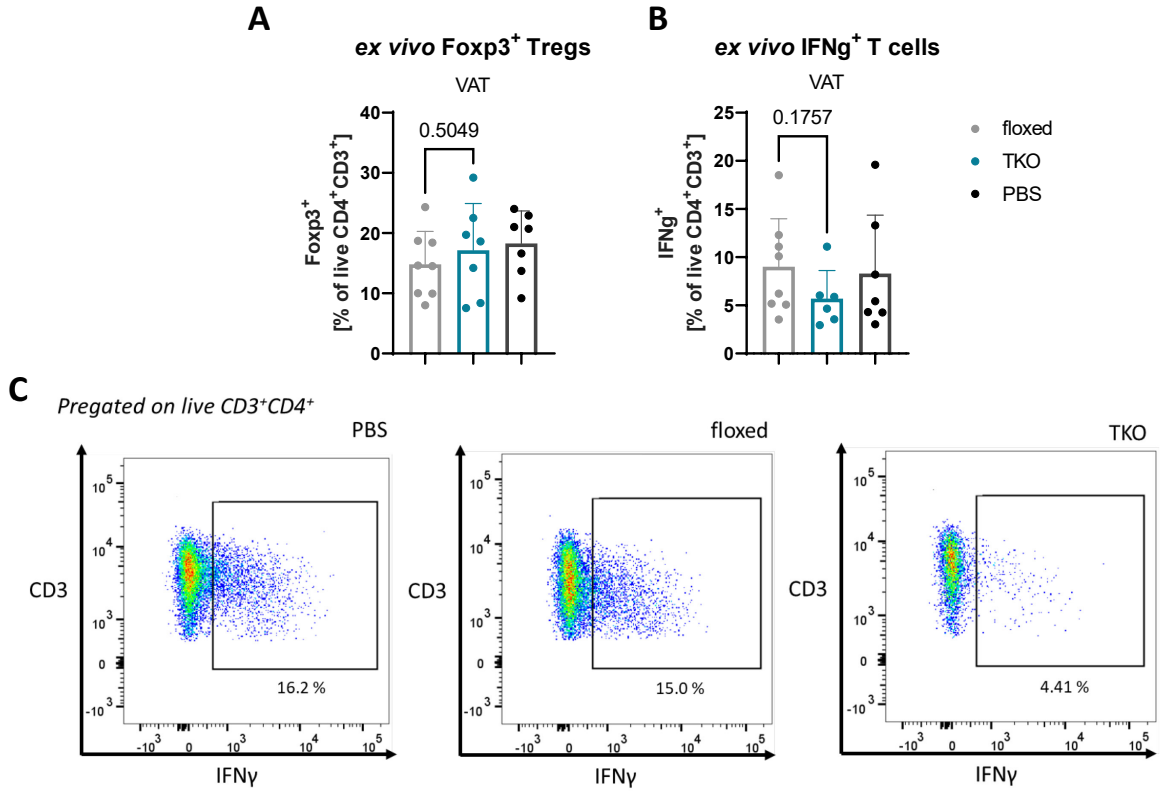

Figure 18: Adoptive transfer of GLP1R-deficient Tregs reduces IFNγ expression in VAT of ob/ob mice. Adoptive transfer of Tregs from GLP1R TKO or floxed mice into the ob/ob animals. FC analysis of (A) Foxp3$^+$ Treg frequencies and (B) percentages of IFNγ-expressing T cells in VAT of ob/ob recipient mice. Summary bar plots, each data point represents a biological replicate. Student's t-test. (C) Representative FC staining example of IFNγ expression.

5.8 Lack of T cell-specific GLP1R increases Treg stability in VAT of HFHS diet-fed mice

Elevated Foxp3 expression in adoptively transferred GLP1R-deficient Tregs, as well as augmented frequencies of Tregs in VAT of HFHS diet-fed GLP1R TKO animals have risen the question of improved stability of Treg phenotype in absence of GLP1R signaling in the proinflammatory environment. Since Treg stability has been shown to be linked to the DNA methylation of the conserved non-coding sequence 2 (CNS2) in the first intron of Foxp3 (Floess et al., 2007), I utilized high-resolution melting (HRM) PCR and pyrosequencing to assess the methylation status of Foxp3 CNS2 in sorted Tregs from VAT of HFHS diet-fed GLP1R TKO and floxed mice according to the protocols established in our lab (Scherm et al., 2019). As a result, I observed a clear, although yet not significant tendency towards diminished Foxp3 CNS2 methylation in Tregs from GLP1R TKO animals (**Figure 19**). This outcome indicates a more stable Foxp3 expression and consequently Treg phenotype in absence of GLP1R signaling in the context of inflammation, which is in line with findings indicated above.

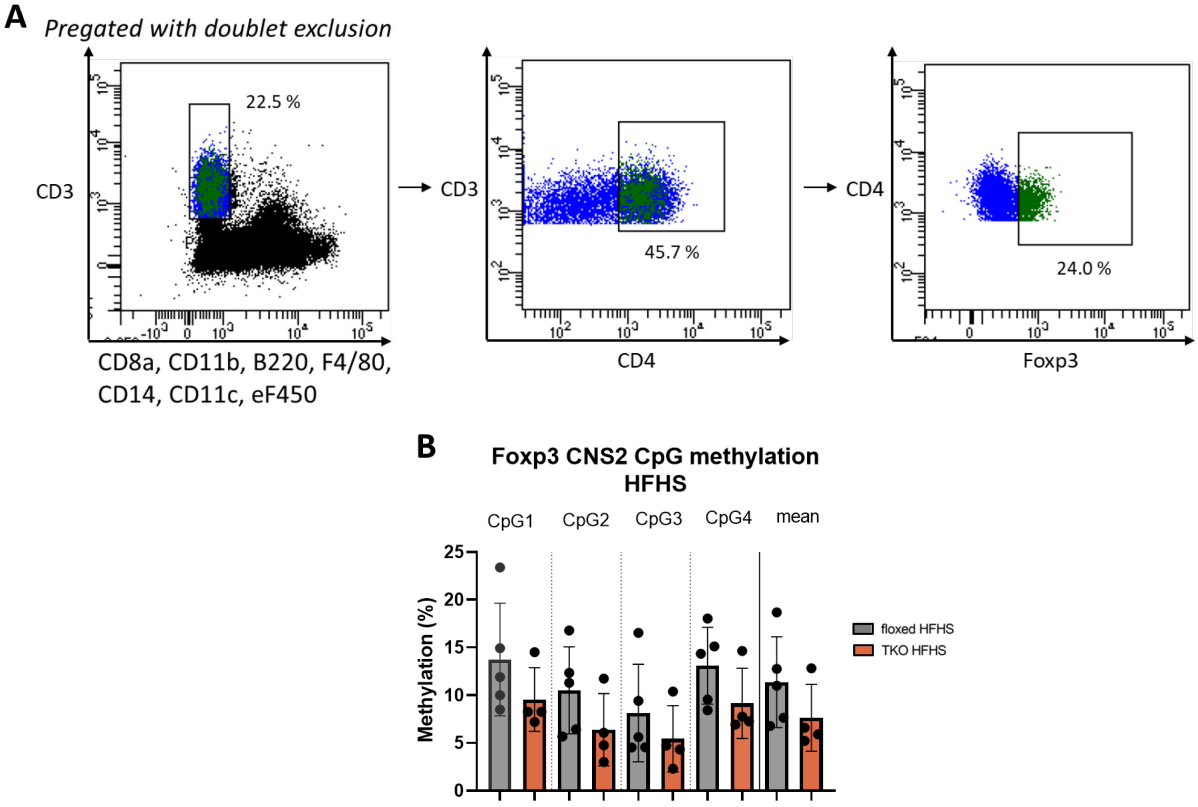

Figure 19: Lack of GLP1R signaling in T cells decreases CNS2 Foxp3 methylation in Tregs. Methylation analysis of the Foxp3 CNS2 in Tregs from VAT of HFHS diet-fed GLP1R TKO vs. floxed mice.

(A) Sorting strategy. (B) Summary scatter plot, four CpG sites and their mean. Each data point represents a biological replicate. Ordinary one-way ANOVA.

5.9 Two clusters of Tregs in VAT of HFHS diet-fed mice

To understand the mechanistic underpinnings of the described observations, we performed unbiased profiling of sorted $CD4^+$ T cells from VAT of GLP1R TKO vs. floxed mice upon HFHS or SD using droplet-based scRNAseq. We analyzed 2 biological replicates in each group, which were distinctly labeled with cell hashing antibodies and pooled together for sequencing. Following the implementation of algorithms for noise reduction and data integration (see Methods), 11 clusters were identified and annotated based on the differentially expressed genes. **Figure 20** represents the subsets of the differentially expressed genes that illustrate the difference between those clusters. Their distribution among the biological replicates did not show any abnormalities, except for the SD-fed floxed mouse #1, which displayed high abundance of pathogenic Th17 cells (data not shown).

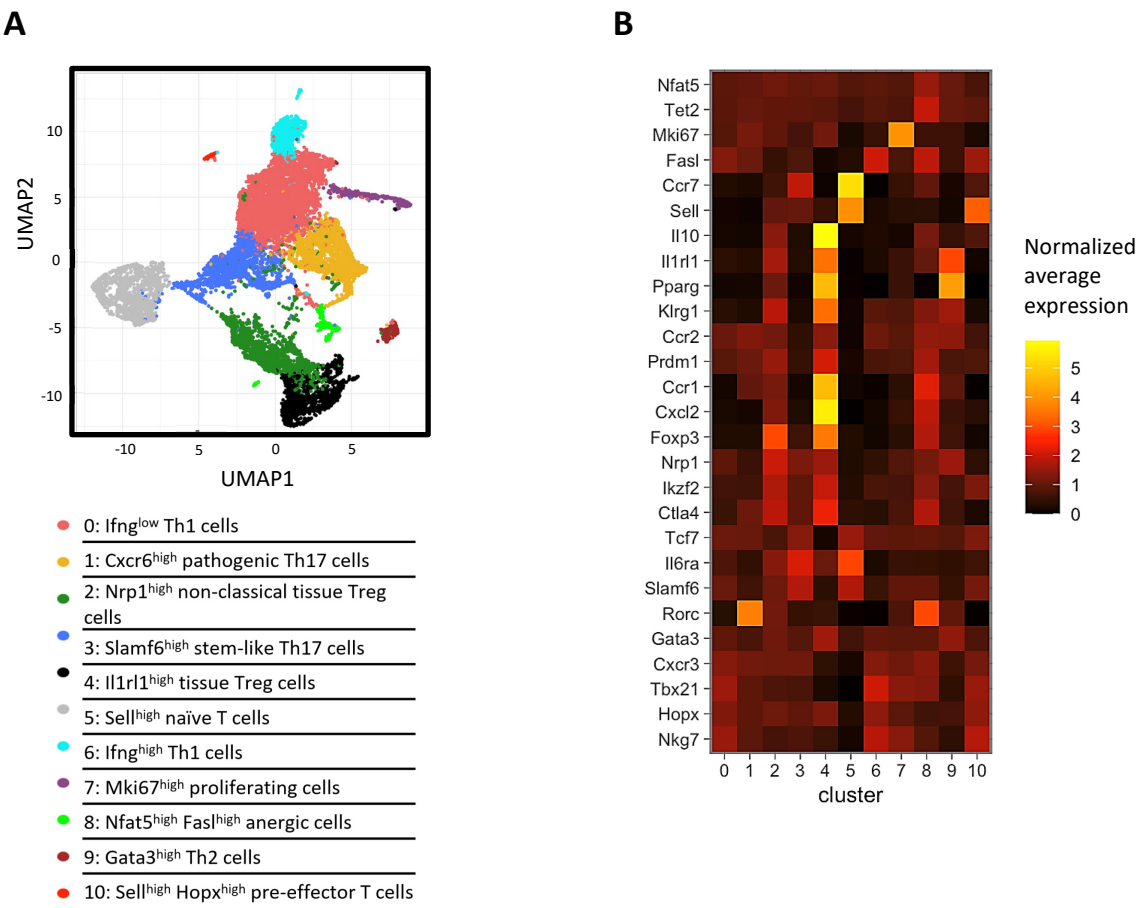

Figure 20: scRNAseq identifies 11 clusters of CD4⁺ T cells in VAT of HFHS diet-fed animals. Single cell mRNA sequencing on CD4⁺ T cells sorted from VAT of HFHS diet- or SD-fed GLP1R TKO or floxed mice (4 groups, 2 mice per group). (A) UMAP embedding of the sorted CD4⁺ T cells pooled from all mice after applying noise reduction (MAGIC) and data integration (Seurat). The colors denote clusters. The cluster annotation is made based on the differentially expressed genes. (B) Heat map shows normalized expression of selected differentially expressed genes in each cluster.

Two clusters of Tregs, namely cluster 2 and cluster 4, were identified along this procedure. While cluster 4 was to a similar level represented in almost all animals, cluster 2 showed paramount increase in VAT of HFHS diet-fed GLP1R TKO animals (**Figure 21**, A). Along with that, cluster 2 in GLP1R TKO animals contained higher numbers of cells expressing IL10, which in sum, resulted in the higher level of IL10 transcripts from both clusters in HFHS diet-fed GLP1R TKO mice (**Figure 21**, B). By these means, our transcriptional analysis was in line with the observed *in vivo* phenotype in GLP1R TKO mice and

identified cluster 2 being responsible for the rise of Tregs and corresponding IL10 levels in VAT of HFHS diet-fed GLP1R TKO mice.

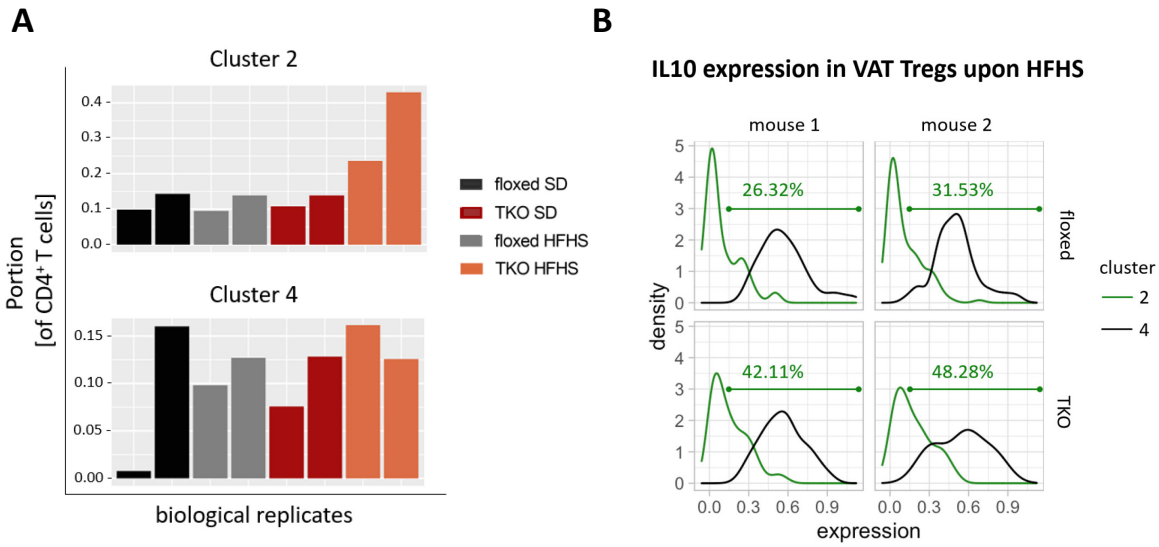

Figure 21: Cluster 2 Tregs are responsible for the rise of VAT Treg frequencies in GLP1R TKO mice upon HFHS diet. (A) The bar plot shows the relative size of cluster 2 or cluster 4 in each mouse. Each bar represents an individual mouse. (B) The histograms show *Il10* expression subjected first to noise reduction (MAGIC) and then to data integration (Seurat).

Having found that cluster 2, rather than cluster 4, contributes more to the increase in VAT Tregs in GLP1R TKO mice upon HFHS diet, we aimed at characterizing both of these Treg populations in greater detail. Interestingly, cluster 4 exhibited characteristics of the VAT Treg signature profile, with high expression of *Klrg1*, *Il1rl1*, *Gata3*, *Il10*, *Ccr2* and *Batf* (**Figure 22**, A). On the contrary, the most differentially expressed genes in cluster 2 encompassed *Ms4a4b* and *Ms4a6b* coding for Treg transmembrane costimulatory molecules (Howie et al., 2009) and *Itgb1* coding for integrin β1 involved in the contact-mediated suppression in Tregs (Klann et al., 2018). Two other transcripts significantly prevalent in cluster 2 code for molecules *Tcf7* and *Nrp1* and are related to the maintenance and stability of the Treg phenotype (Delgoffe et al., 2013, Junius et al., 2021, Yang et al., 2019).

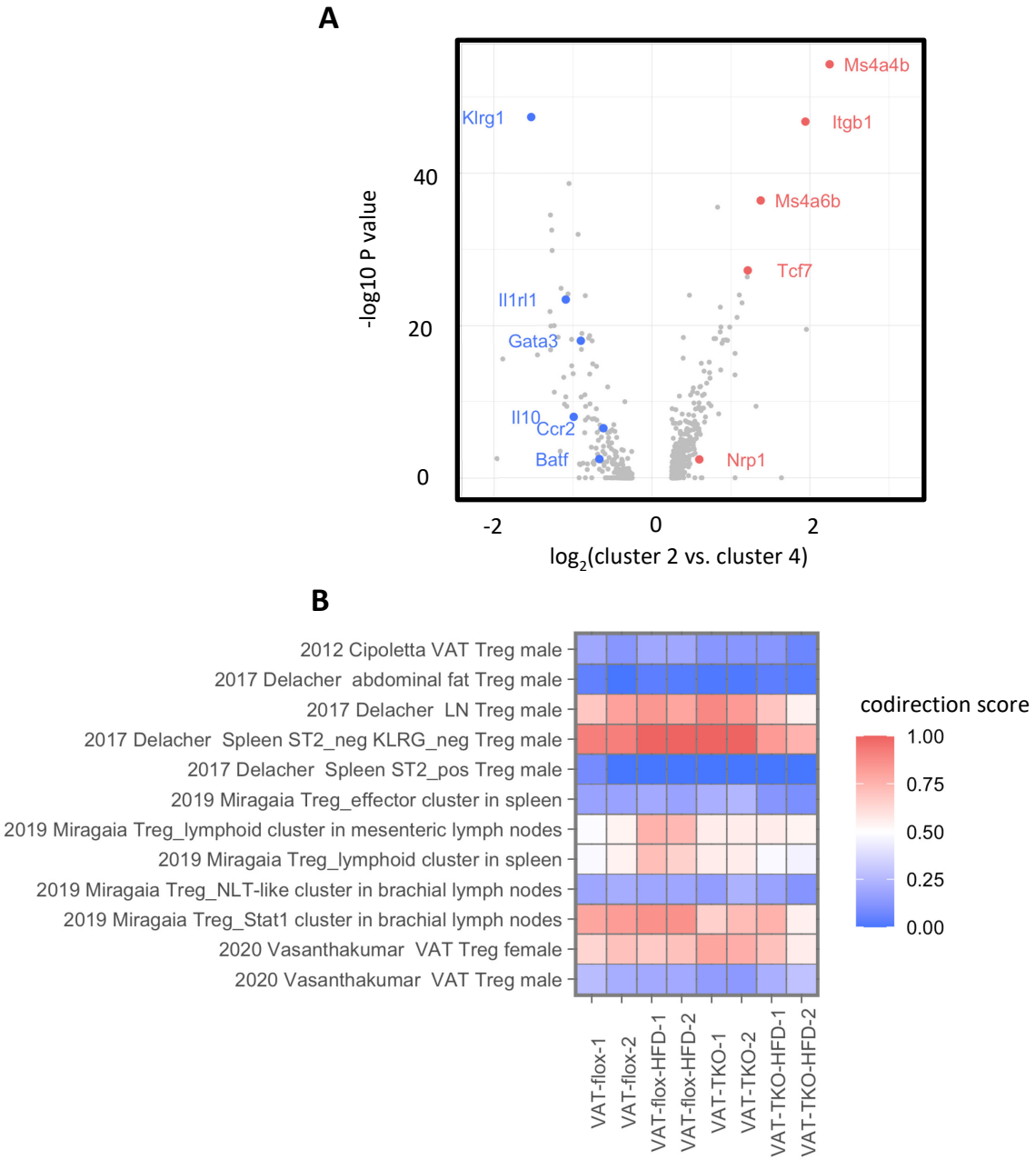

Figure 22: Cluster 4 rather than cluster 2 displays the transcriptional phenotype of classical VAT Tregs. (A) The volcano plot shows the difference in transcript count between cluster 2 and cluster 4 identified with build-in Seurat tools. Selected genes known for upregulation in classical VAT Tregs or in Tregs of peripheral lymphoid tissue are highlighted in blue and red respectively. (B) The heat map shows the codirection score of the indicated signatures in cluster 2 in comparison to cluster 4 (see Methods).

Having observed, that cluster 4 rather than cluster 2 is transcriptionally more similar to classical VAT Tregs, we next assessed the degree of this similarity in both clusters by comparison with published VAT Treg signature profiles (Vasanthakumar et al., 2020, Cipolletta et al., 2012, Delacher et al., 2017, Miragaia et al., 2019). We therefore calculated the similarity of each signature (as the portion of codirected genes (see Methods)) to the difference in the expression between cluster 2 and cluster 4 (**Figure 22**, B). The highest codirection score represents gene sets enriched in cluster 2 relative to cluster 4. Cluster 2 had high transcriptional overlap with signatures of Tregs from lymphoid organs. On the contrary, signatures from VAT Tregs correlated more with gene sets from cluster 4, which resulted in lower codirection score. Interestingly, we observed differences in codirection within the cluster 2 between the genotypes. So, in GLP1R TKO mice fed HFHS diet, cluster 2 exhibited slightly higher degree of similarity to VAT Treg-related transcriptional programs, than their counterparts from floxed controls did.

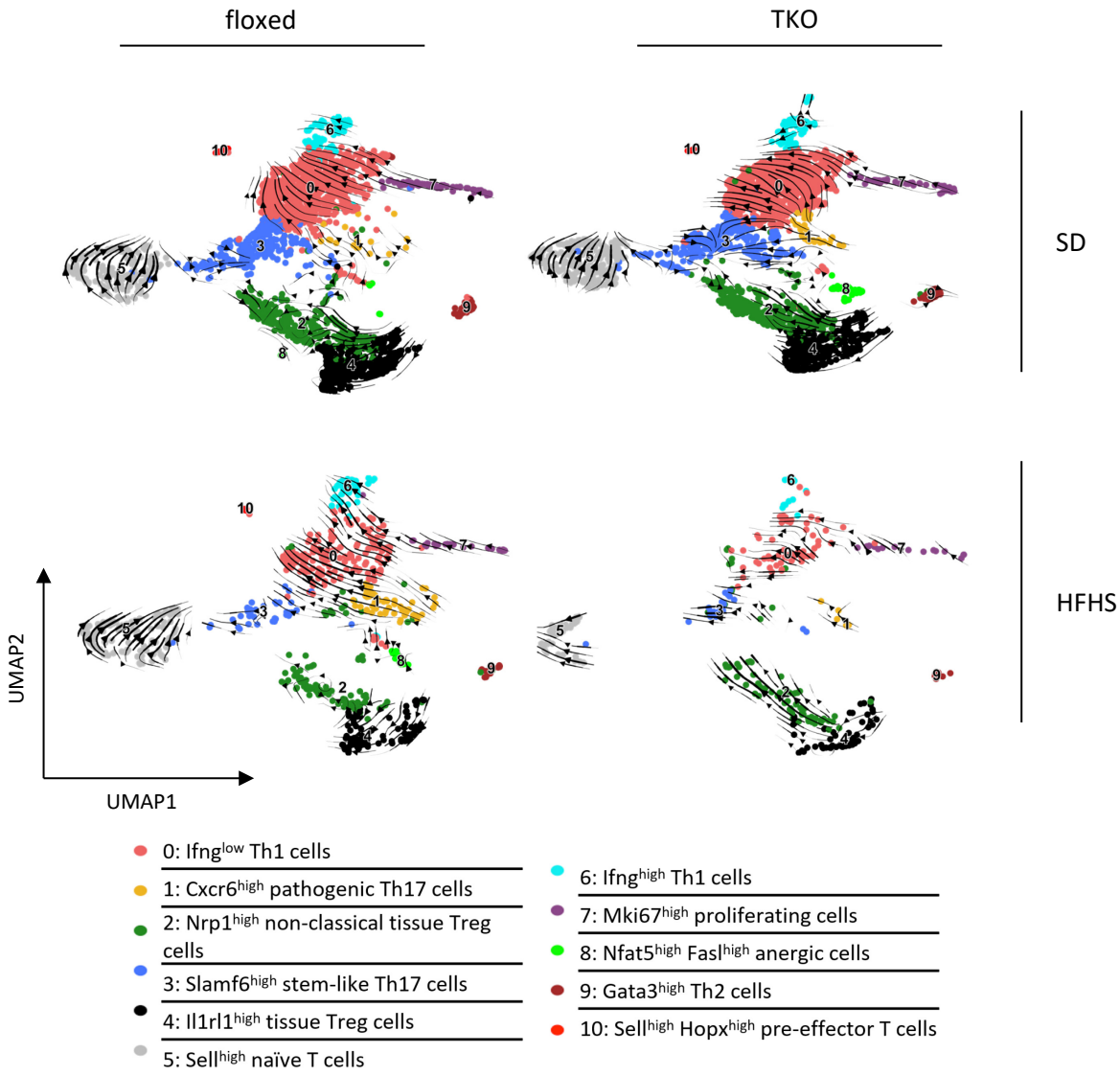

Figure 23: Velocity analysis indicates the dedifferentiation of cluster 4 into the cluster 2. Differentiation trajectories of T cells were inferred by applying scVelo to the spliced and unspliced transcript counts obtained with Velocyto from sorted CD4⁺ T cells. scVelo was applied to each mouse individually. The UMAP embedding was taken from the **Figure 20**.

The expansion of cluster 2 in GLP1R TKO mice upon HFHS diet, as well as its higher similarity to classical VAT Tregs initially prompted us to assume, that cluster 2 represents the precursor population for cluster 4. However, this hypothesis was disproved by the RNA-velocity analysis, a method, which predicts transcriptional dynamics by assessing spliced vs. unspliced transcripts. As annotated by vectors (**Figure 23**), RNA-velocity analysis identified sequential dedifferentiation of VAT Treg cluster 4 to cluster 2 in all independently processed samples.

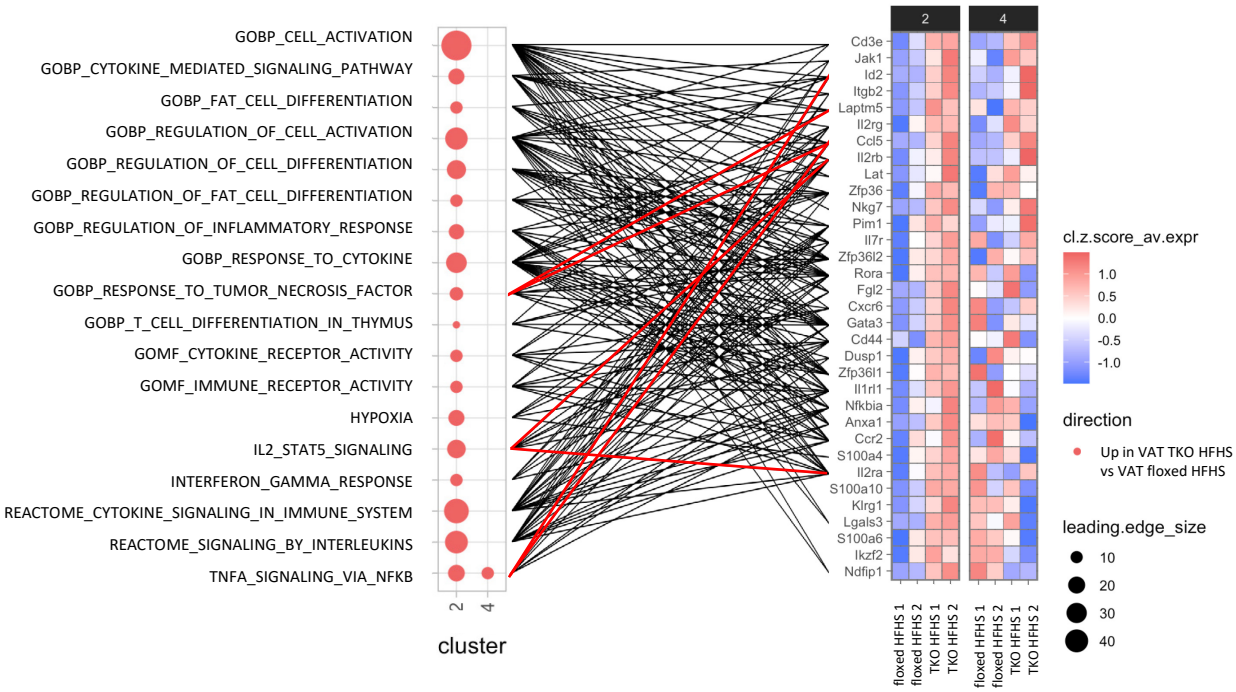

Figure 24: Signaling pathways upregulated in HFHS VAT of GLP1R TKO vs. floxed mice. Genes up- or downregulated in GLP1R TKO mice in comparison to floxed mice both fed HFHS diet were tested using GSEA in cluster 2 and cluster 4 individually. The heat map shows the leading-edge genes pooled from the significantly-enriched gene sets. The bubble diagram displays the number of leading-edge genes (see Methods) in some of those gene sets. The straight lines connect the genes in the heat map to the gene sets, in whose leading edges those genes were found. The lines referring to the genes within the specific gene sets discussed in the text are highlighted in red.

Therefore, we aimed to understand the transcriptional differences between the cells of different genotypes within the same cluster that would underly the observed dynamics of differentiation and could clarify the expansion of cluster 2 in VAT of HFHS diet-fed GLP1R TKO animals. For that we performed an unsupervised search within the variety of publicly available transcriptional signatures using Gene Set Enrichment Analysis (GSEA). As a result, we identified several signatures statistically different between the genotypes in cluster 2 or cluster 4 or in both of them. From these signatures we extracted the leading-edge genes identified by GSEA and assessed their expression among the biological samples and clusters (**Figure 24**, right). In sake of interpretability we focused on the signatures that correspond to sufficiently broad immune and metabolic functions (**Figure 24**, left). In this analysis we identified signaling pathways indicative for

cell activation and response to cytokines and interleukins among the most upregulated in HFHS diet-fed GLP1R TKO mice relative to floxed controls specifically in cluster 2. Moreover, multiple genes with the highest difference in the mean expression between GLP1R TKO and floxed mice (*Id2*, *Lamptm5*, *Ccl5*) belonged to the TNFα signaling pathway. In addition, the components of IL2/STAT5 signaling (*Il2rb*, *Il2ra*), as well as certain VAT Treg markers (*Gata3*, *Il1rl1*, *Ccr2* and *Klrg1*) were also identified to be higher expressed in cluster 2 in GLP1R TKO mice compared to floxed controls.

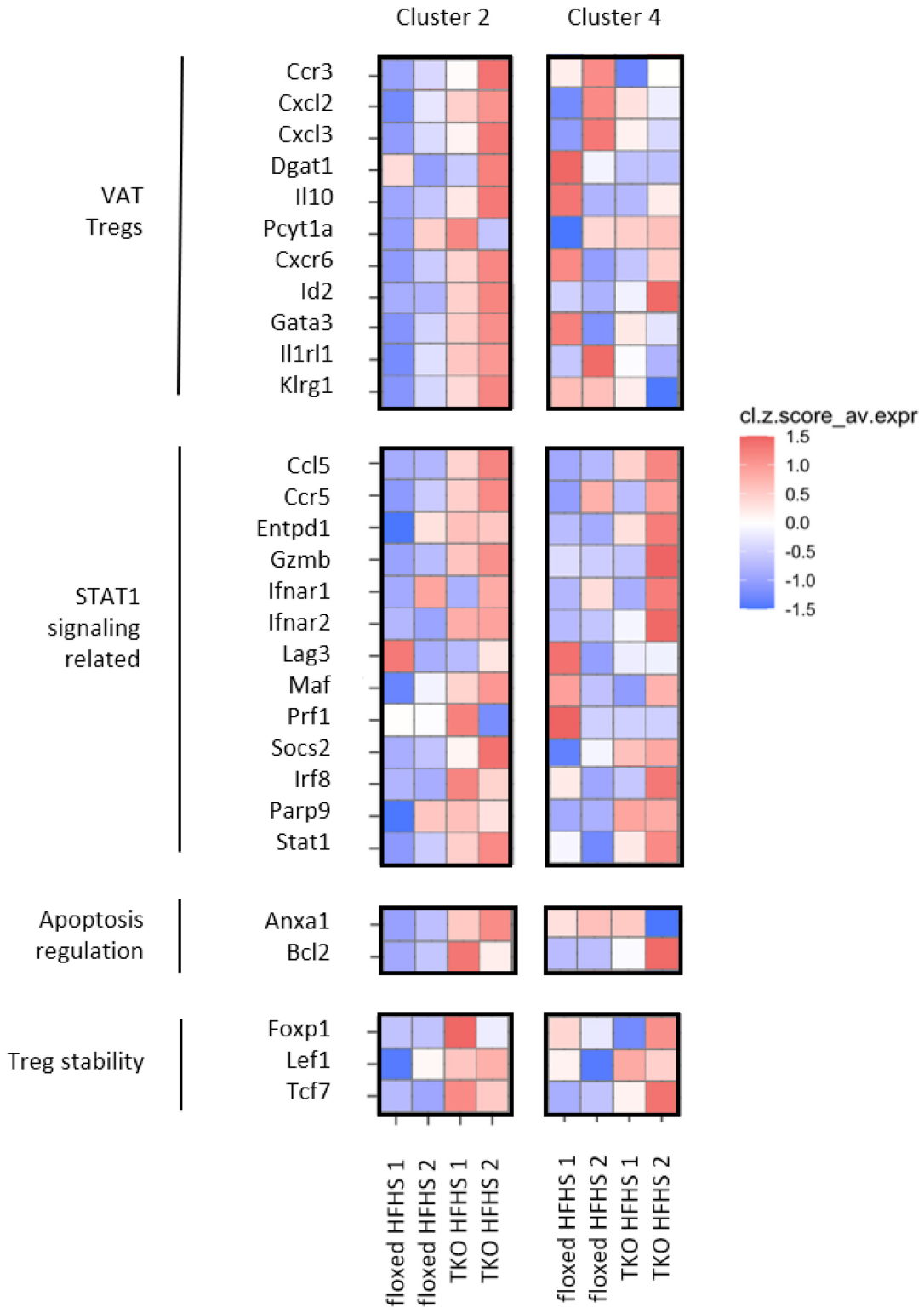

Figure 25: Supervised analysis of designated genes corresponding to signaling pathways or biological function in cluster 2 and cluster 4 in GLP1R TKO vs. floxed mice upon HFHS diet. Four sets of genes highly relevant for specific biological functions in T cells identified based on literature analysis. The heat map shows the expression of these genes normalized within each cluster individually.

To complement our findings about the biological processes differentially regulated between the HFHS diet-fed GLP1R TKO and floxed mice, we proceeded with the deeper analysis of the signatures relevant for Treg biology constructed with a literature-based approach. We identified several signatures composed of the genes with well-documented relevance for the respective biological processes, which appeared too short to be analyzed by GSEA (**Figure 25**). Among them the genes related to VAT Tregs (Cipolletta et al., 2012, Frias et al., 2019), STAT1 signaling (Stewart et al., 2013), Treg stability (Yang et al., 2019, Ren et al., 2019) as well as some genes involved in the regulation of apoptosis (Murase et al., 2013, Yang et al., 2013) demonstrated a coherent trend for upregulation in GLP1R-deficient cluster 2 Tregs relative to their floxed counterparts. The expression of the signatures' members *Anxa1*, *Cxcr6*, *Ccl5*, *Tcf7*, *Stat1*, *Gata3*, *Klrg1* and *Il1rl1* were statistically-different between the two groups of animals (see Methods) with low variation within each group.

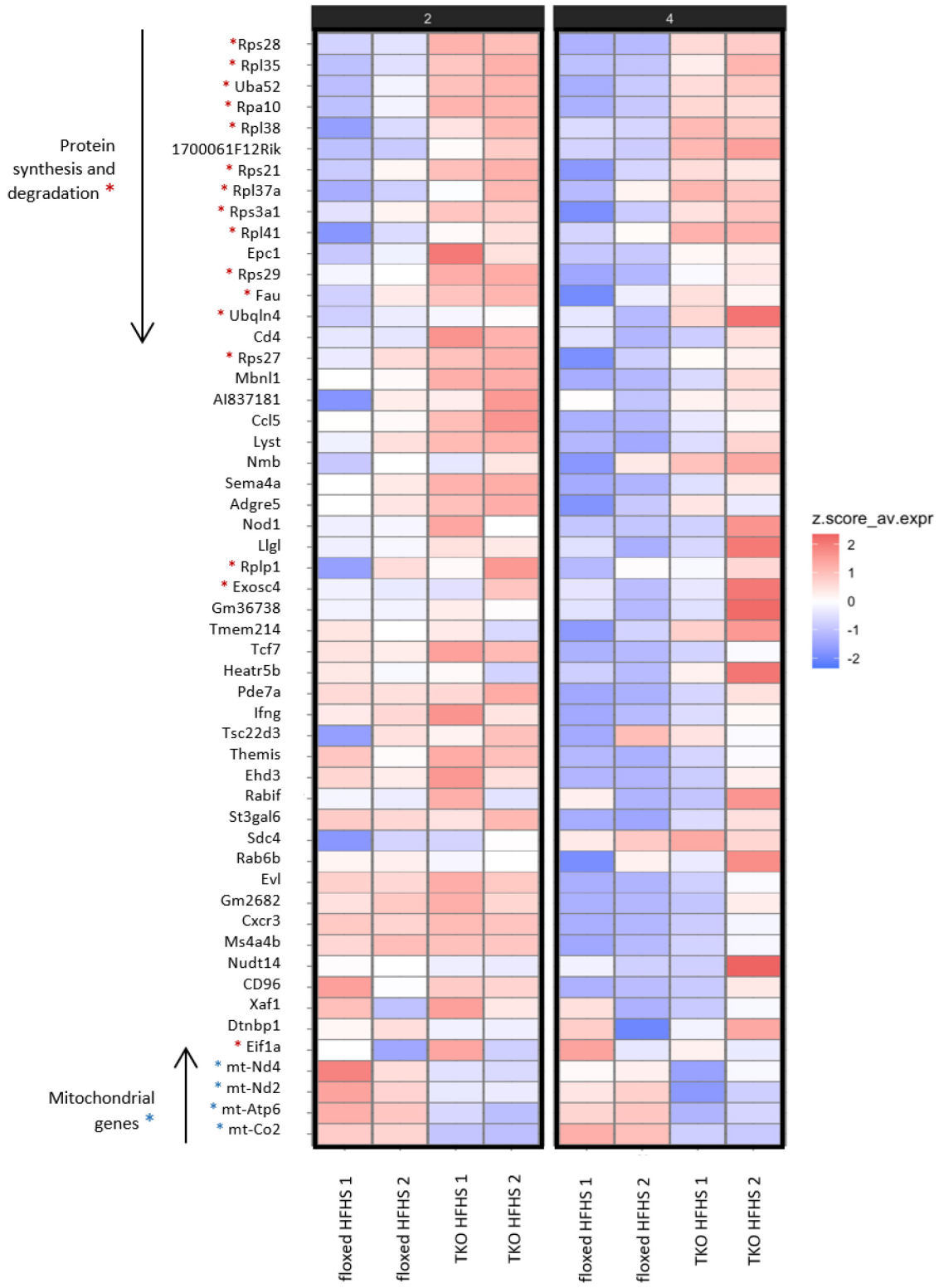

Figure 26: Mitochondrial genes and genes involved in protein synthesis and degradation are highly affected by absence of GLP1R in VAT Tregs of HFHS died-fed mice. The Seurat build-in tool for identification of differentially expressed genes was used to compare transcript counts of sorted $CD4^+$ T cells between GLP1R TKO and floxed mice both fed HFHS diet. The heat map shows the genes that have statistically-different expression between mice of different genotype, but not between mice of the same genotype (see Methods).

An additional unsupervised approach was used to decipher the differences in Tregs from both clusters, in which gene expression data without correction for batch-effect was screened for the most statistically significant differentially expressed genes between GLP1R TKO VAT Tregs upon HFHS diet and their floxed counterparts (**Figure 26**). Among these genes a higher prevalence of transcripts coding for ribosomal proteins, or proteins involved in protein synthesis and degradation were observed in GLP1R-deficient Tregs in comparison to floxed controls in both clusters (e.g. *Rps28*, *Rpl35*, *Uba52*). The significantly downregulated genes, on the contrary, mostly included mitochondrial genes (*mt-Nd4*, *mt-Nd2*, *mt-Atp6*, *mt-Co2*). The possible influence of the batch-effect cannot be ruled out in this case, since no algorithms for its elimination were applied here. However, these results may signify the changes in the cell-intrinsic metabolism, potentially including protein synthesis and mitochondrial activity or stress, which however should be addressed and validated by further experiments.

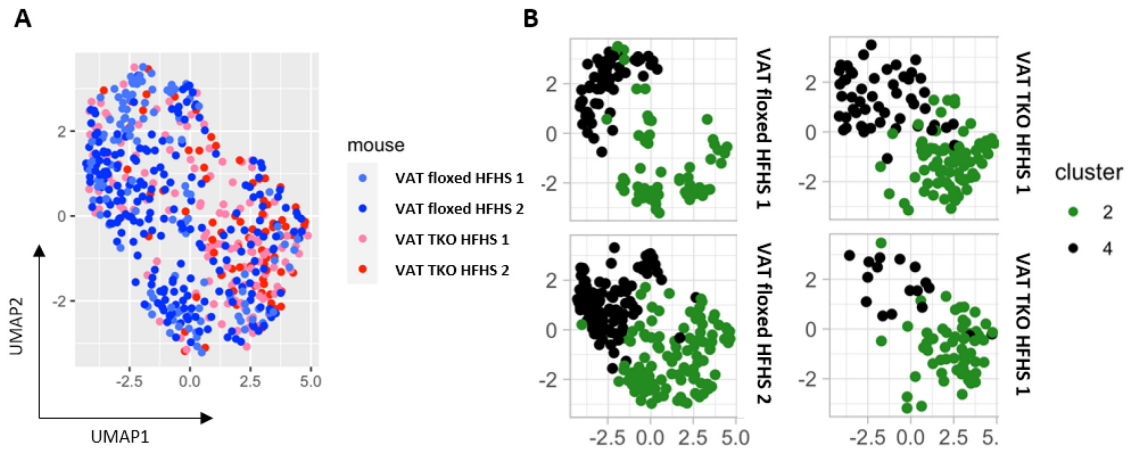

Figure 27: Dimensionality reduction of expression profiles without correction for batch-effect confirmed the robustness of separation between cluster 2 and cluster 4. UMAP embedding created for transcript counts of cluster 2 and cluster 4 of GLP1R TKO or floxed mice both fed HFHS diet pooled together without noise reduction and data integration. (A) The color code represents individual mice. (B) The color code represents clusters.

In the end, we wanted to confirm, that the transcriptional similarity of GLP1R-deficient cluster 2 Tregs to cluster 4 and classical VAT Tregs was not introduced by applied processing algorithms. For that we constructed UMAP embedding of the expression values of clusters 2 and 4 without noise reduction and batch-effect correction. We found that in these coordinates the distance between the samples was smaller than the distance between the clusters (**Figure 27**). Therefore, this method demonstrates the robustness of our clusterization method and reliability of our observations.

6 Discussion

During the last decades the prevalence of overweight and obesity worldwide has risen with alarming rates and became epidemic. This implies that obesity is not the mere lack of discipline or consequence of bad personal choices. Supported by recent studies in the field, obesity has been recognized as a chronic, relapsing, multi-factorial, neurobehavioral disease with pathophysiology including genetic and environmental factors (Obesity Medicine Association, (OMA)). It is a multisystemic disorder and represents the main risk factor for multiple comorbidities, including the cardiovascular disease being the leading cause of death in 2012 (WHO, 2021a). It reduces the quality of life and shortens the life span placing the burden on the society and economy. Therefore, obesity requires further research to improve our understanding of the disease mechanisms to design and optimize medical interventions.

Obesity is accompanied by chronic, low-grade inflammation, which plays a crucial role in the development of insulin resistance and T2DM. The studies demonstrating increase in proinflammatory cytokine production in adipocytes itself, as well as accompanying infiltration of proinflammatory immune cells in AT upon obesity, have for the first time highlighted the close interconnection of immune and metabolic systems. Hotamisligil in his works proposed the idea, that such close interconnection is a conserved throughout evolution mechanism, which is beneficial for the adaptation to fluctuations in the nutrient environment (Hotamisligil, 2017, Hotamisligil, 2006). Such organismal organization helped to ensure functioning of both metabolic and immune system in an energy-efficient way, which is highly relevant for the survival, especially upon food scarcity. To support this hypothesis Hotamisligil argues, that both systems have the common evolutionary origin, which in *Drosophila* is represented by the fat body. This organ simultaneously performs liver, AT and immune functions. Another argument supporting this view is the functional overlap of adipocytes and immune cells. So, adipocytes themselves were demonstrated to acquire immune-like phagocytotic and antimicrobial activity (Caputa et al., 2022, Cousin et al., 2001). At the same time cytokines influence energy intake and energy expansion (Wallenius et al., 2002, Zorrilla Eric et al., 2007, Pamir et al., 2009). In addition and as described previously in this thesis, ongoing inflammation in AT directly

acts on adipocytes influencing their insulin sensitivity and production of adipokines, which in turn regulate systemic metabolism.

To limit this inflammation and to restore immunometabolic balance the population of VAT Tregs comes into play. Their unique role in integrating systemic and tissue healthy function with immune homeostasis is very well described in the literature. This special role is again reflected in their molecular signature, orchestrated by the expression of PPARγ, the adipocyte master regulator. PPARγ induces the tissue-specific metabolic re-wiring of Tregs as a part of their adaptation to the metabolic environment (Cipolletta, 2014). The additional environmental cues, either inflammatory or metabolic, perform the fine-tuning, constantly influencing VAT Tregs. We and others have shown, that some environmental cues, such as HFHS diet, intermittent fasting and cold exposure have an impact on abundance and phenotype of VAT Tregs (Feuerer et al., 2009, Wang et al., 2022, Becker et al., 2017). But what about the direct effect of the food intake and Treg response to metabolic hormones?

We and others could previously identify the expression of multiple metabolic hormone receptors in Tregs, which offers a potential molecular interface for integration of metabolic changes with phenotype and function of Tregs. This hypothesis is supported by the recent reports demonstrating the role of these metabolic signaling pathways in Tregs for their function in safeguarding a healthy metabolism (Wu et al., 2020) and our unpublished data). In this thesis, I focused on the role of GLP1 and its signaling, as a possible molecular mediator between food intake as a systemic switch from fasted state to satiety and Treg response to such metabolic reprogramming. For that we generated a mouse model with CD4 T cell-specific deletion of GLP1R. This model enabled us to assess the role of GLP1R signaling not only for established Tregs, but also to identify effects on the induction and development of Tregs from naïve CD4 T cells. Indeed, GLP1R signaling interfered with *de novo* induction of Tregs *in vitro* under subimmunogenic conditions and in a polyclonal setting. In accordance with that, we observed a slight tendency to increased frequencies of Tregs in SI of GLP1R TKO animals, accompanied by their significant phenotypic changes. These phenotypic changes comprise significantly higher expression of RORγt and CCR6, specifically characteristic for the peripherally induced in response to intestinal microbiota Tregs. Interestingly, at the steady state I could not

identify similar changes in Tregs in colon of GLP1R TKO animals, neither in Treg frequencies, nor in their Th17-related phenotype (data not shown). The reason for that might be the clear structural, metabolic and immunological differences of these tissue compartments. Although the colon is known to have higher microbiota content, it contains a much thicker mucus layer, which prevents direct contact of microbiota with epithelial immune cells (Atuma et al., 2001). The distribution, phenotype and properties of the antigen presenting cells (APCs), which are crucial for peripheral *in vivo* Treg induction are also different in SI and colon ((Coombes et al., 2007), reviewed in (Bowcutt et al., 2014)). For example, although there is less mechanistic data describing the induction of Tregs specific for microbiota, different mechanisms have been proposed for Treg induction in response to soluble antigens in SI and colon. So, the induction of SI Tregs has been described to occur mainly in mesLN and in response to $CD103^+$ DCs (Jaensson et al., 2008, Coombes et al., 2007). On the contrary, the main inductive sites for Tregs in the distal part of the colon were shown to be caudial and iliac LNs, where mainly the independent of $CD103^+$ DCs process of Treg induction takes place (Veenbergen et al., 2016). In addition to that, $CD103^+$ DC residing in duodenum (in SI) exhibited more tolerogenic phenotype than their counterparts in colon-draining LNs, which was boosted by microbiota (Esterházy et al., 2019).

All these evidences underlie the complex compartmentalized regulation of gut-resident immune subsets, where CD4 T cell-intrinsic GLP1R signaling seems to interfere with the regulation of $ROR\gamma t^+$ Tregs at the steady state specifically in SI. This situation is changed upon inflammation. In accordance to the data reporting an impaired ability of $CD103^+$ DC to induce Tregs in the setting of inflammation (Laffont et al., 2010), my preliminary results show the increase in SI $ROR\gamma t^+$ Tregs previously observed at steady state to vanish upon DSS-induced colitis. At the same time, I observed tendentially increased frequencies of Tregs and $Il10^+$ Tregs at the main site of inflammation- in colon. This increase in tolerogenic Tregs was accompanied by a reduced colon weight to length ratio mirroring the amelioration of the disease. I assume, that this effect is rather linked to a superior capability of GLP1R-deficient Tregs to withstand proinflammatory milieu and to establish a tolerogenic environment.

The evidence supporting this statement has been observed throughout the study in multiple disease models and in various tissues. So, when I transferred GLP1R-deficient Tregs into the immunodeficient lymphopenic Rag KO hosts, these Tregs better maintained Foxp3 expression than their floxed counterparts did. In VAT they produced higher amounts of anti-inflammatory cytokines, including IL10, and could better suppress the expression of proinflammatory cytokines IFNγ and IL17 from WT responder cells. In colon, GLP1R-deficient Tregs as bystanders established better environment for the *de novo* Treg induction from cotransferred WT naïve GLP1R competent T cells. All these effects collectively contributed to the amelioration of inflammation in tissues of GLP1R TKO Treg recipients.

A similar phenomenon was observed in the model of the weight gain-induced mild chronic inflammation in mice subjected to HFHS. Multiple previous reports have demonstrated a severe reduction of VAT resident Tregs in animals fed HFHS diet (Cipolletta et al., 2015, Cipolletta et al., 2012, Feuerer et al., 2009). My data propose, that in the absence of GLP1R signaling a HFHS diet has an opposite, rather beneficial effects on VAT Treg frequencies, restoring their levels to those observed in control floxed mice upon SD. In line with my observations in the adoptive transfer model, upon HFHS diet GLP1R-deficient VAT Tregs showed a more stable Treg phenotype and Foxp3 expression as indicated by the reduced methylation state of relevant CNS2 CpG sites.

These data indicate, that GLP1R-deficient Tregs can better tolerate a proinflammatory environment, which provided beneficial effects on systemic metabolic health as well. Thus, HFHS diet-fed GLP1R TKO animals were leaner than their floxed counterparts and demonstrated improved metabolic parameters. To exclude that the advantageous effects on systemic metabolism were the mere consequence of differences in the body weight between GLP1R TKO and floxed mice, the adoptive transfer of either GLP1R TKO or floxed Tregs was performed. The tendentially reduced IFNγ expression in VAT, indicative of the reduced inflammation, as well es tendentially improved glucose tolerance in GLP1R-deficient Treg recipients support our hypothesis that Tregs are at least partially responsible for the improved metabolic heath in GLP1R TKO mice in the setting of HFHS diet. However, we do not know, whether GLP1R-defficient Tregs positively regulate the systemic metabolism solemnly by suppressing inflammation, or whether additional

mechanisms might be involved. So, He et al. proposed the idea, that intraepithelial lymphocytes (IEL) in SI utilize their GLP1R expression to control systemic bioavailability of GLP1 (He et al., 2019), which might then affect the metabolic parameters systemically. Yet, this study has some disadvantages. There were no cell-specific KO models used and GLP1 availability was measured exclusively in cell cultures. In addition and in our experience, the GLP1R antibodies used in the above-mentioned study have limited efficacy and specificity, therefore, additional studies are needed to confirm these results.

Furthermore, the possible interference of microbiota in the interconnection of metabolic parameters and Treg abundance in SI and VAT cannot be ruled out in our study. Recently, a considerable amount of literature has emerged, that describes a tight interrelationship between microbiota, obesity and the immune system. Apparently, HFHS diet impacts microbiota composition by changing the composition of nutrient substrates or by affecting the gut epithelial integrity (Singh et al., 2020, Cani et al., 2008). In turn, microbiota ware reported to influence systemic metabolic parameters, such as weight gain, energy expenditure, insulin resistance (Ridaura et al., 2013, Turnbaugh et al., 2006). Some studies implicate immune cells to be the main part of this bidirectional crosstalk (Garidou et al., 2015), since both, microbiota and diet composition are known to affect immune cell populations in the gut. Therefore, there is a clear evidence of strong association between the systemic metabolic control, microbiota and immune processes, although the exact mechanisms are not yet clear. However, given the Treg phenotype observed in the gut of GLP1R TKO mice, it is therefore possible that the impact on the microbiota might be a potential way of how GLP1R-deficient Tregs improve systemic metabolic health.

The single cell transcriptome analysis could confirm the observed *in vivo* increase in VAT Tregs in GLP1R TKO mice upon HFHS diet. Importantly, it revealed the Tregs of a particular cluster 2 to be responsible for this rise in GLP1R-deficient VAT Tregs. This cluster 2 in its transcription profile was different from the established and described in the literature classical VAT Tregs (Delacher et al., 2017, Feuerer et al., 2009, Vasanthakumar et al., 2020), which in our screen were identified as cluster 4. In contrast with our initial hypothesis of cluster 2 being the precursor population for terminally differentiated VAT tissue Tregs, the velocity analysis of our sequencing data rather proved the opposite. It

suggested the cluster 4 to give rise to the cluster 2 by dedifferentiation and downregulation of the VAT Treg specific program. An increase in the abundance of cluster 2 Tregs in metabolically healthier GLP1R TKO animals may therefore at first sight seem to be contradictory considering the crucial role of this VAT specific program for phenotype, maintenance and function of VAT Tregs, as well as VAT metabolic integrity. However, such transcriptional remodeling might be a part of an adaptational program of GLP1R-deficient Tregs to the challenging proinflammatory metabolic environment, enabling the switch from a VAT tissue program, which might be ineffective or even detrimental upon excess of lipids, hypoxia and oxidative stress in obese VAT, to a more anti-inflammatory state.

In accordance with this hypothesis we observed, that cluster 2 Tregs upregulated a set of genes associated with the "core" Treg phenotype, their stability and suppressive function programs. So, the most differentially upregulated genes in cluster 2 were genes coding the two family members of MS4A transmembrane molecules, MS4A4B and MS4A6B, which in Tregs were reported to support their ability to perceive low level Ag signals and sustain their regulatory function in response to such Ags (Howie et al., 2009). Moreover, cluster 2 Tregs expressed higher levels of characteristic for activated Tregs transcripts *S100a4*, *S100a6*, migratory molecules *Cxcr3* and *Itgb1* (Zemmour et al., 2018), as well *Nrp1*, linked to Treg stability (Junius et al., 2021). Interestingly, some other genes associated with the stability of the Treg phenotype and survival (*Tcf7*, *Lef1*, *Foxp1*) were specifically enriched in cluster 2 in GLP1R TKO Tregs and may account for the expansion of cluster 2 Tregs in VAT of GLP1R TKO animals upon HFHS diet (Yang et al., 2019, Ren et al., 2019).

In addition to the divergent abundancy of cluster 2 Tregs in HFHS diet-fed GLP1R TKO and floxed mice, substantial differences in the transcriptional profile within the clusters were observed between the mouse cohorts with different genotypes. In absence of GLP1R signaling cluster 2 Tregs retained higher degree of similarity to cluster 4, maintaining higher activity of VAT Treg associated transcriptional programs than their GLP1-sufficient counterparts. So, GLP1R-deficient cluster 2 Tregs expressed higher levels of several classical VAT Treg signature genes, such as *Gata3*, *Il1rl1*, *Ccr2* and *Klrg1*, potentially maintaining the essential basal activity of VAT Treg specific transcriptional program

for tissue adaptation. In line with that, *Id2* was found to be among the most differentially upregulated genes in GLP1R TKO mice relative to floxed controls in both, cluster 2 and cluster 4. Frias et al. have previously demonstrated, that VAT Tregs express high levels of *Id2*, which is crucial for their maintenance and phenotype. Treg-specific deletion of *Id2* leads to a reduction of Treg population in VAT, as well as their lower expression of *Gata3*, *Ilrl1*, *Klrg1* and *Ccr2*, which was consistent with our sequencing data (Frias et al., 2019). Additionally, the absence of ID2 impaired the ability of Tregs to produce IL10. Accordingly, we also observed an increase in *Il10* transcripts in GLP1R-deficient Tregs specifically from cluster 2 Tregs, as well as increased overall IL10 levels, as mRNA in transcription profile and as protein in various *in vivo* models.

CD69 is another marker associated with tissue Treg phenotype, which was upregulated in the absence of GLP1R signaling in both, cluster 2 and cluster 4. The recent research findings have described the involvement of CD69 in the regulation of multiple aspects of Treg biology. So, CD69 was shown to control Treg differentiation, probably through the interaction with JAK3/STAT5 (Martín et al., 2010). Moreover, CD69 is involved in the regulation of tissue retention of Tregs, by blocking the egress function of S1P1 (Shiow et al., 2006). In addition to its immunological function, CD69 is implicated in the regulation of intrinsic cell metabolism. In a complex with CD98 it controls an amino acid uptake providing the link to mTOR signaling and T cell differentiation (Sinclair et al., 2013).

Both, CD69 and ID2, were described to be implicated in the maintenance of T cell populations upon hypoxia, since diminished activity of hypoxia-associated pathways are crucial for the cell survival upon low oxygen conditions. In accordance with that, GSEA analysis identified hypoxia-associated pathways to be stronger activated in cluster 2 in HFHS diet-fed GLP1R TKO mice relative to floxed controls. Since hypoxia is described to favor Foxp3 induction and stability, higher activity of this pathway can be an additional element of the metabolic adaptation of GLP1R-deficient cluster 2 Tregs to the proinflammatory microenvironment in obese VAT (Ben-Shoshan et al., 2008, Clambey Eric et al., 2012).

Likewise, we detected enriched transcripts of genes associated with response to proinflammatory signals, as well as TNFα via NFκb signaling, which might be directed to increase the functional maturation of Tregs. The members of the TNFRSF family in Tregs

are described to promote Treg development and maturation and shape the Treg TCR repertoire towards those of high affinity (Mahmud et al., 2014). Mechanistically, the link between the TCR signals and Treg differentiation partially relies on the increase in Treg sensitivity to low doses of IL2 (Mahmud et al., 2014). This was also mirrored in our screen, since higher activity of IL2/STAT5 signaling was observed in GLP1R TKO cluster 2 Tregs. IL2 via its downstream target STAT5 are critical players in the development of Tregs and are important for their maintenance and homeostasis (Burchill et al., 2007, Fontenot et al., 2005). In addition, STAT5 acts directly on the CNS2 region preventing the loss of Foxp3 expression in the presence of proinflammatory cytokines (Feng et al., 2014). By these means, the higher activity of IL2/STAT5 signaling in GLP1R-defecient cluster 2 Tregs may support the maintenance and stability of Tregs in the proinflammatory environment of obese VAT.

Since GLP1 represents a molecular messenger to convey the signal of food intake and nutrient abundancy, one therefore could assume, that the effect of GLP1 on immune cells must involve metabolic reprogramming. Our transcriptional analysis was not able to provide clear and compelling evidence of significant enrichment in specific metabolic programs in Tregs in absence of GLP1R signaling on the mRNA level. However, the direct comparison of transcription profiles (without batch-effect correction) of VAT Tregs from cluster 2 and cluster 4 upon HFHS diet between the genotypes resulted in several mitochondrial genes being reduced and ribosomal genes being significantly more abundant in GLP1R TKO animals. These data should be interpreted with caution and further validated and confirmed, to exclude a potential batch-effect. However, reduced mitochondrial gene transcripts may indicate mitochondrial stress triggered by absence of GLP1R, which was similarly observed by Timper et al. in the model of astrocyte-specific ablation of GLP1R (Timper et al., 2020). This would be in accordance with a higher activity of STAT1 signaling in GLP1R-deficient Tregs, which can be triggered by type I IFNs in response to mitochondrial DNA (mtDNA) release into cytosol upon mitochondrial stress (Field et al., 2020). Correspondingly, it leads to induction of IL10 expression in Tregs, which is in agreement with higher IL10 expression observed in GLP1R Tregs (Zhang et al., 2011).

In the astrocytes, cell-specific deletion and corresponding mitochondrial stress was accompanied by enhanced glucose uptake (Timper et al., 2020). The main signaling pathway downstream of glucose uptake is mTOR, evolutionally conserved metabolic pathway, which integrate environmental (immune and metabolic) cues to regulate cellular growth, proliferation and differentiation. The higher abundancy of ribosomal transcripts in GLP1R TKO mice may indicate the higher protein synthesis as a result of higher mTOR pathway activity. In line, IL2/STAT5 signaling or RORα, which in the transcription profile screen were more present in GLP1R-deficient Tregs, are also known to drive mTOR signaling (Chi et al., 2021, Procaccini et al., 2010). Tregs utilize mTOR for their migration, proliferation and expansion (Gerriets et al., 2016, Procaccini et al., 2010), whereas for their basal metabolism or at the stage of differentiation Tregs are described to mainly operate on fatty acid oxidation (FAO)-fueled oxidative phosphorylation (OXPHOS) (Michalek et al., 2011, Howie et al., 2017). Notably, Howie et al. have demonstrated, that upregulation of OXPHOS and subsequent increase in fatty acid metabolism protected Tregs from fatty acid-induced apoptosis in the environments with elevated fatty acids (Howie et al., 2017). VAT represents such environment, in which Tregs express PPARγ to promote and maintain fatty acid metabolism (Cipolletta et al., 2012). Since HFHS leads to the loss of VAT-specific signature, including PPARγ and PPARγ-dependent fatty acid metabolism (Li et al., 2021b), the mTOR-mediated lipogenesis may compensate for the loss of PPARγ-driven fatty acid uptake and oxidation machinery to restore OXPHOS and fatty acid metabolism for VAT Treg survival and homeostasis. Therefore, the hypothesis, that the ablation of GLP1/GLP1R signaling augments mTOR activity to support Treg intrinsic metabolism particularly in the inflammatory environment will be in line with observed superior tolerogenic character of GLP1R-defecient Tregs in models of acute and chronic inflammation. Additional experiments are yet needed to confirm this hypothesis.

In a nutshell, in frame of my doctoral thesis we identified intriguing and rather unexpected insights into the Treg adaptation to the metabolically challenging proinflammatory environment in absence of GLP1R signaling. These results might seem controversial to the multiple reports describing numerous beneficial effects of GLP1 in various tissues, including the lowering of the body weight and reduction of inflammation. Though, most of these studies are based on the systemic effects induced by GLP1 or GLP1R agonists

and represent their sum metabolic effect throughout the organism. In a such setting, the opposing effects of GLP1 in distinct tissue compartments cannot be identified and studied. Accordingly, such an opposing effect was demonstrated by Timper et al. in the model of astrocyte-specific deletion of GLP1R. Aiming to specifically address the role of GLP1R signaling in astrocytes, the authors have demonstrated such opposing effect, whereby the ablation of GLP1R signaling in astrocytes interfered with astrocyte cell metabolism and enhanced systemic glucose metabolism (Timper et al., 2020). Similarly, here we show that the ablation of GLP1R signaling in CD4 T cells also positively affects systemic metabolic parameters. Taking into account the limited efficacy of GLPR agonists in lowering body weight (~3-10%) (Müller et al., 2019), identification of tissues and cell populations in which cell-intrinsic activity of GLP1R signaling negatively affect the sum positive metabolic effect of GLP1R agonists will help to optimize GLP1-based treatments.

References

AKKAYA, B., OYA, Y., AKKAYA, M., AL SOUZ, J., HOLSTEIN, A. H., KAMENYEVA, O., KABAT, J., MATSUMURA, R., DORWARD, D. W., GLASS, D. D. & SHEVACH, E. M. 2019. Regulatory T cells mediate specific suppression by depleting peptide–MHC class II from dendritic cells. *Nature Immunology,* 20**,** 218-231.

ANSARI, S., HABOUBI, H. & HABOUBI, N. 2020. Adult obesity complications: challenges and clinical impact. *Ther Adv Endocrinol Metab,* 11**,** 2042018820934955.

ATHAUDA, D., MACLAGAN, K., SKENE, S. S., BAJWA-JOSEPH, M., LETCHFORD, D., CHOWDHURY, K., HIBBERT, S., BUDNIK, N., ZAMPEDRI, L., DICKSON, J., LI, Y., AVILES-OLMOS, I., WARNER, T. T., LIMOUSIN, P., LEES, A. J., GREIG, N. H., TEBBS, S. & FOLTYNIE, T. 2017. Exenatide once weekly versus placebo in Parkinson's disease: a randomised, double-blind, placebo-controlled trial. *The Lancet,* 390**,** 1664-1675.

ATUMA, C., STRUGALA, V., ALLEN, A. & HOLM, L. 2001. The adherent gastrointestinal mucus gel layer: thickness and physical state in vivo. *American Journal of Physiology-Gastrointestinal and Liver Physiology,* 280**,** G922-G929.

BAGGER, J. I., HOLST, J. J., HARTMANN, B., ANDERSEN, B., KNOP, F. K. & VILSBØLL, T. 2015. Effect of Oxyntomodulin, Glucagon, GLP-1, and Combined Glucagon +GLP-1 Infusion on Food Intake, Appetite, and Resting Energy Expenditure. *The Journal of Clinical Endocrinology & Metabolism,* 100**,** 4541-4552.

BARRAGÁN, J. M., RODRÍGUEZ, R. E., ENG, J. & BLÁZQUEZ, E. 1996. Interactions of exendin-(9–39) with the effects of glucagon-like peptide-1-(7–36) amide and of exendin-4 on arterial blood pressure and heart rate in rats. *Regulatory Peptides,* 67**,** 63-68.

BECKER, M., LEVINGS, M. K. & DANIEL, C. 2017. Adipose-tissue regulatory T cells: Critical players in adipose-immune crosstalk. *Eur J Immunol,* 47**,** 1867-1874.

BEN-SHOSHAN, J., MAYSEL-AUSLENDER, S., MOR, A., KEREN, G. & GEORGE, J. 2008. Hypoxia controls CD4+CD25+ regulatory T-cell homeostasis via hypoxia-inducible factor-1α. *European Journal of Immunology,* 38**,** 2412-2418.

BENNETT, C. L., CHRISTIE, J., RAMSDELL, F., BRUNKOW, M. E., FERGUSON, P. J., WHITESELL, L., KELLY, T. E., SAULSBURY, F. T., CHANCE, P. F. & OCHS, H. D. 2001. The immune dysregulation, polyendocrinopathy, enteropathy, X-linked syndrome (IPEX) is caused by mutations of FOXP3. *Nature Genetics,* 27**,** 20-21.

BERGEN, V., LANGE, M., PEIDLI, S., WOLF, F. A. & THEIS, F. J. 2020. Generalizing RNA velocity to transient cell states through dynamical modeling. *Nature Biotechnology,* 38**,** 1408-1414.

BHASKARAN, K., DOUGLAS, I., FORBES, H., DOS-SANTOS-SILVA, I., LEON, D. A. & SMEETH, L. 2014. Body-mass index and risk of 22 specific cancers: a population-based cohort study of 5·24 million UK adults. *The Lancet,* 384**,** 755-765.

BI, G., BIAN, Y., LIANG, J., YIN, J., LI, R., ZHAO, M., HUANG, Y., LU, T., ZHAN, C., FAN, H. & WANG, Q. 2021. Pan-cancer characterization of metabolism-related biomarkers

identifies potential therapeutic targets. *Journal of Translational Medicine,* 19**,** 219.

BOWCUTT, R., FORMAN, R., GLYMENAKI, M., CARDING, S. R., ELSE, K. J. & CRUICKSHANK, S. M. 2014. Heterogeneity across the murine small and large intestine. *World J Gastroenterol,* 20**,** 15216-32.

BRAY, G. A., KIM, K. K., WILDING, J. P. H. & WORLD OBESITY, F. 2017. Obesity: a chronic relapsing progressive disease process. A position statement of the World Obesity Federation. *Obes Rev,* 18**,** 715-723.

BRUNKOW, M. E., JEFFERY, E. W., HJERRILD, K. A., PAEPER, B., CLARK, L. B., YASAYKO, S.-A., WILKINSON, J. E., GALAS, D., ZIEGLER, S. F. & RAMSDELL, F. 2001. Disruption of a new forkhead/winged-helix protein, scurfin, results in the fatal lymphoproliferative disorder of the scurfy mouse. *Nature Genetics,* 27**,** 68-73.

BULLOCK, B. P., HELLER, R. S. & HABENER, J. F. 1996. Tissue distribution of messenger ribonucleic acid encoding the rat glucagon-like peptide-1 receptor. *Endocrinology,* 137**,** 2968-2978.

BURCHILL, M. A., YANG, J., VOGTENHUBER, C., BLAZAR, B. R. & FARRAR, M. A. 2007. IL-2 Receptor β-Dependent STAT5 Activation Is Required for the Development of Foxp3+ Regulatory T Cells. *The Journal of Immunology,* 178**,** 280-290.

BURZYN, D., KUSWANTO, W., KOLODIN, D., SHADRACH, J. L., CERLETTI, M., JANG, Y., SEFIK, E., TAN, T. G., WAGERS, A. J., BENOIST, C. & MATHIS, D. 2013. A special population of regulatory T cells potentiates muscle repair. *Cell,* 155**,** 1282-95.

BUTEAU, J., EL-ASSAAD, W., RHODES, C. J., ROSENBERG, L., JOLY, E. & PRENTKI, M. 2004. Glucagon-like peptide-1 prevents beta cell glucolipotoxicity. *Diabetologia,* 47**,** 806-15.

BUTEAU, J., FOISY, S., JOLY, E. & PRENTKI, M. 2003. Glucagon-like peptide 1 induces pancreatic beta-cell proliferation via transactivation of the epidermal growth factor receptor. *Diabetes,* 52**,** 124-32.

CAMPOS, R. V., LEE, Y. C. & DRUCKER, D. J. 1994. Divergent tissue-specific and developmental expression of receptors for glucagon and glucagon-like peptide-1 in the mouse. *Endocrinology,* 134**,** 2156-2164.

CANI, P. D., BIBILONI, R., KNAUF, C., WAGET, A. L., NEYRINCK, A. M., DELZENNE, N. M. & BURCELIN, R. M. 2008. Changes in Gut Microbiota Control Metabolic Endotoxemia-Induced Inflammation in High-Fat Diet–Induced Obesity and Diabetes in Mice. *Diabetes,* 57**,** 1470-1481.

CAPUTA, G., MATSUSHITA, M., SANIN, D. E., KABAT, A. M., EDWARDS-HICKS, J., GRZES, K. M., POHLMEYER, R., STANCZAK, M. A., CASTOLDI, A., CUPOVIC, J., FORDE, A. J., APOSTOLOVA, P., SEIDL, M., VAN TEIJLINGEN BAKKER, N., VILLA, M., BAIXAULI, F., QUINTANA, A., HACKL, A., FLACHSMANN, L., HÄSSLER, F., CURTIS, J. D., PATTERSON, A. E., HENNEKE, P., PEARCE, E. L. & PEARCE, E. J. 2022. Intracellular infection and immune system cues rewire adipocytes to acquire immune function. *Cell Metabolism,* 34**,** 747-760.e6.

CHALLA, T. D., BEATON, N., ARNOLD, M., RUDOFSKY, G., LANGHANS, W. & WOLFRUM, C. 2012. Regulation of Adipocyte Formation by GLP-1/GLP-1R Signaling*. *Journal of Biological Chemistry,* 287**,** 6421-6430.

CHI, X., JIN, W., BAI, X., ZHAO, X., SHAO, J., LI, J., SUN, Q., SU, B., WANG, X., YANG, X. O. & DONG, C. 2021. RORα is critical for mTORC1 activity in T cell-mediated colitis. *Cell Reports,* 36**,** 109682.

CIPOLLETTA, D. 2014. Adipose tissue-resident regulatory T cells: phenotypic specialization, functions and therapeutic potential. *Immunology,* 142**,** 517-525.

CIPOLLETTA, D., COHEN, P., SPIEGELMAN BRUCE, M., BENOIST, C. & MATHIS, D. 2015. Appearance and disappearance of the mRNA signature characteristic of Treg cells in visceral adipose tissue: Age, diet, and PPARγ effects. *Proceedings of the National Academy of Sciences,* 112**,** 482-487.

CIPOLLETTA, D., FEUERER, M., LI, A., KAMEI, N., LEE, J., SHOELSON, S. E., BENOIST, C. & MATHIS, D. 2012. PPAR-gamma is a major driver of the accumulation and phenotype of adipose tissue Treg cells. *Nature,* 486**,** 549-53.

CLAMBEY ERIC, T., MCNAMEE EÓIN, N., WESTRICH JOSEPH, A., GLOVER LOUISE, E., CAMPBELL ERIC, L., JEDLICKA, P., DE ZOETEN EDWIN, F., CAMBIER JOHN, C., STENMARK KURT, R., COLGAN SEAN, P. & ELTZSCHIG HOLGER, K. 2012. Hypoxia-inducible factor-1 alpha–dependent induction of FoxP3 drives regulatory T-cell abundance and function during inflammatory hypoxia of the mucosa. *Proceedings of the National Academy of Sciences,* 109**,** E2784-E2793.

COOMBES, J. L., SIDDIQUI, K. R. R., ARANCIBIA-CÁRCAMO, C. V., HALL, J., SUN, C.-M., BELKAID, Y. & POWRIE, F. 2007. A functionally specialized population of mucosal CD103+ DCs induces Foxp3+ regulatory T cells via a TGF-β– and retinoic acid–dependent mechanism. *Journal of Experimental Medicine,* 204**,** 1757-1764.

COUSIN, B., ANDRÉ, M., CASTEILLA, L. & PÉNICAUD, L. 2001. Altered macrophage-like functions of preadipocytes in inflammation and genetic obesity. *Journal of Cellular Physiology,* 186**,** 380-386.

CRETNEY, E., XIN, A., SHI, W., MINNICH, M., MASSON, F., MIASARI, M., BELZ, G. T., SMYTH, G. K., BUSSLINGER, M., NUTT, S. L. & KALLIES, A. 2011. The transcription factors Blimp-1 and IRF4 jointly control the differentiation and function of effector regulatory T cells. *Nature Immunology,* 12**,** 304-311.

DEACON, C. F., JOHNSEN, A. H. & HOLST, J. J. 1995. Degradation of glucagon-like peptide-1 by human plasma in vitro yields an N-terminally truncated peptide that is a major endogenous metabolite in vivo. *The Journal of Clinical Endocrinology & Metabolism,* 80**,** 952-957.

DEACON, C. F., PRIDAL, L., KLARSKOV, L., OLESEN, M. & HOLST, J. J. 1996. Glucagon-like peptide 1 undergoes differential tissue-specific metabolism in the anesthetized pig. *American Journal of Physiology-Endocrinology and Metabolism,* 271**,** E458-E464.

DELACHER, M., IMBUSCH, C. D., HOTZ-WAGENBLATT, A., MALLM, J. P., BAUER, K., SIMON, M., RIEGEL, D., RENDEIRO, A. F., BITTNER, S., SANDERINK, L., PANT, A., SCHMIDLEITHNER, L., BRABAND, K. L., ECHTENACHTER, B., FISCHER, A., GIUNCHIGLIA, V., HOFFMANN, P., EDINGER, M., BOCK, C., REHLI, M., BRORS, B.,

SCHMIDL, C. & FEUERER, M. 2020. Precursors for Nonlymphoid-Tissue Treg Cells Reside in Secondary Lymphoid Organs and Are Programmed by the Transcription Factor BATF. *Immunity,* 52**,** 295-312 e11.

DELACHER, M., IMBUSCH, C. D., WEICHENHAN, D., BREILING, A., HOTZ-WAGENBLATT, A., TRAGER, U., HOFER, A. C., KAGEBEIN, D., WANG, Q., FRAUHAMMER, F., MALLM, J. P., BAUER, K., HERRMANN, C., LANG, P. A., BRORS, B., PLASS, C. & FEUERER, M. 2017. Genome-wide DNA-methylation landscape defines specialization of regulatory T cells in tissues. *Nat Immunol,* 18**,** 1160-1172.

DELGOFFE, G. M., WOO, S.-R., TURNIS, M. E., GRAVANO, D. M., GUY, C., OVERACRE, A. E., BETTINI, M. L., VOGEL, P., FINKELSTEIN, D., BONNEVIER, J., WORKMAN, C. J. & VIGNALI, D. A. A. 2013. Stability and function of regulatory T cells is maintained by a neuropilin-1–semaphorin-4a axis. *Nature,* 501**,** 252-256.

DRUCKER, D. J. & ASA, S. 1988. Glucagon gene expression in vertebrate brain. *Journal of Biological Chemistry,* 263**,** 13475-13478.

DURING, M. J., CAO, L., ZUZGA, D. S., FRANCIS, J. S., FITZSIMONS, H. L., JIAO, X., BLAND, R. J., KLUGMANN, M., BANKS, W. A., DRUCKER, D. J. & HAILE, C. N. 2003. Glucagon-like peptide-1 receptor is involved in learning and neuroprotection. *Nature Medicine,* 9**,** 1173-1179.

ELLER, K., KIRSCH, A., WOLF, A. M., SOPPER, S., TAGWERKER, A., STANZL, U., WOLF, D., PATSCH, W., ROSENKRANZ, A. R. & ELLER, P. 2011. Potential Role of Regulatory T Cells in Reversing Obesity-Linked Insulin Resistance and Diabetic Nephropathy. *Diabetes,* 60**,** 2954-2962.

ESTERHÁZY, D., CANESSO, M. C. C., MESIN, L., MULLER, P. A., DE CASTRO, T. B. R., LOCKHART, A., ELJALBY, M., FARIA, A. M. C. & MUCIDA, D. 2019. Compartmentalized gut lymph node drainage dictates adaptive immune responses. *Nature,* 569**,** 126-130.

FAUSTINO, L., MUCIDA, D., KELLER, A. C., DEMENGEOT, J., BORTOLUCI, K., SARDINHA, L. R., CARLA TAKENAKA, M., BASSO, A. S., FARIA, A. M. & RUSSO, M. 2012. Regulatory T cells accumulate in the lung allergic inflammation and efficiently suppress T-cell proliferation but not Th2 cytokine production. *Clin Dev Immunol,* 2012**,** 721817.

FENG, Y., ARVEY, A., CHINEN, T., VAN DER VEEKEN, J., GASTEIGER, G. & RUDENSKY, ALEXANDER Y. 2014. Control of the Inheritance of Regulatory T Cell Identity by a cis Element in the Foxp3 Locus. *Cell,* 158**,** 749-763.

FERNANDEZ, J. & VALDEOLMILLOS, M. 1999. Glucose-dependent stimulatory effect of glucagon-like peptide 1(7-36) amide on the electrical activity of pancreatic beta-cells recorded in vivo. *Diabetes,* 48**,** 754-757.

FEUERER, M., HERRERO, L., CIPOLLETTA, D., NAAZ, A., WONG, J., NAYER, A., LEE, J., GOLDFINE, A. B., BENOIST, C., SHOELSON, S. & MATHIS, D. 2009. Lean, but not obese, fat is enriched for a unique population of regulatory T cells that affect metabolic parameters. *Nat Med,* 15**,** 930-9.

FIELD, C. S., BAIXAULI, F., KYLE, R. L., PULESTON, D. J., CAMERON, A. M., SANIN, D. E., HIPPEN, K. L., LOSCHI, M., THANGAVELU, G., CORRADO, M., EDWARDS-HICKS, J., GRZES, K. M., PEARCE, E. J., BLAZAR, B. R. & PEARCE, E. L. 2020. Mitochondrial

Integrity Regulated by Lipid Metabolism Is a Cell-Intrinsic Checkpoint for Treg Suppressive Function. *Cell Metab,* 31**,** 422-437.e5.

FLOESS, S., FREYER, J., SIEWERT, C., BARON, U., OLEK, S., POLANSKY, J., SCHLAWE, K., CHANG, H.-D., BOPP, T., SCHMITT, E., KLEIN-HESSLING, S., SERFLING, E., HAMANN, A. & HUEHN, J. 2007. Epigenetic Control of the foxp3 Locus in Regulatory T Cells. *PLOS Biology,* 5**,** e38.

FONTENOT, J. D., RASMUSSEN, J. P., GAVIN, M. A. & RUDENSKY, A. Y. 2005. A function for interleukin 2 in Foxp3-expressing regulatory T cells. *Nature Immunology,* 6**,** 1142-1151.

FRIAS, A. B., JR., HYZNY, E. J., BUECHEL, H. M., BEPPU, L. Y., XIE, B., JURCZAK, M. J. & D'CRUZ, L. M. 2019. The Transcriptional Regulator Id2 Is Critical for Adipose-Resident Regulatory T Cell Differentiation, Survival, and Function. *J Immunol,* 203**,** 658-664.

GARIDOU, L., POMIÉ, C., KLOPP, P., WAGET, A., CHARPENTIER, J., ALOULOU, M., GIRY, A., SERINO, M., STENMAN, L., LAHTINEN, S., DRAY, C., IACOVONI, JASON S., COURTNEY, M., COLLET, X., AMAR, J., SERVANT, F., LELOUVIER, B., VALET, P., EBERL, G., FAZILLEAU, N., DOUIN-ECHINARD, V., HEYMES, C. & BURCELIN, R. 2015. The Gut Microbiota Regulates Intestinal CD4 T Cells Expressing RORγt and Controls Metabolic Disease. *Cell Metabolism,* 22**,** 100-112.

GAVIN, M. A., RASMUSSEN, J. P., FONTENOT, J. D., VASTA, V., MANGANIELLO, V. C., BEAVO, J. A. & RUDENSKY, A. Y. 2007. Foxp3-dependent programme of regulatory T-cell differentiation. *Nature,* 445**,** 771-775.

GERRIETS, V. A., KISHTON, R. J., JOHNSON, M. O., COHEN, S., SISKA, P. J., NICHOLS, A. G., WARMOES, M. O., DE CUBAS, A. A., MACIVER, N. J., LOCASALE, J. W., TURKA, L. A., WELLS, A. D. & RATHMELL, J. C. 2016. Foxp3 and Toll-like receptor signaling balance Treg cell anabolic metabolism for suppression. *Nature Immunology,* 17**,** 1459-1466.

HADJIYANNI, I., BAGGIO, L. L., POUSSIER, P. & DRUCKER, D. J. 2008. Exendin-4 modulates diabetes onset in nonobese diabetic mice. *Endocrinology,* 149**,** 1338-49.

HADJIYANNI, I., SIMINOVITCH, K. A., DANSKA, J. S. & DRUCKER, D. J. 2010. Glucagon-like peptide-1 receptor signalling selectively regulates murine lymphocyte proliferation and maintenance of peripheral regulatory T cells. *Diabetologia,* 53**,** 730-740.

HARE, K. J., VILSBØLL, T., ASMAR, M., DEACON, C. F., KNOP, F. K. & HOLST, J. J. 2010. The Glucagonostatic and Insulinotropic Effects of Glucagon-Like Peptide 1 Contribute Equally to Its Glucose-Lowering Action. *Diabetes,* 59**,** 1765-1770.

HASSAN, M., LATIF, N. & YACOUB, M. 2012. Adipose tissue: friend or foe? *Nat Rev Cardiol,* 9**,** 689-702.

HE, S., KAHLES, F., RATTIK, S., NAIRZ, M., MCALPINE, C. S., ANZAI, A., SELGRADE, D., FENN, A. M., CHAN, C. T., MINDUR, J. E., VALET, C., POLLER, W. C., HALLE, L., ROTLLAN, N., IWAMOTO, Y., WOJTKIEWICZ, G. R., WEISSLEDER, R., LIBBY, P., FERNÁNDEZ-HERNANDO, C., DRUCKER, D. J., NAHRENDORF, M. & SWIRSKI, F. K. 2019. Gut intraepithelial T cells calibrate metabolism and accelerate cardiovascular disease. *Nature,* 566**,** 115-119.

HEMMERS, S., SCHIZAS, M. & RUDENSKY, A. Y. 2020. T reg cell–intrinsic requirements for ST2 signaling in health and neuroinflammation. *Journal of Experimental Medicine,* 218.

HEPPNER, K. M., MARKS, S., HOLLAND, J., OTTAWAY, N., SMILEY, D., DIMARCHI, R. & PEREZ-TILVE, D. 2015. Contribution of brown adipose tissue activity to the control of energy balance by GLP-1 receptor signalling in mice. *Diabetologia,* 58**,** 2124-2132.

HILARY E. WILSON-PÉREZ, A. P. C., KAREN K. RYAN, BAILING LI,1 DARLEEN A. SANDOVAL, DORIS STOFFERS, DANIEL J. DRUCKER, DIEGO PÉREZ-TILVE, AND RANDY J. SEELEY 2013. Vertical Sleeve Gastrectomy Is Effective in Two Genetic Mouse Models of Glucagon-Like Peptide 1 Receptor Deficiency. *DIABETES,* 62.

HILL, J. A., FEUERER, M., TASH, K., HAXHINASTO, S., PEREZ, J., MELAMED, R., MATHIS, D. & BENOIST, C. 2007. Foxp3 Transcription-Factor-Dependent and -Independent Regulation of the Regulatory T Cell Transcriptional Signature. *Immunity,* 27**,** 786-800.

HOTAMISLIGIL, G. S. 2006. Inflammation and metabolic disorders. *Nature,* 444**,** 860-867.

HOTAMISLIGIL, G. S. 2017. Inflammation, metaflammation and immunometabolic disorders. *Nature,* 542**,** 177-185.

HOWIE, D., COBBOLD, S. P., ADAMS, E., TEN BOKUM, A., NECULA, A. S., ZHANG, W., HUANG, H., ROBERTS, D. J., THOMAS, B., HESTER, S. S., VAUX, D. J., BETZ, A. G. & WALDMANN, H. 2017. Foxp3 drives oxidative phosphorylation and protection from lipotoxicity. *JCI Insight,* 2.

HOWIE, D., NOLAN, K. F., DALEY, S., BUTTERFIELD, E., ADAMS, E., GARCIA-RUEDA, H., THOMPSON, C., SAUNDERS, N. J., COBBOLD, S. P., TONE, Y., TONE, M. & WALDMANN, H. 2009. MS4A4B Is a GITR-Associated Membrane Adapter, Expressed by Regulatory T Cells, Which Modulates T Cell Activation. *The Journal of Immunology,* 183**,** 4197-4204.

ITO, M., KOMAI, K., MISE-OMATA, S., IIZUKA-KOGA, M., NOGUCHI, Y., KONDO, T., SAKAI, R., MATSUO, K., NAKAYAMA, T., YOSHIE, O., NAKATSUKASA, H., CHIKUMA, S., SHICHITA, T. & YOSHIMURA, A. 2019. Brain regulatory T cells suppress astrogliosis and potentiate neurological recovery. *Nature,* 565**,** 246-250.

JAENSSON, E., URONEN-HANSSON, H., PABST, O., EKSTEEN, B., TIAN, J., COOMBES, J. L., BERG, P.-L., DAVIDSSON, T., POWRIE, F., JOHANSSON-LINDBOM, B. & AGACE, W. W. 2008. Small intestinal CD103+ dendritic cells display unique functional properties that are conserved between mice and humans. *Journal of Experimental Medicine,* 205**,** 2139-2149.

JORSAL, T., RHEE, N. A., PEDERSEN, J., WAHLGREN, C. D., MORTENSEN, B., JEPSEN, S. L., JELSING, J., DALBØGE, L. S., VILMANN, P., HASSAN, H., HENDEL, J. W., POULSEN, S. S., HOLST, J. J., VILSBØLL, T. & KNOP, F. K. 2018. Enteroendocrine K and L cells in healthy and type 2 diabetic individuals. *Diabetologia,* 61**,** 284-294.

JUNIUS, S., MAVROGIANNIS, A. V., LEMAITRE, P., GERBAUX, M., STAELS, F., MALVIYA, V., BURTON, O., GERGELITS, V., SINGH, K., TADEO, R. Y. T., RAES, J., HUMBLET-BARON, S., LISTON, A. & SCHLENNER, S. M. 2021. Unstable regulatory T cells,

enriched for naïve and Nrp1neg cells, are purged after fate challenge. *Science Immunology,* 6**,** eabe4723.

KALIN, S., BECKER, M., OTT, V. B., SERR, I., HOSP, F., MOLLAH, M. M. H., KEIPERT, S., LAMP, D., ROHNER-JEANRENAUD, F., FLYNN, V. K., SCHERM, M. G., NASCIMENTO, L. F. R., GERLACH, K., POPP, V., DIETZEN, S., BOPP, T., KRISHNAMURTHY, P., KAPLAN, M. H., SERRANO, M., WOODS, S. C., TRIPAL, P., PALMISANO, R., JASTROCH, M., BLUHER, M., WOLFRUM, C., WEIGMANN, B., ZIEGLER, A. G., MANN, M., TSCHOP, M. H. & DANIEL, C. 2017. A Stat6/Pten Axis Links Regulatory T Cells with Adipose Tissue Function. *Cell Metab,* 26**,** 475-492 e7.

KANOSKI, S. E., FORTIN, S. M., ARNOLD, M., GRILL, H. J. & HAYES, M. R. 2011. Peripheral and Central GLP-1 Receptor Populations Mediate the Anorectic Effects of Peripherally Administered GLP-1 Receptor Agonists, Liraglutide and Exendin-4. *Endocrinology,* 152**,** 3103-3112.

KIM, J. M., RASMUSSEN, J. P. & RUDENSKY, A. Y. 2007. Regulatory T cells prevent catastrophic autoimmunity throughout the lifespan of mice. *Nature Immunology,* 8**,** 191-197.

KIM KWANG, S., HONG, S.-W., HAN, D., YI, J., JUNG, J., YANG, B.-G., LEE JUN, Y., LEE, M. & SURH CHARLES, D. 2016. Dietary antigens limit mucosal immunity by inducing regulatory T cells in the small intestine. *Science,* 351**,** 858-863.

KLANN, J. E., KIM, S. H., REMEDIOS, K. A., HE, Z., METZ, P. J., LOPEZ, J., TYSL, T., OLVERA, J. G., ABLACK, J. N., CANTOR, J. M., BOLAND, B. S., YEO, G., ZHENG, Y., LU, L. F., BUI, J. D., GINSBERG, M. H., PETRICH, B. G. & CHANG, J. T. 2018. Integrin Activation Controls Regulatory T Cell-Mediated Peripheral Tolerance. *J Immunol,* 200**,** 4012-4023.

KOBIE, J. J., SHAH, P. R., YANG, L., REBHAHN, J. A., FOWELL, D. J. & MOSMANN, T. R. 2006. T regulatory and primed uncommitted CD4 T cells express CD73, which suppresses effector CD4 T cells by converting 5'-adenosine monophosphate to adenosine. *J Immunol,* 177**,** 6780-6.

KOLODIN, D., VAN PANHUYS, N., LI, C., MAGNUSON, A. M., CIPOLLETTA, D., MILLER, C. M., WAGERS, A., GERMAIN, R. N., BENOIST, C. & MATHIS, D. 2015. Antigen- and cytokine-driven accumulation of regulatory T cells in visceral adipose tissue of lean mice. *Cell Metab,* 21**,** 543-57.

KOOLE, C., PABREJA, K., SAVAGE, EMILIA E., WOOTTEN, D., FURNESS, SEBASTIAN G. B., MILLER, LAURENCE J., CHRISTOPOULOS, A. & SEXTON, PATRICK M. 2013. Recent advances in understanding GLP-1R (glucagon-like peptide-1 receptor) function. *Biochemical Society Transactions,* 41**,** 172-179.

LA MANNO, G., SOLDATOV, R., ZEISEL, A., BRAUN, E., HOCHGERNER, H., PETUKHOV, V., LIDSCHREIBER, K., KASTRITI, M. E., LÖNNERBERG, P., FURLAN, A., FAN, J., BORM, L. E., LIU, Z., VAN BRUGGEN, D., GUO, J., HE, X., BARKER, R., SUNDSTRÖM, E., CASTELO-BRANCO, G., CRAMER, P., ADAMEYKO, I., LINNARSSON, S. & KHARCHENKO, P. V. 2018. RNA velocity of single cells. *Nature,* 560**,** 494-498.

LAFFONT, S., SIDDIQUI, K. R. R. & POWRIE, F. 2010. Intestinal inflammation abrogates the tolerogenic properties of MLN CD103+ dendritic cells. *European Journal of Immunology,* 40**,** 1877-1883.

LARSEN, P. J., TANG-CHRISTENSEN, M., HOLST, J. J. & ØRSKOV, C. 1997. Distribution of glucagon-like peptide-1 and other preproglucagon-derived peptides in the rat hypothalamus and brainstem. *Neuroscience,* 77**,** 257-270.

LI, C., DISPIRITO, J. R., ZEMMOUR, D., SPALLANZANI, R. G., KUSWANTO, W., BENOIST, C. & MATHIS, D. 2018. TCR Transgenic Mice Reveal Stepwise, Multi-site Acquisition of the Distinctive Fat-Treg Phenotype. *Cell*.

LI, C., MUNOZ-ROJAS, A. R., WANG, G., MANN, A. O., BENOIST, C. & MATHIS, D. 2021a. PPARgamma marks splenic precursors of multiple nonlymphoid-tissue Treg compartments. *Proc Natl Acad Sci U S A,* 118.

LI, C., WANG, G., SIVASAMI, P., RAMIREZ, R. N., ZHANG, Y., BENOIST, C. & MATHIS, D. 2021b. Interferon-α-producing plasmacytoid dendritic cells drive the loss of adipose tissue regulatory T cells during obesity. *Cell Metabolism,* 33**,** 1610-1623.e5.

LI, M., ZHAO, W., WANG, Y., JIN, L., JIN, G., SUN, X., WANG, W., WANG, K., XU, X., HAO, J., JIN, R., FU, W., SUN, Y., CHANG, Y., HUANG, X., ZHOU, X., WU, H., ZHANG, K. & GE, Q. 2020. A wave of Foxp3(+) regulatory T cell accumulation in the neonatal liver plays unique roles in maintaining self-tolerance. *Cell Mol Immunol,* 17**,** 507-518.

LÓPEZ-FERRERAS, L., RICHARD, J. E., NOBLE, E. E., EEROLA, K., ANDERBERG, R. H., OLANDERSSON, K., TAING, L., KANOSKI, S. E., HAYES, M. R. & SKIBICKA, K. P. 2018. Lateral hypothalamic GLP-1 receptors are critical for the control of food reinforcement, ingestive behavior and body weight. *Molecular Psychiatry,* 23**,** 1157-1168.

MACOTELA, Y., BOUCHER, J., TRAN, T. T. & KAHN, C. R. 2009. Sex and Depot Differences in Adipocyte Insulin Sensitivity and Glucose Metabolism. *Diabetes,* 58**,** 803-812.

MAHMUD, S. A., MANLOVE, L. S., SCHMITZ, H. M., XING, Y., WANG, Y., OWEN, D. L., SCHENKEL, J. M., BOOMER, J. S., GREEN, J. M., YAGITA, H., CHI, H., HOGQUIST, K. A. & FARRAR, M. A. 2014. Costimulation via the tumor-necrosis factor receptor superfamily couples TCR signal strength to the thymic differentiation of regulatory T cells. *Nature Immunology,* 15**,** 473-481.

MARTÍN, P., GÓMEZ, M., LAMANA, A., CRUZ-ADALIA, A., RAMÍREZ-HUESCA, M., URSA MARÍA, Á., YÁÑEZ-MO, M. & SÁNCHEZ-MADRID, F. 2010. CD69 Association with Jak3/Stat5 Proteins Regulates Th17 Cell Differentiation. *Molecular and Cellular Biology,* 30**,** 4877-4889.

MATHIS, D. 2013. Immunological goings-on in visceral adipose tissue. *Cell Metab,* 17**,** 851-9.

MICHALEK, R. D., GERRIETS, V. A., JACOBS, S. R., MACINTYRE, A. N., MACIVER, N. J., MASON, E. F., SULLIVAN, S. A., NICHOLS, A. G. & RATHMELL, J. C. 2011. Cutting Edge: Distinct Glycolytic and Lipid Oxidative Metabolic Programs Are Essential for Effector and Regulatory CD4+ T Cell Subsets. *The Journal of Immunology,* 186**,** 3299.

MIRAGAIA, R. J., GOMES, T., CHOMKA, A., JARDINE, L., RIEDEL, A., HEGAZY, A. N., WHIBLEY, N., TUCCI, A., CHEN, X., LINDEMAN, I., EMERTON, G., KRAUSGRUBER, T., SHIELDS, J., HANIFFA, M., POWRIE, F. & TEICHMANN, S. A. 2019. Single-Cell Transcriptomics of Regulatory T Cells Reveals Trajectories of Tissue Adaptation. *Immunity,* 50**,** 493-504.e7.

MOJSOV, S., WEIR, G. C. & HABENER, J. F. 1987. Insulinotropin: glucagon-like peptide I (7-37) co-encoded in the glucagon gene is a potent stimulator of insulin release in the perfused rat pancreas. *The Journal of Clinical Investigation,* 79**,** 616-619.

MOLOFSKY, ARI B., VAN GOOL, F., LIANG, H.-E., VAN DYKEN, STEVEN J., NUSSBAUM, JESSE C., LEE, J., BLUESTONE, JEFFREY A. & LOCKSLEY, RICHARD M. 2015. Interleukin-33 and Interferon-γ Counter-Regulate Group 2 Innate Lymphoid Cell Activation during Immune Perturbation. *Immunity,* 43**,** 161-174.

MÜLLER, T. D., FINAN, B., BLOOM, S. R., D'ALESSIO, D., DRUCKER, D. J., FLATT, P. R., FRITSCHE, A., GRIBBLE, F., GRILL, H. J., HABENER, J. F., HOLST, J. J., LANGHANS, W., MEIER, J. J., NAUCK, M. A., PEREZ-TILVE, D., POCAI, A., REIMANN, F., SANDOVAL, D. A., SCHWARTZ, T. W., SEELEY, R. J., STEMMER, K., TANG-CHRISTENSEN, M., WOODS, S. C., DIMARCHI, R. D. & TSCHÖP, M. H. 2019. Glucagon-like peptide 1 (GLP-1). *Molecular Metabolism,* 30**,** 72-130.

MURASE, K., KAWANO, Y., RYAN, J., MATSUOKA, K.-I., BASCUG, G., MCDONOUGH, S., SMITH, R. W., COWENS, K., LAZO-KALLANIAN, S., DALEY, J., KORETH, J., SOIFFER, R. J., LETAI, A. & RITZ, J. 2013. Low-Dose IL-2 Induces Bcl2 Expression and Resistance To Apoptosis In CD4 Regulatory T Cells. *Blood,* 122**,** 3475-3475.

NOSBAUM, A., PREVEL, N., TRUONG, H. A., MEHTA, P., ETTINGER, M., SCHARSCHMIDT, T. C., ALI, N. H., PAULI, M. L., ABBAS, A. K. & ROSENBLUM, M. D. 2016. Cutting Edge: Regulatory T Cells Facilitate Cutaneous Wound Healing. *J Immunol,* 196**,** 2010-4.

NOYAN-ASHRAF, M. H., MOMEN, M. A., BAN, K., SADI, A.-M., ZHOU, Y.-Q., RIAZI, A. M., BAGGIO, L. L., HENKELMAN, R. M., HUSAIN, M. & DRUCKER, D. J. 2009. GLP-1R Agonist Liraglutide Activates Cytoprotective Pathways and Improves Outcomes After Experimental Myocardial Infarction in Mice. *Diabetes,* 58**,** 975-983.

OGAWA, C., BANKOTI, R., NGUYEN, T., HASSANZADEH-KIABI, N., NADEAU, S., PORRITT, R. A., COUSE, M., FAN, X., DHALL, D., EBERL, G., OHNMACHT, C. & MARTINS, G. A. 2018. Blimp-1 Functions as a Molecular Switch to Prevent Inflammatory Activity in Foxp3+ Regulatory T Cells. *Cell Reports,* 25**,** 19-28.e5.

OHNMACHT, C., PARK, J.-H., CORDING, S., WING, J. B., ATARASHI, K., OBATA, Y., GABORIAU-ROUTHIAU, V., MARQUES, R., DULAUROY, S., FEDOSEEVA, M., BUSSLINGER, M., CERF-BENSUSSAN, N., BONECA, I. G., VOEHRINGER, D., HASE, K., HONDA, K., SAKAGUCHI, S. & EBERL, G. 2015. The microbiota regulates type 2 immunity through RORγt+ T cells. *Science,* 349**,** 989.

OMA. *What Is Obesity?* [Online]. Obesity Medicine Association. Available: https://obesitymedicine.org/what-is-obesity/ [Accessed 11.08 2022].

ORSKOV, C., RABENHØJ, L., WETTERGREN, A., KOFOD, H. & HOLST, J. J. 1994. Tissue and plasma concentrations of amidated and glycine-extended glucagon-like peptide I in humans. *Diabetes,* 43**,** 535-9.

PAMIR, N., MCMILLEN, T. S., KAIYALA, K. J., SCHWARTZ, M. W. & LEBOEUF, R. C. 2009. Receptors for tumor necrosis factor-alpha play a protective role against obesity and alter adipose tissue macrophage status. *Endocrinology,* 150**,** 4124-34.

PANDIYAN, P., ZHENG, L., ISHIHARA, S., REED, J. & LENARDO, M. J. 2007. CD4+CD25+Foxp3+ regulatory T cells induce cytokine deprivation-mediated apoptosis of effector CD4+ T cells. *Nat Immunol,* 8**,** 1353-62.

PATSOURIS, D., LI, P.-P., THAPAR, D., CHAPMAN, J., OLEFSKY, J. M. & NEELS, J. G. 2008. Ablation of CD11c-Positive Cells Normalizes Insulin Sensitivity in Obese Insulin Resistant Animals. *Cell Metabolism,* 8**,** 301-309.

PETERS, J. H., KOENEN, H. J. P. M., FASSE, E., TIJSSEN, H. J., IJZERMANS, J. N. M., GROENEN, P. J. T. A., SCHAAP, N. P. M., KWEKKEBOOM, J. & JOOSTEN, I. 2013. Human secondary lymphoid organs typically contain polyclonally-activated proliferating regulatory T cells. *Blood,* 122**,** 2213-2223.

PROCACCINI, C., DE ROSA, V., GALGANI, M., ABANNI, L., CALÌ, G., PORCELLINI, A., CARBONE, F., FONTANA, S., HORVATH, T. L., LA CAVA, A. & MATARESE, G. 2010. An Oscillatory Switch in mTOR Kinase Activity Sets Regulatory T Cell Responsiveness. *Immunity,* 33**,** 929-941.

QIU, R., ZHOU, L., MA, Y., ZHOU, L., LIANG, T., SHI, L., LONG, J. & YUAN, D. 2020. Regulatory T Cell Plasticity and Stability and Autoimmune Diseases. *Clinical Reviews in Allergy & Immunology,* 58**,** 52-70.

REN, J., HAN, L., TANG, J., LIU, Y., DENG, X., LIU, Q., HAO, P., FENG, X., LI, B., HU, H. & WANG, H. 2019. Foxp1 is critical for the maintenance of regulatory T-cell homeostasis and suppressive function. *PLoS Biol,* 17**,** e3000270.

RIDAURA, V. K., FAITH, J. J., REY, F. E., CHENG, J., DUNCAN, A. E., KAU, A. L., GRIFFIN, N. W., LOMBARD, V., HENRISSAT, B., BAIN, J. R., MUEHLBAUER, M. J., ILKAYEVA, O., SEMENKOVICH, C. F., FUNAI, K., HAYASHI, D. K., LYLE, B. J., MARTINI, M. C., URSELL, L. K., CLEMENTE, J. C., VAN TREUREN, W., WALTERS, W. A., KNIGHT, R., NEWGARD, C. B., HEATH, A. C. & GORDON, J. I. 2013. Gut Microbiota from Twins Discordant for Obesity Modulate Metabolism in Mice. *Science,* 341**,** 1241214.

RKI. *Overweight and Obesity* [Online]. Available: https://www.rki.de/EN/Content/Health_Monitoring/Main_Topics/Overweight_Obesity/obesity_node.html [Accessed 08.08 2022].

ROUILLÉ, Y., MARTIN, S. & STEINER, D. F. 1995. Differential Processing of Proglucagon by the Subtilisin-like Prohormone Convertases PC2 and PC3 to Generate either Glucagon or Glucagon-like Peptide (∗). *Journal of Biological Chemistry,* 270**,** 26488-26496.

SALINERO, A. E., ANDERSON, B. M. & ZULOAGA, K. L. 2018. Sex differences in the metabolic effects of diet-induced obesity vary by age of onset. *International Journal of Obesity,* 42**,** 1088-1091.

SAUER, S., BRUNO, L., HERTWECK, A., FINLAY, D., LELEU, M., SPIVAKOV, M., KNIGHT, Z. A., COBB, B. S., CANTRELL, D., O'CONNOR, E., SHOKAT, K. M., FISHER, A. G. & MERKENSCHLAGER, M. 2008. T cell receptor signaling controls Foxp3 expression via PI3K, Akt, and mTOR. *Proc Natl Acad Sci U S A,* 105**,** 7797-802.

SCHERM, M. G., SERR, I., ZAHM, A. M., SCHUG, J., BELLUSCI, S., MANFREDINI, R., SALB, V. K., GERLACH, K., WEIGMANN, B., ZIEGLER, A.-G., KAESTNER, K. H. & DANIEL, C. 2019. miRNA142-3p targets Tet2 and impairs Treg differentiation and stability in models of type 1 diabetes. *Nature Communications,* 10**,** 5697.

SCHIERING, C., KRAUSGRUBER, T., CHOMKA, A., FROHLICH, A., ADELMANN, K., WOHLFERT, E. A., POTT, J., GRISERI, T., BOLLRATH, J., HEGAZY, A. N., HARRISON, O. J., OWENS, B. M. J., LOHNING, M., BELKAID, Y., FALLON, P. G. & POWRIE, F. 2014. The alarmin IL-33 promotes regulatory T-cell function in the intestine. *Nature,* 513**,** 564-568.

SCROCCHI, L. A., BROWN, T. J., MACLUSKY, N., BRUBAKER, P. L., AUERBACH, A. B., JOYNER, A. L. & DRUCKER, D. J. 1996. Glucose intolerance but normal satiety in mice with a null mutation in the glucagon-like peptide 1 receptor gene. *Nat Med,* 2**,** 1254-8.

SECHER, A., JELSING, J., BAQUERO, A. F., HECKSHER-SØRENSEN, J., COWLEY, M. A., DALBØGE, L. S., HANSEN, G., GROVE, K. L., PYKE, C., RAUN, K., SCHÄFER, L., TANG-CHRISTENSEN, M., VERMA, S., WITGEN, B. M., VRANG, N. & KNUDSEN, L. B. 2014. The arcuate nucleus mediates GLP-1 receptor agonist liraglutide-dependent weight loss. *Journal of Clinical Investigation,* 124**,** 4473-4488.

SEFIK, E., GEVA-ZATORSKY, N., OH, S., KONNIKOVA, L., ZEMMOUR, D., MCGUIRE, A. M., BURZYN, D., ORTIZ-LOPEZ, A., LOBERA, M., YANG, J., GHOSH, S., EARL, A., SNAPPER, S. B., JUPP, R., KASPER, D., MATHIS, D. & BENOIST, C. 2015. MUCOSAL IMMUNOLOGY. Individual intestinal symbionts induce a distinct population of RORγ^{+} regulatory T cells. *Science (New York, N.Y.),* 349**,** 993-997.

SERR, I., WEIGMANN, B., FRANKE, R. K. & DANIEL, C. 2014. Treg vaccination in autoimmune type 1 diabetes. *BioDrugs,* 28**,** 7-16.

SHIOW, L. R., ROSEN, D. B., BRDICKOVÁ, N., XU, Y., AN, J., LANIER, L. L., CYSTER, J. G. & MATLOUBIAN, M. 2006. CD69 acts downstream of interferon-alpha/beta to inhibit S1P1 and lymphocyte egress from lymphoid organs. *Nature,* 440**,** 540-4.

SIMONSSON, E. & AHRÉN, B. 1998. Potentiated β-cell response to non-glucose stimuli in insulin-resistant C57BL/6J mice. *European Journal of Pharmacology,* 350**,** 243-250.

SINCLAIR, L. V., ROLF, J., EMSLIE, E., SHI, Y.-B., TAYLOR, P. M. & CANTRELL, D. A. 2013. Control of amino-acid transport by antigen receptors coordinates the metabolic reprogramming essential for T cell differentiation. *Nature Immunology,* 14**,** 500-508.

SINGH, R. P., HALAKA, D. A., HAYOUKA, Z. & TIROSH, O. 2020. High-Fat Diet Induced Alteration of Mice Microbiota and the Functional Ability to Utilize Fructooligosaccharide for Ethanol Production. *Frontiers in Cellular and Infection Microbiology,* 10.

STEWART, C. A., METHENY, H., IIDA, N., SMITH, L., HANSON, M., STEINHAGEN, F., LEIGHTY, R. M., ROERS, A., KARP, C. L., MÜLLER, W. & TRINCHIERI, G. 2013. Interferon-dependent IL-10 production by Tregs limits tumor Th17 inflammation. *J Clin Invest,* 123**,** 4859-74.

STUART, T., BUTLER, A., HOFFMAN, P., HAFEMEISTER, C., PAPALEXI, E., MAUCK, W. M., HAO, Y., STOECKIUS, M., SMIBERT, P. & SATIJA, R. 2019. Comprehensive Integration of Single-Cell Data. *Cell,* 177**,** 1888-1902.e21.

SUBRAMANIAN, A., TAMAYO, P., MOOTHA, V. K., MUKHERJEE, S., EBERT, B. L., GILLETTE, M. A., PAULOVICH, A., POMEROY, S. L., GOLUB, T. R., LANDER, E. S. & MESIROV, J. P. 2005. Gene set enrichment analysis: A knowledge-based approach for interpreting genome-wide expression profiles. *Proceedings of the National Academy of Sciences,* 102**,** 15545-15550.

SUNDSTEDT, A., O'NEILL, E. J., NICOLSON, K. S. & WRAITH, D. C. 2003. Role for IL-10 in suppression mediated by peptide-induced regulatory T cells in vivo. *J Immunol,* 170**,** 1240-8.

SZUREK, E., CEBULA, A., WOJCIECH, L., PIETRZAK, M., REMPALA, G., KISIELOW, P. & IGNATOWICZ, L. 2015. Differences in Expression Level of Helios and Neuropilin-1 Do Not Distinguish Thymus-Derived from Extrathymically-Induced CD4+Foxp3+ Regulatory T Cells. *PLOS ONE,* 10**,** e0141161.

TIMPER, K., DEL RÍO-MARTÍN, A., CREMER, A. L., BREMSER, S., ALBER, J., GIAVALISCO, P., VARELA, L., HEILINGER, C., NOLTE, H., TRIFUNOVIC, A., HORVATH, T. L., KLOPPENBURG, P., BACKES, H. & BRÜNING, J. C. 2020. GLP-1 Receptor Signaling in Astrocytes Regulates Fatty Acid Oxidation, Mitochondrial Integrity, and Function. *Cell Metabolism,* 31**,** 1189-1205.e13.

TURNBAUGH, P. J., LEY, R. E., MAHOWALD, M. A., MAGRINI, V., MARDIS, E. R. & GORDON, J. I. 2006. An obesity-associated gut microbiome with increased capacity for energy harvest. *Nature,* 444**,** 1027-1031.

USSHER, J. R. & DRUCKER, D. J. 2014. Cardiovascular Actions of Incretin-Based Therapies. *Circulation Research,* 114**,** 1788-1803.

VAHL, T. P., PATY, B. W., FULLER, B. D., PRIGEON, R. L. & D'ALESSIO, D. A. 2003. Effects of GLP-1-(7-36)NH2, GLP-1-(7-37), and GLP-1- (9-36)NH2 on intravenous glucose tolerance and glucose-induced insulin secretion in healthy humans. *J Clin Endocrinol Metab,* 88**,** 1772-9.

VAN DIJK, D., SHARMA, R., NAINYS, J., YIM, K., KATHAIL, P., CARR, A. J., BURDZIAK, C., MOON, K. R., CHAFFER, C. L., PATTABIRAMAN, D., BIERIE, B., MAZUTIS, L., WOLF, G., KRISHNASWAMY, S. & PE'ER, D. 2018. Recovering Gene Interactions from Single-Cell Data Using Data Diffusion. *Cell,* 174**,** 716-729.e27.

VASANTHAKUMAR, A., CHISANGA, D., BLUME, J., GLOURY, R., BRITT, K., HENSTRIDGE, D. C., ZHAN, Y., TORRES, S. V., LIENE, S., COLLINS, N., CAO, E., SIDWELL, T., LI, C., SPALLANZANI, R. G., LIAO, Y., BEAVIS, P. A., GEBHARDT, T., TREVASKIS, N., NUTT, S. L., ZAJAC, J. D., DAVEY, R. A., FEBBRAIO, M. A., MATHIS, D., SHI, W. & KALLIES, A. 2020. Sex-specific adipose tissue imprinting of regulatory T cells. *Nature*.

VASANTHAKUMAR, A., MORO, K., XIN, A., LIAO, Y., GLOURY, R., KAWAMOTO, S., FAGARASAN, S., MIELKE, L. A., AFSHAR-STERLE, S., MASTERS, S. L., NAKAE, S., SAITO, H., WENTWORTH, J. M., LI, P., LIAO, W., LEONARD, W. J., SMYTH, G. K., SHI, W., NUTT, S. L., KOYASU, S. & KALLIES, A. 2015. The transcriptional regulators IRF4, BATF and IL-33 orchestrate development and maintenance of adipose tissue–resident regulatory T cells. *Nature Immunology,* 16**,** 276-285.

VEENBERGEN, S., VAN BERKEL, L. A., DU PRÉ, M. F., HE, J., KARRICH, J. J., COSTES, L. M. M., LUK, F., SIMONS-OOSTERHUIS, Y., RAATGEEP, H. C., CEROVIC, V., CUPEDO, T., MOWAT, A. M., KELSALL, B. L. & SAMSOM, J. N. 2016. Colonic tolerance develops in the iliac lymph nodes and can be established independent of CD103+ dendritic cells. *Mucosal Immunology,* 9**,** 894-906.

VENDRELL, J., EL BEKAY, R., PERAL, B., GARCÍA-FUENTES, E., MEGIA, A., MACIAS-GONZALEZ, M., REAL, J. F., JIMENEZ-GOMEZ, Y., ESCOTÉ, X., PACHÓN, G., SIMÓ, R., SELVA, D. M., MALAGÓN, M. M. & TINAHONES, F. J. 2011. Study of the Potential Association of Adipose Tissue GLP-1 Receptor with Obesity and Insulin Resistance. *Endocrinology,* 152**,** 4072-4079.

VON BOEHMER, H. 2005. Mechanisms of suppression by suppressor T cells. *Nat Immunol,* 6**,** 338-44.

WALLENIUS, V., WALLENIUS, K., AHRÉN, B., RUDLING, M., CARLSTEN, H., DICKSON, S. L., OHLSSON, C. & JANSSON, J.-O. 2002. Interleukin-6-deficient mice develop mature-onset obesity. *Nature Medicine,* 8**,** 75-79.

WANG, C., ZHANG, X., LUO, L., LUO, Y., YANG, X., DING, X., WANG, L., LE, H., FELDMAN, L. E. R., MEN, X., YAN, C., HUANG, W., FENG, Y., LIU, F., YANG, X. O. & LIU, M. 2022. Adipocyte-derived PGE2 is required for intermittent fasting–induced Treg proliferation and improvement of insulin sensitivity. *JCI Insight,* 7.

WANG, S.-X., XIE, Y., ZHOU, X., SHA, W.-W., WANG, W.-L., HAN, L.-P., WANG, J.-C. & YU, D.-M. 2010. [Effect of glucagon-like peptide-1 on hypoxia-reoxygenation induced injury in neonatal rat cardiomyocytes]. *Zhonghua xin xue guan bing za zhi,* 38**,** 72-75.

WEI, Y. & MOJSOV, S. 1995. Tissue-specific expression of the human receptor for glucagon-like peptide-I: brain, heart and pancreatic forms have the same deduced amino acid sequences. *FEBS Letters,* 358**,** 219-224.

WEISBERG, S. P., MCCANN, D., DESAI, M., ROSENBAUM, M., LEIBEL, R. L. & FERRANTE, A. W., JR. 2003. Obesity is associated with macrophage accumulation in adipose tissue. *The Journal of Clinical Investigation,* 112**,** 1796-1808.

WHEATON, J. D., YEH, C.-H. & CIOFANI, M. 2017. Cutting Edge: c-Maf Is Required for Regulatory T Cells To Adopt RORγt(+) and Follicular Phenotypes. *Journal of immunology (Baltimore, Md. : 1950),* 199**,** 3931-3936.

WHO. 2021a. *Noncommunicable diseases* [Online]. Available: https://www.who.int/news-room/fact-sheets/detail/noncommunicable-diseases [Accessed 11.08 2022].

WHO. 2021b. *Obesity and overweight* [Online]. Available: https://www.who.int/news-room/fact-sheets/detail/obesity-and-overweight [Accessed 08.08 2022].

WOHLFERT, E. A., GRAINGER, J. R., BOULADOUX, N., KONKEL, J. E., OLDENHOVE, G., RIBEIRO, C. H., HALL, J. A., YAGI, R., NAIK, S., BHAIRAVABHOTLA, R., PAUL, W. E., BOSSELUT, R., WEI, G., ZHAO, K., OUKKA, M., ZHU, J. & BELKAID, Y. 2011. GATA3 controls Foxp3^{+} regulatory T cell fate during inflammation in mice. *The Journal of clinical investigation,* 121**,** 4503-4515.

WU, D., WONG, C. K., HAN, J. M., ORBAN, P. C., HUANG, Q., GILLIES, J., MOJIBIAN, M., GIBSON, W. T. & LEVINGS, M. K. 2020. T reg–specific insulin receptor deletion prevents diet-induced and age-associated metabolic syndrome. *Journal of Experimental Medicine,* 217**,** e20191542.

XU, H., BARNES, G. T., YANG, Q., TAN, G., YANG, D., CHOU, C. J., SOLE, J., NICHOLS, A., ROSS, J. S., TARTAGLIA, L. A. & CHEN, H. 2003. Chronic inflammation in fat plays a crucial role in the development of obesity-related insulin resistance. *The Journal of Clinical Investigation,* 112**,** 1821-1830.

XUE, S., WASSERFALL, C. H., PARKER, M., BRUSKO, T. M., MCGRAIL, S., MCGRAIL, K., MOORE, M., CAMPBELL-THOMPSON, M., SCHATZ, D. A., ATKINSON, M. A. & HALLER, M. J. 2008. Exendin-4 Therapy in NOD Mice with New-Onset Diabetes Increases Regulatory T Cell Frequency. *Annals of the New York Academy of Sciences,* 1150**,** 152-156.

YANG, B. H., HAGEMANN, S., MAMARELI, P., LAUER, U., HOFFMANN, U., BECKSTETTE, M., FÖHSE, L., PRINZ, I., PEZOLDT, J., SUERBAUM, S., SPARWASSER, T., HAMANN, A., FLOESS, S., HUEHN, J. & LOCHNER, M. 2016. Foxp3+ T cells expressing RORγt represent a stable regulatory T-cell effector lineage with enhanced suppressive capacity during intestinal inflammation. *Mucosal Immunology,* 9**,** 444-457.

YANG, B. H., WANG, K., WAN, S., LIANG, Y., YUAN, X., DONG, Y., CHO, S., XU, W., JEPSEN, K., FENG, G. S., LU, L. F., XUE, H. H. & FU, W. 2019. TCF1 and LEF1 Control Treg Competitive Survival and Tfr Development to Prevent Autoimmune Diseases. *Cell Rep,* 27**,** 3629-3645.e6.

YANG, Y. H., SONG, W., DEANE, J. A., KAO, W., OOI, J. D., NGO, D., KITCHING, A. R., MORAND, E. F. & HICKEY, M. J. 2013. Deficiency of Annexin A1 in CD4+; T Cells Exacerbates T Cell–Dependent Inflammation. *The Journal of Immunology,* 190**,** 997.

ZEMMOUR, D., ZILIONIS, R., KINER, E., KLEIN, A. M., MATHIS, D. & BENOIST, C. 2018. Single-cell gene expression reveals a landscape of regulatory T cell phenotypes shaped by the TCR. *Nature Immunology,* 19**,** 291-301.

ZHANG, L., YUAN, S., CHENG, G. & GUO, B. 2011. Type I IFN Promotes IL-10 Production from T Cells to Suppress Th17 Cells and Th17-Associated Autoimmune Inflammation. *PLOS ONE,* 6**,** e28432.

ZORRILLA ERIC, P., SANCHEZ-ALAVEZ, M., SUGAMA, S., BRENNAN, M., FERNANDEZ, R., BARTFAI, T. & CONTI, B. 2007. Interleukin-18 controls energy homeostasis by suppressing appetite and feed efficiency. *Proceedings of the National Academy of Sciences,* 104**,** 11097-11102.

Acknowledgement

First and foremost, I would like to express my deepest gratitude to my mentor and supervisor Prof. Dr. Carolin Daniel for supporting me all the way through the path of my PhD degree. I'm sincerely thankful for her optimistic attitude and enthusiasm, her trust and encouragement, which helped me to overcome all the hurdles and doubts. I really appreciate her effort and dedication to provide the resources and give the extraordinary opportunity for professional and personal growth for myself and each member of the research group.

I also want to thank the members of my Thesis Committee: Prof. Dr. Susanna Hofmann and Prof. Dr. Kathrin Schumann for external supervision of my project. I am very grateful for their interest in the topic, for the constructive feedback and helpful comments that have definitely contributed to the progress and success of this project.

Moreover, I would address my special thanks to Dr. Alexey Surnov, who made an enormous contribution to this project by supporting the scRNAseq analysis and executing the computational and statistical part of it. I appreciate Alexeys' curiosity, great attention to details, logical thinking and constant striving for careful and precise examination of information. His humor, kind attitude and willingness to help made this time of intense and productive cooperation pleasant and fun.

In addition, I also want to thank all other fellows of the research group for the friendly and joyful atmosphere in the lab. I really enjoyed working in such an inspiring and motivating environment, with such talented, creative and intelligent people and to have the opportunity to learn from them. Especially, I would like to express my gratitude to Maike Becker and Hannah Hipp for their supportive attitude and willingness to help.

Last but not least, I would like to thank my family and my husband for supporting me spiritually throughout this project and my whole life. I am enormous grateful to them for their unconditional love and never-ending encouragement, which gave me the strength and patience over the hard years of PhD Thesis. Thank you!

Affidavit

LMU LUDWIG-MAXIMILIANS-UNIVERSITÄT MÜNCHEN

Promotionsbüro
Medizinische Fakultät

MMRS

Eidesstattliche Versicherung

Opaleva, Daria

Name, Vorname

Ich erkläre hiermit an Eides statt, dass ich die vorliegende Dissertation mit dem Titel:

The role of GLP1R signaling for the tissue-specific adaptation of regulatory T cells

……

selbständig verfasst, mich außer der angegebenen keiner weiteren Hilfsmittel bedient und alle Erkenntnisse, die aus dem Schrifttum ganz oder annähernd übernommen sind, als solche kenntlich gemacht und nach ihrer Herkunft unter Bezeichnung der Fundstelle einzeln nachgewiesen habe.

Ich erkläre des Weiteren, dass die hier vorgelegte Dissertation nicht in gleicher oder in ähnlicher Form bei einer anderen Stelle zur Erlangung eines akademischen Grades eingereicht wurde.

München, 09.08.2023 — Daria Opaleva

Ort, Datum — Unterschrift Doktorandin bzw. Doktorand

Publications

Poster presentation at the international conference:

DARIA OPALEVA, MAIKE BECKER, ALEXEY SURNOV, ISABELLE SERR, MICHAEL STERR, MATTHIAS TSCHÖP, CAROLIN DANIEL. 2022 June 26-28. The absence of GLP1 receptor in T cells restores adipose tissue Tregs and metabolic parameters upon hypercaloric challenge. *Cell Symposium Translational Immunometabolism*, Basel, Switzerland.